Canadian Light Source | Centre canadien de rayonnement synchrotron

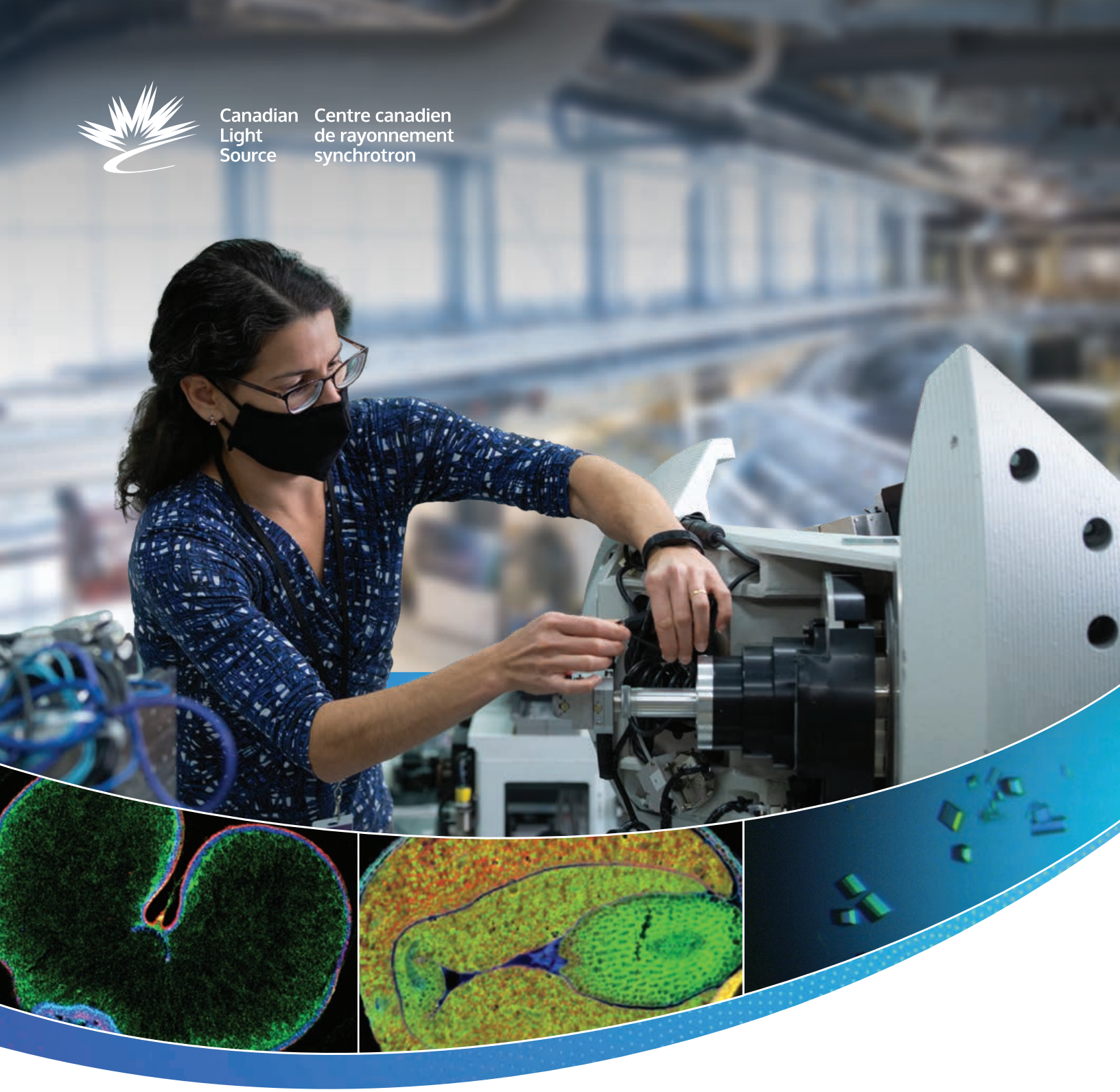

Research Report | 2021

CANADIAN LIGHT SOURCE INC.

ACKNOWLEDGEMENTS

FUNDING PARTNERS

The Canadian Light Source thanks all of our funding partners for their commitment to the advancement of science and innovation.

OPERATING

CAPITAL

USER INSTITUTIONS

Agriculture and Agri-Food Canada (AAFC)
Balmoral Hall School
Bishop Carroll High School
Canadian Light Source Inc.
Canadian Museum of Nature
Center for High Pressure Science & Technology Advanced Research (HPSTAR)
Chinese Academy of Agricultural Science
Chinook School Division
CSIR- Central Glass and Ceramic Research Institute
Dalhousie University
Donostia International Physics Center
Drexel University
École Polytechnique de Montréal
Environment and Climate Change Canada, Aquatic Ecosystem Protection Research Division
Environment Climate Change Canada
Federal University of Minas Gerais (UFMG)
FTXT Energy Technology Co., Ltd. Baoding Branch
Fudan University
Global Institute for Food Security
Halifax Grammar School
Helix Biostructures LLC
IBM T.J. Watson Research Center
InnoTech Alberta Inc.
Institut National de la Recherche Scientifique (INRS)
Institute for Energy, Environment and Sustainable Communities
Institute of Applied Ecology
Institute of Environmental and Sustainable Development in Agriculture
Instituto de Investigaciones en Tecnología Química (INTEQUI, UNSL-CONICET)
James Madison University
Lanzhou University
Lawrence Berkeley National Laboratory
Leibniz Institute for Solid State Physics and Materials Research Dresden (IFW Dresden)
Massachusetts Eye and Ear
Massachusetts Institute of Technology
Max Planck Institute for Chemical Physics of Solids
Max Planck Institute for Solid State Research
McGill University
McMaster University
Meadowridge Independent School
Meadowridge School
MicroBeam Advancement, Inc.
National Research Council of Canada
Natural Resources Canada
Notre Dame High School
Palustris Environmental
Queen's University
Royal Saskatchewan Museum
Saskatchewan Cancer Agency
Saskatchewan Food Industry Development Centre Inc.
Saskatchewan Polytechnic
Savannah River National Laboratory
Shanghai Advanced Research Institute, Chinese Academy of Sciences
Shanghai Institute of Applied Physics
ShanghaiTech University
Soochow University, Functional Nano & Soft Material Laboratory
Southwest Petroleum University
Sundre High School
Texas A and M University
The Hospital for Sick Children
TR Labs
Trinity College, Dublin
Trinity University
UChicago Argonne LLC
United States Department of Agriculture, Forest Service
University of Alberta
University of Bayreuth
University of Bristol
University of British Columbia
University of Calgary
University of California, Davis
University of California, Irvine
University of California, San Diego
University of California, Santa Barbara
University of Cambridge
University of Colorado Boulder
University of Guelph
University of Helsinki
University of Illinois at Urbana–Champaign
University of Liverpool
University of Manitoba
University of Minnesota
University of Nevada, Las Vegas
University of New Brunswick
University of North Dakota
University of Ottawa
University of Oulu
University of Quebec, Abitibi-Temiscamingue
University of Regina
University of Rostock
University of Saskatchewan
University of Texas at Austin
University of Texas, Arlington
University of Toronto
University of Victoria
University of Waterloo
University of Western Ontario
University of Wyoming
Virginia Polytechnic and State University
Webber Academy
Yale University

TABLE OF CONTENTS

Canadian Light Source Research Report 2021 | **Editor:** Victoria Martinez
 | **www.lightsource.ca**

Front cover images

Top: Beatriz Moreno Diaz. **Left:** Distribution of sulfur (green), zinc (blue) and manganese (green) in Arborg Oat measured at BioXAS. Courtesy Ganqi Deng. **Center:** Qualitative distribution map of macronutrients (lipids – red, proteins – green, carbohydrates – blue) within a canola seed cross-section measured at Mid-IR by Charlotte Fleet (undergraduate summer student, McMaster). Sample and data curtesy of Janitha Wanasundara and Agriculture and Agri-Food Canada (AAFC). **Right:** Protein crystals

MESSAGE FROM THE **SCIENCE DIRECTOR**

For the second year in a row, CLS staff and users demonstrated their adaptability and resilience in the face of the pandemic. We operated in mail-in mode for most of the year, providing outstanding support to users outside of our province, finally welcoming users from the rest of Canada in September, and international users in December.

The COVID-19 special call for proposals continued to allow the prioritization of vital pandemic-related research. We persevered through a small COVID outbreak in April, repaired damage to our cryo-transfer line caused by a power failure in June, and fixed issues with a klystron in August so rapidly that it had minimal impact on user beamtime.

Top-Up was achieved in July, with a record run in the last few days of the year, and we successfully realigned part of the storage ring and upgraded the bendmagnet at our macromolecular crystallography beamline (CMCF) with very competitive output that supported all the macromolecular crystallography work of our users during the upgrade of the ID beamline..

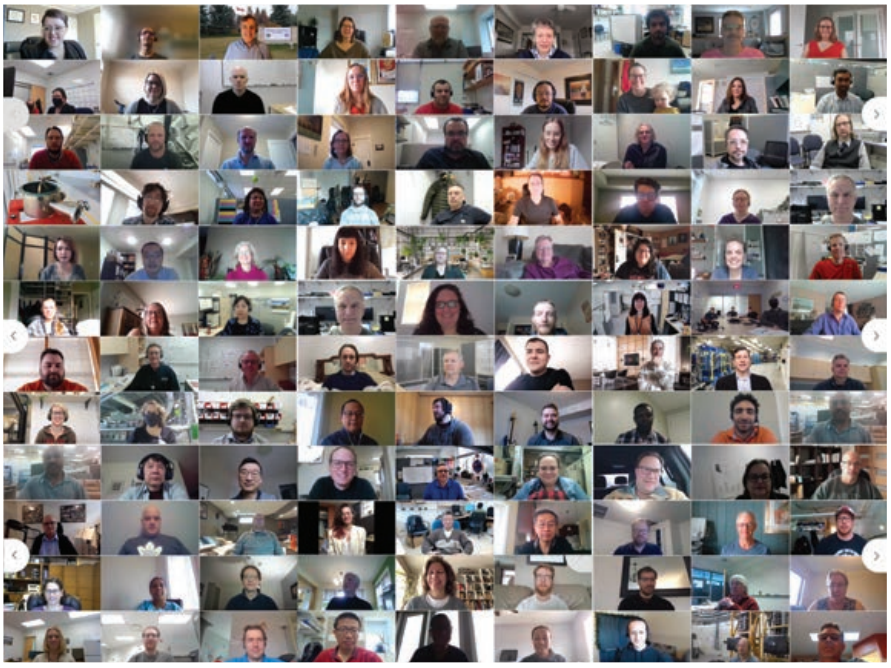

We hosted 986 distinct users from 19 countries, and 44 Canadian institutions from 10 provinces, publishing 518 scientific papers. Once again, the importance of CLS in training the next generation of Canadian scientists is demonstrated by the over 60% of graduate students that used our facility, conducting critical research for their studies and supporting the valuable research by leading scientists across the country.

The quality of science continues to be evident, as highlighted in these pages. From plant imaging and structural biology to Fermi surfaces and fuel cells, our users published in a wide range of areas and contribute to Canada's global science reputation. These publications are competitive with the best beamlines in the world. Furthermore, two successful CFI-IF applications, led by McMaster University, will bring new detectors, robots, and tensile testing capabilities to BXDS and BMIT, as well as an environmental scanning electron microscope for users.

Several beamlines hosted users through the general user program for the first time, including the Brockhouse Diffraction Sector (BXDS), BioXAS-Imaging, and the Quantum Materials Spectroscopy Centre (QMSC). In addition, new capabilities were added to Far-IR, SyLMAND, SGM, BXDS, BMIT, IDEAS, and SM, as a well as a major upgrade to CMCF-ID, which achieved outstanding results competitive with the best beamlines in the world.

We also continued our focus on improving the user experience, with the establishment of a dedicated User Experience Coordinator position, revamped user feedback surveys and processes for acting on feedback, a new and improved website focused on providing information needed by new users, updated peer review process with a new scientific merit rubric, and several improvements to our user portal.

Two significant efforts towards securing the long-term success of CLS are also worth mentioning. We submitted the operating funding proposal for the Canada Foundation for Innovation's Major Science Initiatives program for 2023-2029, and our Board of Directors completed the Strategic Plan for 2022-2032, with wide stakeholder consultation including the Users' Executive Committee and Beamline Teams Leaders, establishing a clear vision and direction for the next decade.

Lastly, we remain committed to continuously improving our service to users and our scientific capabilities, through the maintenance and upgrades of our machine and beamlines, our expert staff, and by ensuring we listen to our users and stakeholders.

Thank you for your valuable contributions to our national research facility.

Gianluigi Botton,
Science Director

Beamlines

The Canadian Light Source houses 22 beamlines, supporting a wide variety of research applications. Each beamline offers a unique spectral range providing different elemental information. To find a beamline that suits your intended research, explore by scientific sector, technique, or spectral range, or search through our Beamline Directory at **www.lightsource.ca**

BEAMLINE GLOSSARY

BioXAS: Biological X-ray Absorption Spectroscopy

BMIT: Biomedical Imaging and Therapy

BXDS: Brockhouse X-Ray Diffraction and Scattering Sector

CLS@APS: CLS at the Advanced Photon Source

CMCF: Canadian Macromolecular Crystallography Facility

Far-IR: Far Infrared Spectroscopy

HXMA: Hard X-ray MicroAnalysis

IDEAS: Industry Development Education Applications Students

Mid-IR: Mid Infrared Spectromicroscopy

QMSC: Quantum Materials Spectroscopy Center

REIXS: Resonant Elastic and Inelastic X-ray Scattering

SGM: High Resolution Spherical Grating Monochromator

SM: Soft X-ray Spectromicroscopy

SXRMB: Soft X-ray Microcharacterization Beamline

SyLMAND: Synchrotron Laboratory for Micro And Nano Devices

VESPERS: Very Sensitive Elemental and Structural Probe Employing Radiation from a Synchrotron

VLS-PGM: Variable Line Spacing Plane Grating Monochromator

BM: Bend Magnet

ID: Insertion Device

FIND A BEAMLINE

FAR-IR

Fundamental studies of molecules in all states of matter

MID-IR

Infrared studies of biological, agricultural, or environmental samples, polymers, art specimens, and more

SGM

Soft x-ray spectroscopy for in-situ and in-operando studies of soil, environmental samples, and catalytic materials

VLS-PGM

High-resolution, low-energy spectroscopic studies

BXDS

Suite of three beamlines for characterizing the structure of materials

BMIT

Beamlines dedicated to 3D imaging of matter, from biological tissues to advanced materials

SyLMAND

X-ray lithography and pre and post-processing laboratories

HXMA

In-situ and ex-situ studies of the chemical state of elements in materials

SXRMB

Medium energy studies in the biological, environmental, and chemical sciences

BioXAS

Dedicated beamlines for imaging and spectroscopy on biological samples and trace element detection/speciation in matter

VESPERS

Hard x-ray microprobe with a wide variety of applications

CMCF

Suite of two beamlines for macromolecular crystallography (MX)

QMSC

Angle-and spin-resolved photoemission spectroscopy (ARPES/SARPES)

REIXS

Soft x-ray scattering for studying the electronic properties of materials, including quantum and nano-scale biomaterials

SM

Spectromicroscopic studies with applications in biological, environment, and materials sciences

LEGEND

- SPECTROSCOPY
- IMAGING / MICROSCOPY
- SCATTERING / DIFFRACTION
- MICROFABRICATION

New Beamline Capabilities

BEAMLINES BY SPECTRAL RANGE

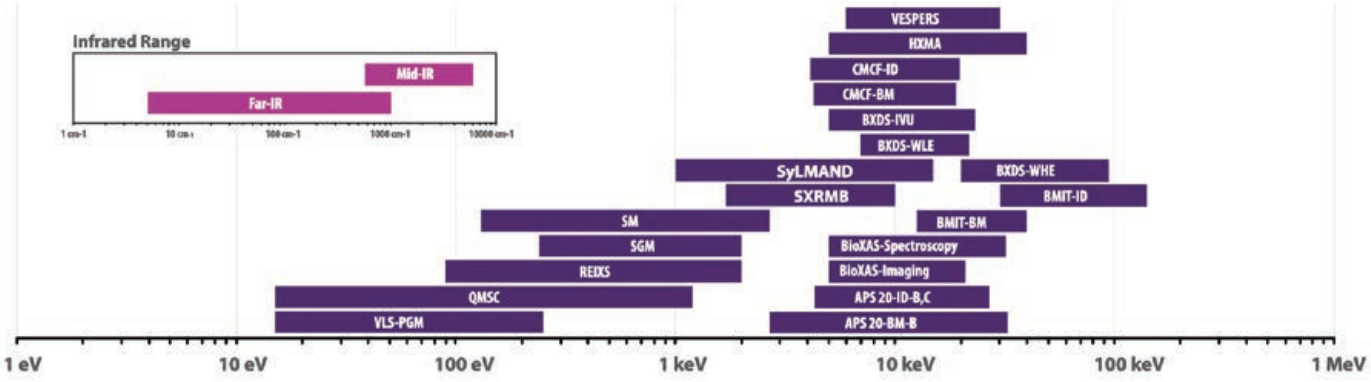

SM: SOFT X-RAY PTYCHOGRAPHY

Detecting and resolving, with high spatial resolution, the interactions between chemical components in lithium-ion battery (LIB) cathodes is challenging but crucial for a better understanding of their degradation mechanisms. Cutting-edge STXM-ptychography was employed to image degradation heterogeneities and the interplay between components in degraded Li-rich cathodes with an unprecedented spatial resolution of 5.6 nm, the best spatial resolution of x-ray microscopy on energy nanomaterials ever achieved. Additionally, subtle chemical modifications

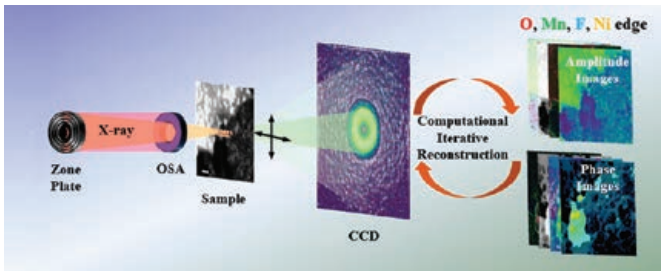

of the degraded LIB cathodes were confirmed by the extension to spectro-ptychography, which demonstrated that fluorine ions are incorporated into the cathode lattice during charging/discharging processes. This effect is is strongly correlated with manganese dissolution and oxygen loss within the secondary cathode particles. The work was led by CLS scientists from the SM beamline and the Industrial group through a close collaboration with other research institutions, making a significant impact on both x-ray microscopy and battery materials analysis. Owing to many years of development work and to strong support from CLS management, particularly for investing in a state-of-the-art UHV x-ray direct-CCD camera, ptychography on SM STXM is actively serving a broad range of research communities.

[1] Sun, Tianxiao, Gang Sun, Fuda Yu, Yongzhi Mao, Renzhong Tai, Xiangzhi Zhang, Guangjie Shao, Zhenbo Wang, Jian Wang, and Jigang Zhou. "Soft X-ray ptychography chemical imaging of degradation in a composite surface-reconstructed Li-rich cathode." ACS nano 15, no. 1 (2020): 1475-1485.

BMIT: ULTRA-FAST X-RAY IMAGING AND TIME-RESOLVED MICROTOMOGRAPHY

X-ray tomographic microscopy is an invaluable non-invasive imaging technique for examining the internal structure of objects and model organisms. Over the past several years BMIT scientists have made a number of modifications to x-ray microtomography (μCT) endstations on BMIT-BM and ID, with support from CLS engineers and software developers. These upgrades enabled new imaging techniques and protocols, including ultra-fast imaging and microtomography. This is of great interest as it allows researchers to capture dynamic effects inside various objects and conduct in situ and in operando studies of processes inside fuel cells, batteries, and other systems. The high flux of the BMIT x-ray beams allows acquisition of many thousands of images each second. In order to exploit this, a high-precision, ultra-fast rotation stage was installed; new sCMOS cameras have been procured; optical efficiency of the detectors has been optimized; and new data acquisition, transfer, and storage solutions have been deployed. A new control system is capable of accurately synchronizing everything in a variety of ways, and is flexible and user-friendly.

With new instruments one can either record up to 100,000 images over 10 seconds or continuously stream up to 500 images per second to data storage. The former is used to capture fast transients while the latter permits time-resolved μCT imaging of processes that can last several tens of minutes.

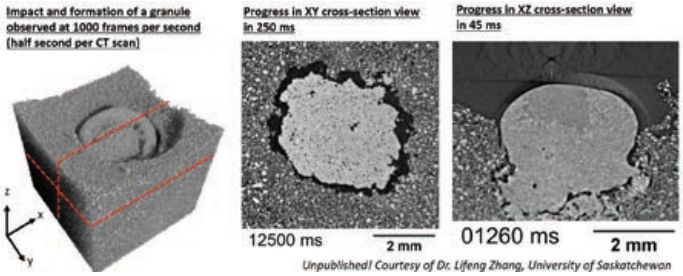

Unpublished! Courtesy of Dr. Lifeng Zhang, University of Saskatchewan

SYLMAND: REACTIVE ION ETCHER

SyLMAND has a new reactive ion etcher (RIE) tool purchased from the Canadian company Plasmionique. The RIE uses argon and oxygen as process gases for plasma treatment, for example in the preparation of highly clean substrate surfaces before fabrication. Argon atoms in the plasma bombard the substrate, removing adsorbed contaminants. Oxygen radicals add a chemical cleaning method by reacting with contaminants, further improving cleaning. Plasma treatment can also be used to modify surface properties, such as for plasma-assisted bonding of microfluidic

devices (PDMS/glass or PDMS/Si) or hydrophilizing fluorinated polymers for fuel cells.

The RIE has recently been upgraded with a UV-Vis-NIR spectrometer for endpoint detection of plasma cleaning processes. Optical emission of plasma-phase fragments of surface coatings or contaminants can be monitored spectroscopically, allowing a greater degree of process automation and verification of surface cleanliness. Future improvements will add reactive process gases to provide dry etching capabilities for materials such as silicon and silicon nitride. This will provide users with greater ability to fabricate micro- and nano-devices in fields such as RF MEMS, x-ray optics, and microfluidics.

SGM: ANAEROBIC SAMPLE HOLDER

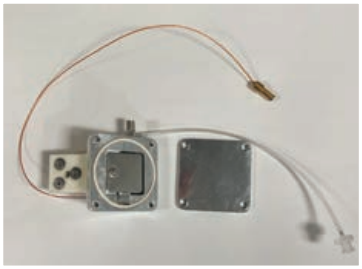

Many of the most important energy materials are highly sensitive to oxygen and water in the atmosphere and have to be handled in an anaerobic environment to maintain their useful properties. This presents a challenge for analyzing these materials using x-ray spectroscopies because the controlled environmental conditions must be maintained throughout the production, preparation, transfer and analysis stages of the experiment. This is particularly important for soft x-ray spectroscopies where probe depths are very shallow and even a brief exposure to atmospheric conditions can degrade the sample surface and affect the measurements.

The development of the SGM beamline anaerobic sample holder addresses the needs of the energy material research community by providing an end-to-end anaerobic sample transfer capability. The system consists of a sealable sample holder that can be loaded and prepared in a glove box. Once the samples are mounted, the system is sealed and the contents are put under vacuum. The holder can then be safely taken from the glove box and loaded into the measurement endstation. When the endstation vacuum reaches the vacuum level inside the holder, the lid falls away, exposing the sample for measurement.

The holder is currently available for general use and can even be an option for mail-in experiments. Recent updates include the addition of electrical feedthroughs for in-situ and operando measurements. Please contact SGM beamline staff to discuss use of the anaerobic sample holder.

BXDS: SAXS ENDSTATION

In 2020, small angle x-ray scattering (SAXS) capabilities moved from HXMA to the recently completed BXDS sector [1]. The in-house developed SAXS instrument has been revised as part of the move. The major components now include scatterless slits, a modular lightweight plastic flight tube up to 4 meters long with silicon nitride entrance window, improved beamstops, and out-of-vacuum Rayonix MX300 detectors. The revised instrument has been in user operation since early 2021, and has now been used by 15 academic groups and industrial clients. Our diverse user community has been applying SAXS to research areas including photovoltaics, polymers, food science, and pharmaceuticals.

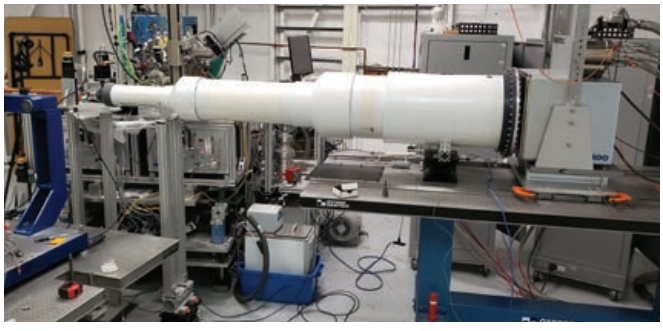

[1] Leontowich, A. F. G., Gomez, A., Moreno, B. D., Muir, D., Spasyuk, D., King, G., Reid, J. W., Kim, C. Y. & Kycia, S. The lower energy diffraction and scattering side bounce beamline for materials science at the Canadian Light Source. *J. Synchrotron Rad.* 28 961-969 (2021). https://doi.org/10.1107/S1600577521002496

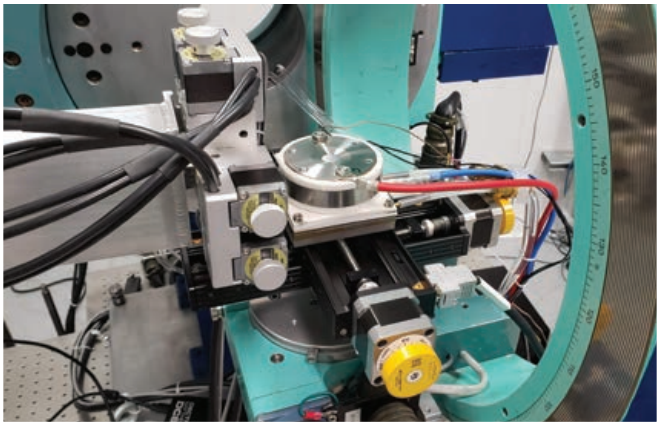

BXDS: IN-SITU BATTERY RESEARCH ON THE WIGGLER HIGH ENERGY BEAMLINE

High energy x-rays can penetrate real life samples like batteries. We can cycle batteries during x-ray diffraction and total scattering experiments, extracting information about the structure and atomic order in the near, medium and long range of battery components such as the anode and cathode materials, and how they evolve during the charge/discharge cycle. This allows to improve the understanding of the structure-property relationship, eventually leading to the creation of more efficient batteries for a greener world.

CMCF: UPGRADE TO THE ID FACILITY

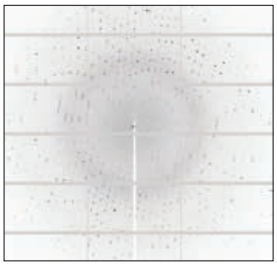

Our CMCF beamline has been undergoing an upgrade over the last two years, and it's now ready for users. This upgrade will allow CMCF to remain among the best x-ray diffraction beamlines in the world, with more intense and tightly focused x-rays, and a faster and more sensitive x-ray detector. Over 60 Canadian protein crystallography laboratories use this unique facility, actively pursuing research in therapeutics and protein engineering that targets cancer, diabetes, infectious diseases and chronic diseases such as Parkinson's, cystic fibrosis and Alzheimer's. These upgrades will enable experiments with smaller and weakly diffracting crystals, the new frontier of macromolecular crystallography. Seen here is the first dataset collected on the new equipment: a high-flux 180-degree dataset, Lysozyme crystal, 1.8 seconds for 360 frames, 0.5 deg/5 msec per frame with attenuated beam.

Far-IR: Learning about the universe with the James Web Space Telescope

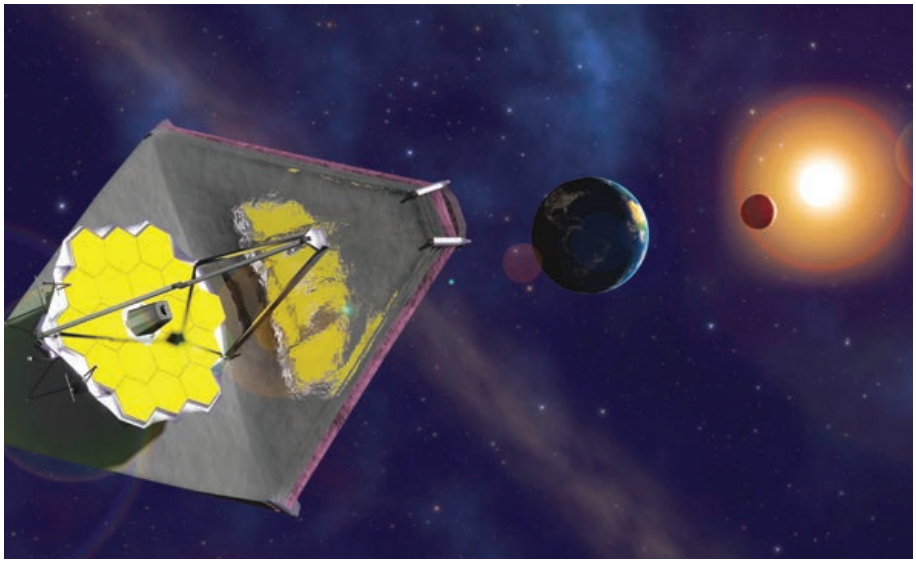

Image courtesy Kevin M. Gill

On December 25th, 2021, the James Web Space telescope successfully launched. It has now collected its first images. One of the instruments onboard the James Web Space telescope is the Mid-Infrared Instrument, which has both a camera and spectrograph operating in the 352 to 2000 cm^{-1} spectral region. This instrument is already collecting a wealth of data about the universe, providing insights into the formation of galaxies, planetary systems, and the origin of life. Reference data, generated back on Earth, is required so that the spectral signatures of molecules can be identified in the data. The Far-Infrared beamline is well positioned to help provide this data due to its high-resolution spectrometer and long-pass temperature-controlled gas cell, which can provide high-quality spectra at a variety of pressures and temperatures for molecules of interest. Recently the Far-IR beamline has been working to extend the temperature range of the gas cell down to 100K to better match the conditions found in space.

Over the last year, Far-IR's users have published several papers that may be relevant to the James Web Space telescope's mission. Methanol is known as a "cosmic weed" molecule as it often appears in satellite spectra and has a very complicated spectrum. Two papers from CLS users may help to identify features caused by methanol in these spectra. Dr. Mukhopadhay published an analysis of the spectrum of CHD_2OH, for the 50-5000 cm^{-1} region [1], and Dr. Lees has published an analysis of the COD-bending fundamental vibration found at 775 cm^{-1}. [2] Dr. Esselman et al. published an analysis of thiazole. [3] Dr. McKellar has continued his work on the astrophysically-important molecule acrolein, publishing an analysis of the states in the 1250 to 1650 cm^{-1} region [4]. Dr. Predoi-Cross et al. have published papers on the spectra of chloroform in the 450-850 cm^{-1} region [5] and deuterated ammonia species in the 60-600 cm^{-1} region [6]. The spectrum of the simple pre-sugar glycolaldehyde in the 450 to 600 cm^{-1} was published by Dr. Raston et al [7].

An important tool for the analysis of astrophysical and atmospheric spectra is the HITRAN database [8]. The newest version of this important database included contributions from papers published using data from the Far-IR beamline, including line lists for formic acid taken from a 2019 paper by Dr. Raston et al. [9] and absorption cross-sections for hydrogen and helium-broadened propane from the 2019 paper by Bernath et al. [10].

While much work has been accomplished, there are many more molecules to study and many more parameters to probe. With the James Web Space Telescope set to provide a wealth of new data about the universe, the Far-IR beamline's goal of enabling a deeper understanding of the universe is more relevant as ever.

1. Mukhopadhyay, Indranath; Billinghurst, B.E. (2021). Very high-resolution synchrotron radiation far-infrared (FIR) spectrum of methanolD2 (CHD_2OH) & millimeter-wave (MMW) measurements involving highly excited torsional vibrational rotational states, and identification of optically pumped FIR laser lines. *Infrared Physics and Technology* 113, 103563. 10.1016/j.infrared.2020.103563.

2. Lees, R.M.; Billinghurst, B.E. (2022). Fourier transform synchrotron spectroscopy of the COD-bending fundamental of CD_3OD. *Journal of Molecular Spectroscopy* 384, 111592. 10.1016/j.jms.2022.111592.

3. Esselman, Brian J.; Zdanovskaia, Maria A.; Adkins, Taylor K.; Billinghurst, Brant E.; Zhao, Jianbao et al. (2021). Millimeter-wave and infrared spectroscopy of thiazole ($c\text{-}C_3H_3NS$) in its ground state and lowest-energy vibrationally excited states (v18, v17, and v13). *Journal of Molecular Spectroscopy* 379, 111493. 10.1016/j.jms.2021.111493.

4. McKellar, A.R.W.; Billinghurst, B.E. (2022). High-resolution infrared spectroscopy of acrolein: The 91, 81, 71, and 61 fundamentals and other vibrational states between 1250 and 1650 cm^{-1}. *Journal of Molecular Spectroscopy* 383, 111563. 10.1016/j.jms.2021.111563.

5. Ceausu-Velcescu, Adina; Pracna, Petr; Margules, Laurent; Predoi-Cross, Adriana (2021). Rotational spectrum of chloroform, "grass-roots among the forest of trees": The v2 = 1, v3 = 2, v5 = 1, and v6 = 3 vibrational states of $CH^{35}Cl_3$. *Journal of Quantitative Spectroscopy and Radiative Transfer* 276, 107937. 10.1016/j.jqsrt.2021.107937.

6. Canè, Elisabetta; Di Lonardo, Gianfranco; Fusina, Luciano; Tamassia, Filippo; Predoi-Cross, Adriana et al. (2022). Mono- and di-deuterated ammonias: Far-infrared spectra and spectroscopic parameters in the ground state. *Journal of Molecular Spectroscopy* 384, 111581. 10.1016/j.jms.2022.111581.

7. Collier, Breanna; Krueger, Kristopher; Miller, Isaac; Zhao, Jianbao; Billinghurst, Brant E. et al. (2021). The Synchrotron-based Far-infrared Spectrum of Glycolaldehyde. *Astrophysical Journal. Supplement Series* 253(2) , 40. 10.3847/1538-4365/abde40.

8. Gordon, I.E.; Rothman, L.S.; Hargreaves, R.J.; Hashemi, R.; Karlovets, E.V. et al. (2022). The HITRAN2020 molecular spectroscopic database. *Journal of Quantitative Spectroscopy and Radiative Transfer* 277, 107949. 10.1016/j.jqsrt.2021.107949.

9. Hull, Killian; Wells, Tyler; Billinghurst, Brant E.; Bunn, Hayley; Raston, Paul L. et al. (2019). Synchrotron-based infrared spectroscopy of formic acid: Confirmation of the reassignment of Fermi-coupled 8 μm states. *AIP Advances* 9(1) , 015021. 10.1063/1.5063010.

10. Wong, Andy; Hewett, Dan; Billinghurst, Brant B.; Hodges, James N.; Bernath, Peter F. et al. (2019). He and H_2 broadened propane cross sections in the 3 μm region at cold temperatures. *Journal of Quantitative Spectroscopy and Radiative Transfer 232*, 104-107. 10.1016/j.jqsrt.2019.04.038.

High-throughput sample processing

Agriculture and environmental samples have complex ecosystems and may experience complex conditions. Crucial to this research is the requirement to analyze tens or hundreds of samples in a high throughput manner. The CLS has worked on increasing the throughput of bulk sample analysis in different beamlines. This entails a dedicated laboratory for bulk sample preparation through fast data collection and data analysis thereby improving the efficiency of synchrotron science (e.g. automated sample weighing, pellet making, multiple sample loading, data collection, fast scanning, improved detectors, and improved pipelines for data analysis). As examples, shown here are the high throughput bulk X-ray absorption spectroscopy data collection setup in the IDEAS beamline from automated pellets prepared from bulk samples (Figure 1), and high throughput X-ray computed tomography data collection at the BMIT-ID beamline, where as many as 15 wheat spikes can be imaged at a time to phenotype the genotypes resistant to Fusarium disease (Figure 2).

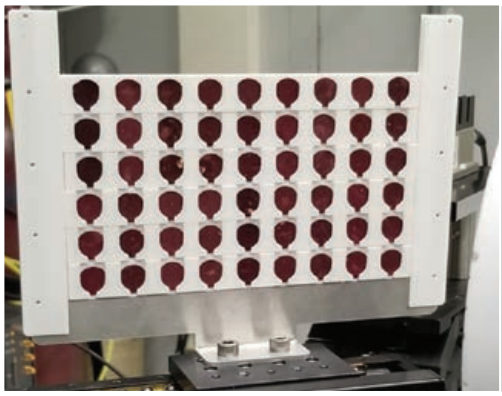

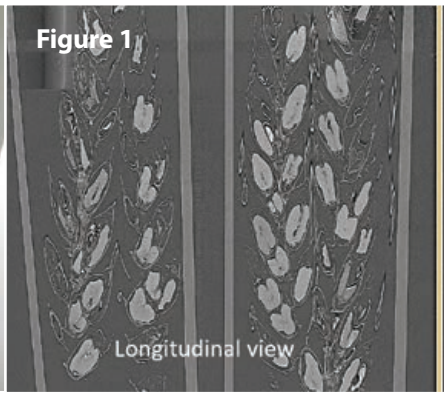

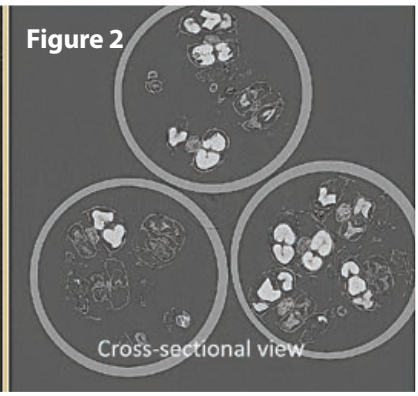

On-site Phytotron

Agriculture researchers can now bring their plants to the CLS and keep them in a controlled environment until the end of their beamtime. Pictured are users from the University of British Columbia and Agriculture and Agri-Food Canada studying large tree samples using our BMIT-ID beamline. Their poplar tree seedlings were scanned last year and the same plants are being scanned again to compare old and new wood growth as well as their adaptability to climate change.

Phytotron

Science Highlights

Throughout this report, the following symbols will be used to indicate the techniques of highlighted research.

- SPECTROSCOPY
- IMAGING / MICROSCOPY
- SCATTERING / DIFFRACTION
- MICROFABRICATION

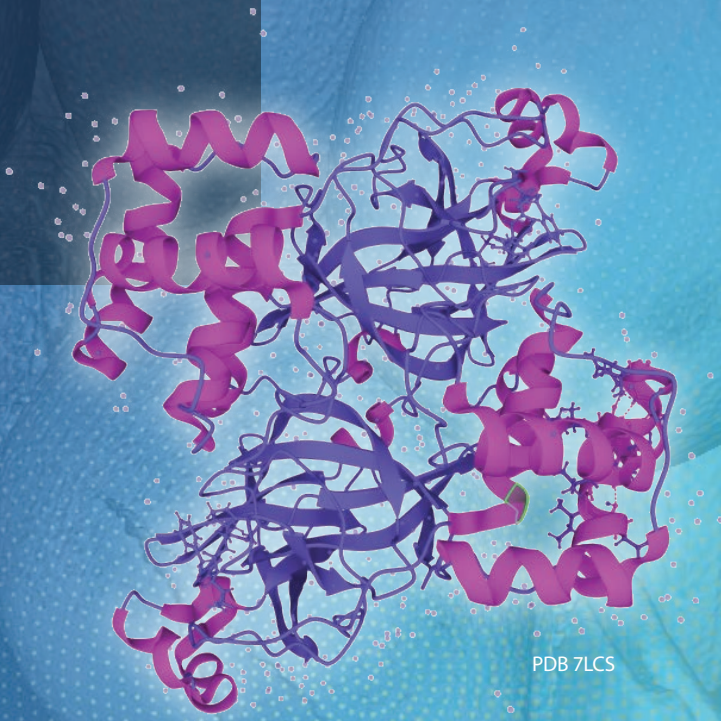

PDB 7LCS

ADVANCED MATERIALS

General synthesis of single-atom catalysts with high metal loading using graphene quantum dots

Xia, Chuan, Yunrui Qiu, Yang Xia, Peng Zhu, Graham King, Xiao Zhang, Zhenyu Wu et al. "General synthesis of single-atom catalysts with high metal loading using graphene quantum dots." *Nature chemistry* 13, no. 9 (2021): 887-894.
DOI: 10.1038/s41557-021-00734-x

CLS data was used to identify the chemical state and site of the catalysts.

BioXAS, BXDS, SXRMB

Transition-metal single-atom catalysts present extraordinary activity per metal atomic site, but suffer from low metal-atom densities (typically less than 5 wt% or 1 at.%), which limits their overall catalytic performance. This work reports a general method for the synthesis of single-atom catalysts with high transition-metal-atom loadings of up to 40 wt% or 3.8 at.%, representing several-fold improvements compared to benchmarks in the literature. Graphene quantum dots, later interweaved into a carbon matrix, were used as a support, providing numerous anchoring sites and thus facilitating the generation of high densities of transition-metal atoms with sufficient spacing between the metal atoms to avoid aggregation. A significant increase in activity in electrochemical CO_2 reduction (used as a representative reaction) was demonstrated on a Ni single-atom catalyst with increased Ni loading.

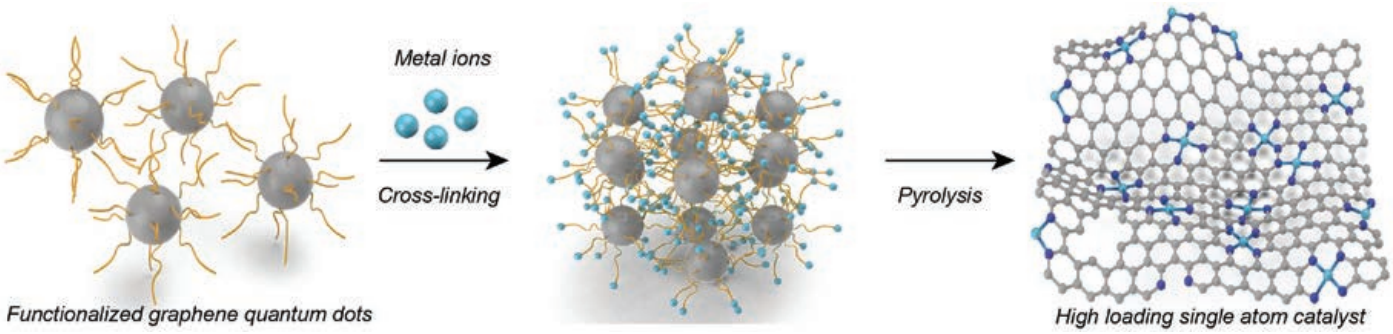

Rice University engineers in collaboration with CLS have led the development of a process that uses functionalized graphene quantum dots to trap transition metals for higher metal loading single-atom catalysis. Illustration courtesy of the Wang Group.

Corresponding authors:
Chuan Xia, University of Electronic Science and Technology of China, Yongfeng Hu , CLS & Haotian Wang, Rice University and Canadian Institute for Advanced Research

High-order replica bands in monolayer FeSe/SrTiO$_3$ revealed by polarization-dependent photoemission spectroscopy

Liu, Chong, Ryan P. Day, Fengmiao Li, Ryan L. Roemer, Sergey Zhdanovich, Sergey Gorovikov, Tor M. Pedersen et al. "High-order replica bands in monolayer FeSe/SrTiO$_3$ revealed by polarization-dependent photoemission spectroscopy." *Nature Communications* 12, no. 1 (2021): 1-8.

The polarization dependent, high resolution ARPES measurements were carried out at the CLS.

QMSC

The mechanism of the enhanced superconductivity in monolayer FeSe/SrTiO$_3$ has been enthusiastically studied and debated over the past decade. One specific observation has been taken to be of central importance: the replica bands in the photoemission spectrum. Although suggestive of electron-phonon interaction in the material, the essence of these spectroscopic features remains highly controversial. In this work, we conduct angle-resolved photoemission spectroscopy measurements on the QMSC beamline on monolayer FeSe/SrTiO$_3$ using linearly polarized photons. This configuration enables unambiguous characterization of the valence electronic structure with a suppression of the spectral background. We consistently observe high-order replica bands derived from various Fe 3d bands, similar to those observed on bare SrTiO$_3$. The intensity of the replica bands is unexpectedly high and different between d_{xy} and d_{yz} bands. Our results provide new insights on the electronic structure of this high-temperature superconductor and the physical origin of the photoemission replica bands.

Corresponding authors:
Fengmiao Li & Ke Zou, Quantum Matter Institute, University of British Columbia

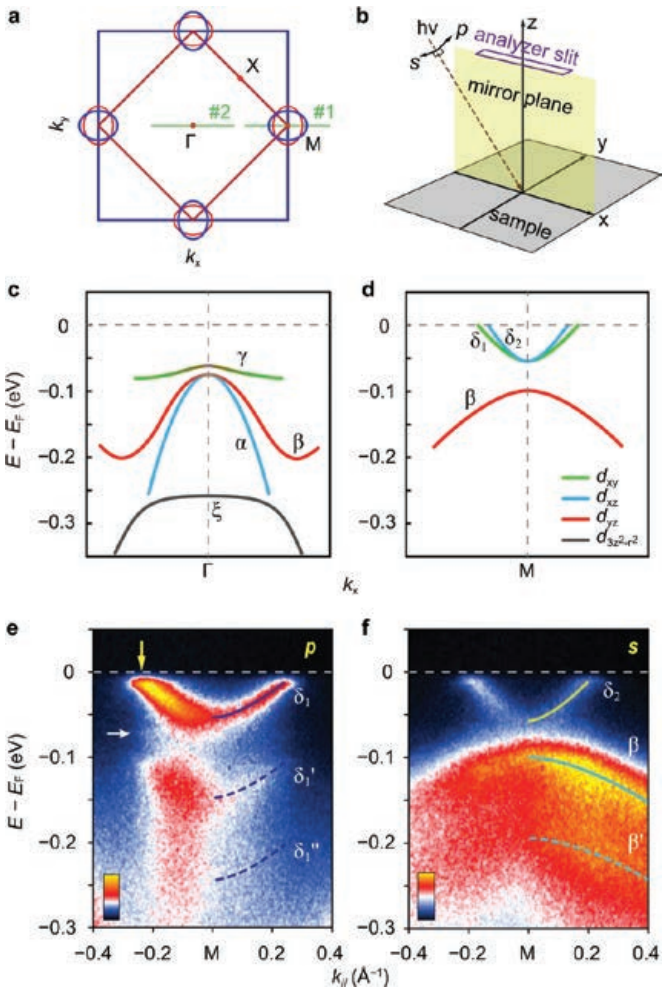

a The 2-Fe (red square) and 1-Fe (blue square) Brillouin zones (BZs), and the sketch of Fermi surfaces (blue and red ellipses) of monolayer FeSe/STO[26]. The green lines are the two cuts for the ARPES in Figs. 1–4. **b** Experimental geometry for linear polarization-dependent ARPES, where *p (s)* indicates the electric field of incident photon is parallel (perpendicular) to the emission plane defined by the analyzer slit. **c, d** Schematic diagram of band structure and orbital characters of monolayer FeSe/STO at Γ and M points, respectively, as determined by this ARPES study and in agreement with refs. 26,27. Here we use the same coordinate system as in **b** to define the *d* orbitals, i.e., x and y along the nearest Fe–Fe directions. Photoemission maps along cut #1, with 24 eV photons in p polarization **(e)** and s polarization **(f)**. The solid and dashed curves indicate principal and replica bands with ~90 meV intervals, respectively. The white arrow indicates the other set of replica band at ~60 meV below the principal band. The yellow arrow indicates the Fermi momentum of the δ1 band, where a superconducting gap is opened.

Multication perovskite 2D/3D interfaces form via progressive dimensional reduction

Proppe, Andrew H., Andrew Johnston, Sam Teale, Arup Mahata, Rafael Quintero-Bermudez, Eui Hyuk Jung, Luke Grater et al. "Multication perovskite 2D/3D interfaces form via progressive dimensional reduction." *Nature communications* 12, no. 1 (2021): 1-9.

In-situ GIWAXS measurements provided insight into the formation of the 2D/3D interface.

HXMA, BXDS

Many of the best-performing perovskite photovoltaic devices make use of 2D/3D interfaces, which improve efficiency and stability – but it remains unclear how the conversion of 3D-to-2D perovskite occurs and how these interfaces are assembled. Here, researchers use in situ Grazing-Incidence Wide-Angle X-Ray Scattering to resolve 2D/3D interface formation during spin-coating. We observe progressive dimensional reduction from 3D to n = 3 → 2 → 1 when we expose (MAPbBr3)0.05(FAPbI3)0.95 perovskites to vinylbenzylammonium ligand cations. Density functional theory simulations suggest ligands incorporate sequentially into the 3D lattice, driven by phenyl ring stacking, progressively bisecting the 3D perovskite into lower-dimensional fragments to form stable interfaces. Slowing the 2D/3D transformation with higher concentrations of antisolvent yields thinner 2D layers formed conformally onto 3D grains, improving carrier extraction and device efficiency (20% 3D-only, 22% 2D/3D). Controlling this progressive dimensional reduction has potential to further improve the performance of 2D/3D perovskite photovoltaics.

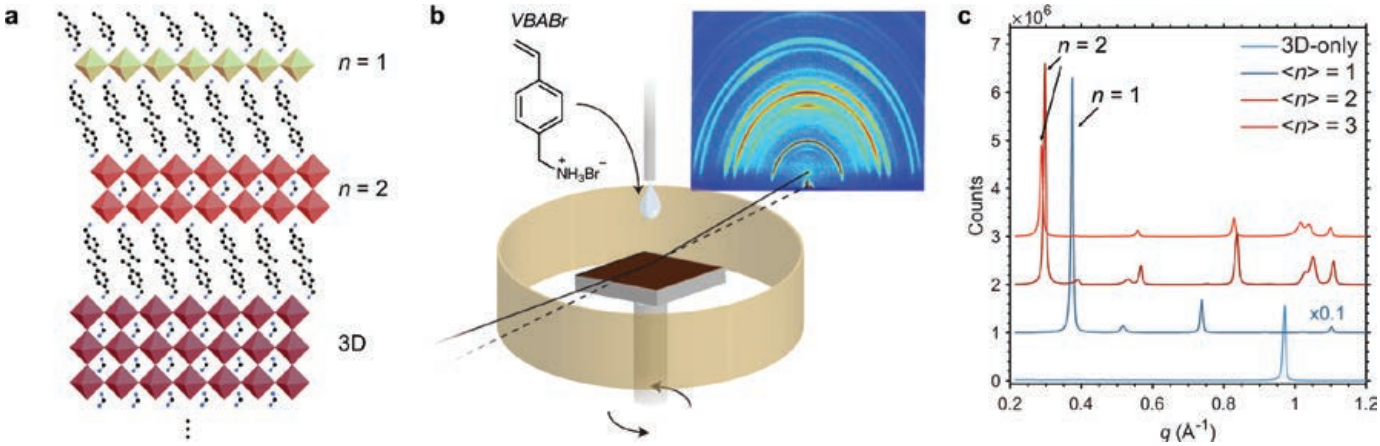

a Illustration of a 2D/3D interface for consecutive layers of 3D, $n = 2$, and $n = 1$ RDPs. **b** Schematic of the in situ GIWAXS experimental system used herein. A solvent dripper is positioned directly above the sample, which is mounted on a motorized pole with double-sided carbon tape. A Kapton shield encircles the spinning sample, prevented liquid from splashing onto the X-ray optics and the detector. VBABr: vinylbenzylammonium bromide. **c** Ex situ XRD patterns of RDP thin films with central n values of 1–3, and 3D control. Patterns are offset for clarity. Note: these are not 2D/3D perovskite thin films, and were synthesized from solutions containing precursor ratios corresponding to each n value.

Corresponding author:
Edward H. Sargent, University of Toronto

Vanishing nematic order beyond the pseudogap phase in overdoped cuprate superconductors

Gupta, Naman K., Christopher McMahon, Ronny Sutarto, Tianyu Shi, Rantong Gong, Haofei I. Wei, Kyle M. Shen et al. "Vanishing nematic order beyond the pseudogap phase in overdoped cuprate superconductors." *Proceedings of the National Academy of Sciences* 118, no. 34 (2021).

RXS and XAS measurements at the CLS were used to probe the electronic nematicity of Nd-LSCO.

REIXS

During the last decade, translational and rotational symmetry-breaking phases—density wave order and electronic nematicity—have been established as generic and distinct features of many correlated electron systems, including pnictide and cuprate superconductors. However, in cuprates, the relationship between these electronic symmetry-breaking phases and the enigmatic pseudogap phase remains unclear. Here, we employ resonant X-ray scattering in a cuprate high-temperature superconductor $La_{1.6-x}Nd_{0.4}Sr_xCuO_4$ (Nd-LSCO) to navigate the cuprate phase diagram, probing the relationship between electronic nematicity of the Cu 3*d* orbitals, charge order, and the pseudogap phase as a function of doping. We find evidence for a considerable decrease in electronic nematicity beyond the pseudogap phase, either by raising the temperature through the pseudogap onset temperature T^* or increasing doping through the pseudogap critical point, p^*. These results establish a clear link between electronic nematicity, the pseudogap, and its associated quantum criticality in overdoped cuprates. Our findings anticipate that electronic nematicity may play a larger role in understanding the cuprate phase diagram than previously recognized, possibly having a crucial role in the phenomenology of the pseudogap phase.

Corresponding author:
David D. Hawthorn, University of Waterloo

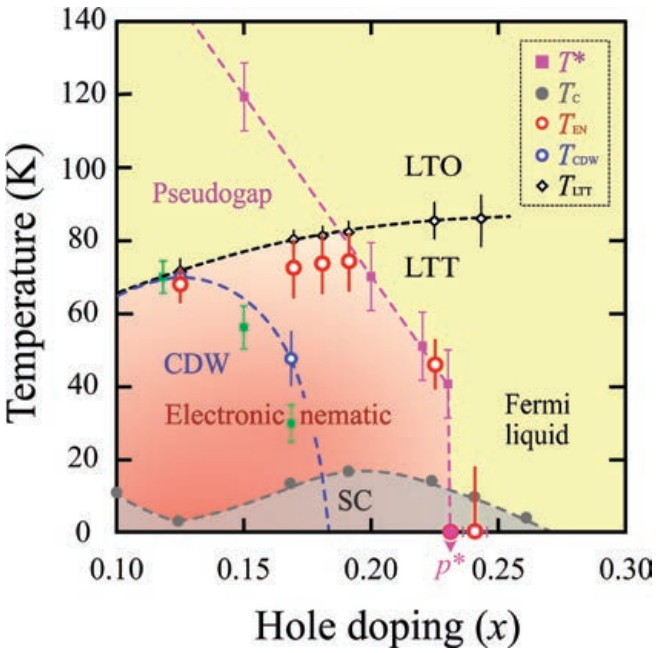

The doping–temperature phase diagram of Nd-LSCO. The structural phase transition from the LTO to LTT phase, T_{LTT} (black diamonds). The onset temperature of the CDW order, T_{CDW}, using resonant X-ray scattering measurement (blue circles) and recent Seebeck coefficient measurement (green squares). The red circles mark the onset of the electronic nematic order in the LTT phase, T_{EN}. The superconducting (SC) transition temperature, T_C (gray circles), has been reported in article ref. 34 on the same series of samples as used for the group's resonant X-ray scattering measurements. The existence of a QCP at p* = 0.23 has been identified in ref. 21. The pseudogap onset temperature, T* (purple squares), as a function of hole doping is measured via the onset of the upturn in electrical resistivity ρ(T) in ref. 23. The black, purple, blue, and gray dotted lines are guides to the eye.

An air-stable and Li-metal-compatible glass-ceramic electrolyte enabling high-performance all-solid-state Li metal batteries

Zhao, Feipeng, Sandamini H. Alahakoon, Keegan Adair, Shumin Zhang, Wei Xia, Weihan Li, Chuang Yu et al. "An air-stable and Li-metal-compatible glass-ceramic electrolyte enabling high-performance all-solid-state Li metal batteries." *Advanced Materials* 33, no. 8 (2021): 2006577.

Synchrotron measurements were used to assess the structure and the stability of the materials.

VESPERS, SXRMB

The development of all-solid-state Li metal batteries (ASSLMBs) has attracted significant attention due to their potential to maximize energy density and improved safety compared to the conventional liquid-electrolyte-based Li-ion batteries. However, it is very challenging to fabricate an ideal solid-state electrolyte (SSE) that simultaneously possesses high ionic conductivity, excellent air-stability, and good Li metal compatibility. Herein, a new glass-ceramic $Li_{3.2}P_{0.8}Sn_{0.2}S_4$ (gc-$Li_{3.2}P_{0.8}Sn_{0.2}S_4$) SSE is synthesized to satisfy the aforementioned requirements, enabling high-performance ASSLMBs at room temperature (RT). Compared with the conventional Li_3PS_4 glass-ceramics, the present gc-$Li_{3.2}P_{0.8}Sn_{0.2}S_4$ SSE with 12% amorphous content has an enlarged unit cell and a high Li+ ion concentration, which leads to 6.2-times higher ionic conductivity (1.21×10^{-3} S cm^{-1} at RT) after a simple cold sintering process. The $(P/Sn)S_4$ tetrahedron inside the gc-$Li_{3.2}P_{0.8}Sn_{0.2}S_4$ SSE is verified to show a strong resistance toward reaction with H_2O in 5%-humidity air, demonstrating excellent air-stability. Moreover, the gc-$Li_{3.2}P_{0.8}Sn_{0.2}S_4$ SSE triggers the formation of Li–Sn alloys at the Li/SSE interface, serving as an essential component to stabilize the interface and deliver good electrochemical performance in both symmetric and full cells. The discovery of this gc-$Li_{3.2}P_{0.8}Sn_{0.2}S_4$ superionic conductor enriches the choice of advanced SSEs and accelerates the commercialization of ASSLMBs.

Corresponding authors:
Yining Huang and Xueliang Sun, University of Western Ontario

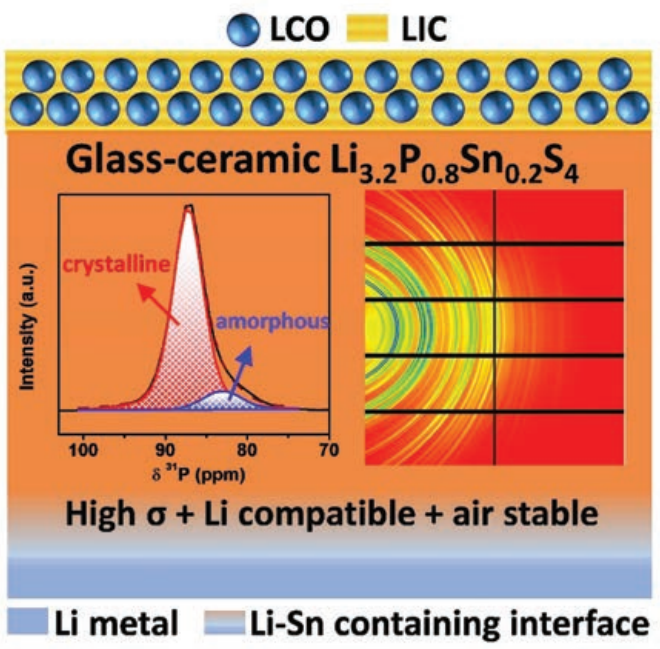

A new glass-ceramic $Li_{3.2}P_{0.8}Sn_{0.2}S_4$ solid-state electrolyte is developed for the first time to simultaneously possesse high ionic conductivity (10^{-3} S cm^{-1} level at room temperature), excellent air-stability (dry room operable), and good Li metal compatibility. This finding is highly expected to accelerate the commercialization of all-solid-state Li metal batteries.

AGRICULTURE

Tempering of cocoa butter and chocolate using minor lipidic components

Chen, Jay, Saeed M. Ghazani, Jarvis A. Stobbs, and Alejandro G. Marangoni. "Tempering of cocoa butter and chocolate using minor lipidic components." *Nature communications* 12, no. 1 (2021): 1-9.

Synchrotron micro-computed tomography was used to reveal the microstructures of chocolate, which helped to confirm that chocolate prepared with the addition of a minor lipidic component can simplify the tempering process in chocolate making.

BMIT

Chocolate manufacture includes a complex tempering procedure to direct the crystallization of cocoa butter towards the formation of fat crystal networks with specific polymorphism, nano- and microstructure, melting behavior, surface gloss and mechanical properties. Here we investigate the effects of adding various minor non-triglyceride lipidic components to refined cocoa butter and chocolate on their physical properties. They find that addition of saturated phosphatidylcholine and phosphatidylethanolamine to neutralized and bleached cocoa butter or molten and recrystallized commercial chocolate at 0.1% (w/w) levels, followed by rapid cooling to 20 °C in the absence of shear, accelerates crystallization, stabilizes the desirable Form V polymorph and induces the formation of chocolate with an optimal microstructure, surface gloss and mechanical strength. Final chocolate structure and properties are comparable to those of a commercial tempered chocolate. Minor lipidic component addition represents an effective way to engineer chocolate material properties at different length scales, thus simplifying the entire tempering process.

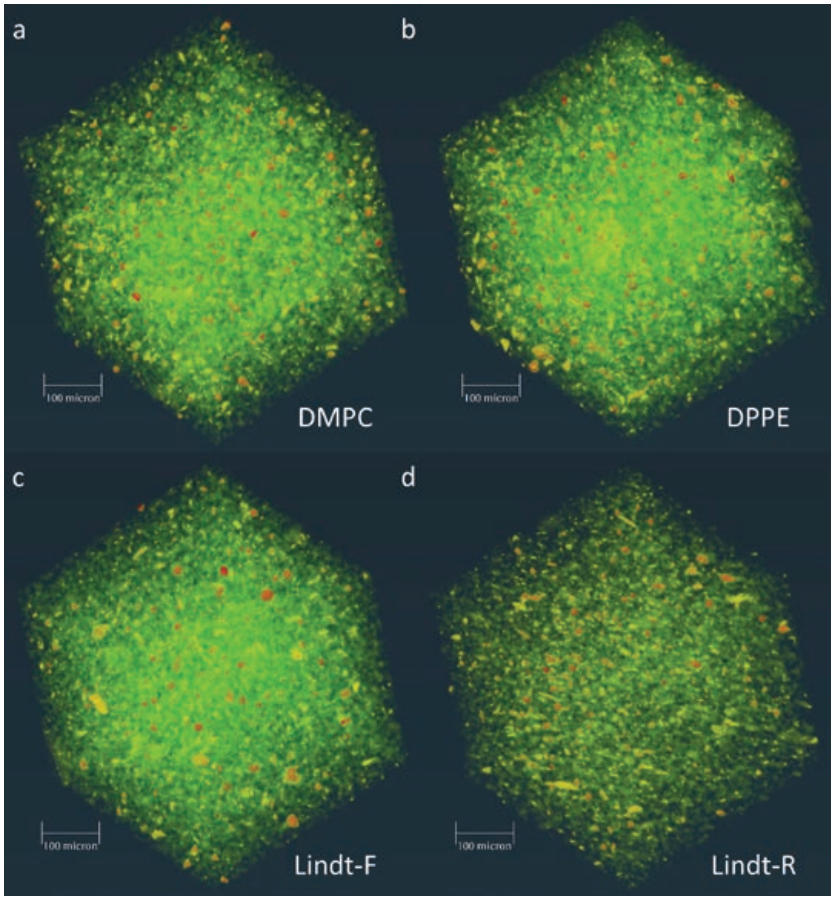

Samples included **a** molten and recrystallized commercial chocolate with added 0.1% (w/w) dimyristoylphosphatidylcholine (DMPC) **b** molten and recrystallized commercial chocolate with added 0.1% (w/w) dipalmitoylphosphatidylethanolamine (DPPE) **c** fresh commercial chocolate (Lindt-F) **d** molten and recrystallized commercial chocolate (Lindt-R)

Corresponding author:
Alejandro Marangoni, University of Guelph

Characterization of canola growth and in-vivo element fate in Canadian prairie under the interferences of tillage and residue treatment

Huang, Jing, Gordon Huang, Xiaying Xin, David Halstead, Katelyn Gaetz, Leila Benmerrouche, Yuwei Wu, Nan Wang, Yupeng Fu, and Jinbo Zhang. "Characterization of canola growth and in-vivo element fate in Canadian prairie under the interferences of tillage and residue treatment." *Journal of Cleaner Production* 320 (2021): 128707.

Synchrotron mid-infrared spectromicroscopy and X-ray fluorescence mapping techniques helped to understand the beneficial effects of post-harvest treatment on canola growth by revealing the organic compounds and elemental distributions in canola seedlings' roots and leaves.

Mid-IR, VESPERS

Canola is one of the main crops produced in Canadian prairies. It is important to provide an effective approach for improving the growth and yield of canola. The effects of tillage and residue management on the growth of canola have been analyzed in this study through evaluating physicochemical features of canola plants under the interferences of tillage and residue treatment. Synchrotron-based FTIR and x-ray fluorescence mapping technologies are used to examine the variation of different organisms and important metal elements in the canola plants at different stages. The effects of interactions among tillage and residue treatments on the growth state of canola plants at different growing stages are various. Content of lipid and protein in mature root are improved with the application of harrow treatment. The application of tillage management is beneficial for the content of some elements, while negatively influences the content of other metal elements.

Corresponding author:
Gordon Huang, Institute for Energy, University of Regina

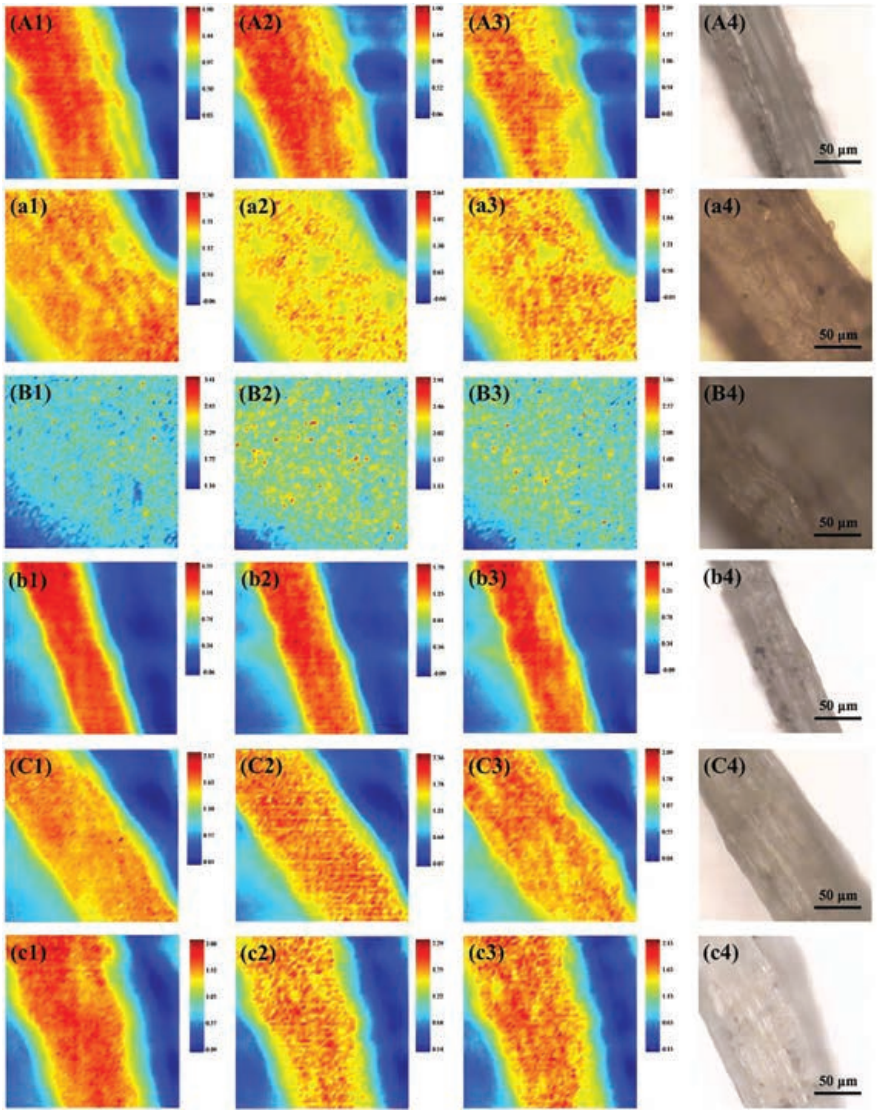

FTIR images of the distribution of lignin at 1250 cm^{-1} (column 1), protein at 1650 cm^{-1} (column 2) and lipid at 1741 cm^{-1} (column 3) on root surfaces of seedlings at 36 days after seeding (A_4, B_4, C_4) and mature plants at 67 days after seeding (a_4, b_4, c_4). Samples in (A_4) and (a_4) come from 2 to 1 part of trial field; Samples in (B_4) and (b_4) come from 2 to 2 part of trial field; Samples in (C_4) and (c_4) come from 2 to 3 part of trial field. In the colored bar, dark blue represents lowest content and dark red represents highest content.

Differential transformation mechanisms of exotic Cr(VI) in agricultural soils with contrasting physio-chemical and biological properties

Wang, Yihao, Jianjun Yang, Hui Han, Yongfeng Hu, Jian Wang, Ya Feng, Baoshan Yu, Xing Xia, and Aminu Darma. "Differential transformation mechanisms of exotic Cr (VI) in agricultural soils with contrasting physio-chemical and biological properties." *Chemosphere* 279 (2021): 130546.

Soft and hard X-ray spectroscopy combined with micro- and nano-scale microscopy helped to reveal the interactions of carboxylic carbon and Mn/Fe oxides in the reduction transformation of Cr(VI). This transformation is stronger in Ultisol soil than in Fluvo-aquic soil.

SXRMB, SM, VESPERS

The transformation mechanisms of Cr(VI) in agricultural soils at the molecular level remain largely unknown due to the multitude of abiotic and biotic factors. In this study, the different speciation and distribution of Cr in two types of agricultural soil (Ultisol and Fluvo-aquic soils) after two weeks of aging was investigated using synchrotron-based X-ray absorption near-edge structure (XANES) spectroscopy, microfocused X-ray fluorescence (μ-XRF) and X-ray transmission microscopy (STXM). The microbial community structure of the two soils was also analyzed via high-throughput sequencing of 16S rRNA. Cr(VI) availability was relatively lower in the Ultisol than in the Fluvo-aquic soil after aging. Cr K-edge bulk XANES and STXM analysis indicated that Cr(VI) was reduced to Cr(III) in both soils. μ-XRF analysis and STXM analysis indicated the predominant association of Cr with Mn/Fe oxides and/or organo-Fe oxides in both soils. Additionally, STXM-coupled imaging and multiedge XANES analyses demonstrated that carboxylic groups were involved in the reduction of Cr(VI) and subsequent retention of Cr(III). 16S rRNA analysis showed considerably different bacterial communities across the two soils. Redundancy analysis (RDA) suggested that soil properties, including the total carbon content, Fe oxide component and pH, were closely linked to Cr(VI)-reducing functional bacteria in the Ultisol, including chromium-reducing bacteria (CRB) (e.g., Bacillus sp.) and dissimilatory iron-reducing (DIRB) (e.g., Shewanella sp.) bacteria, which possibly promoted Cr(VI) reduction. These findings shed light on the molecular-level transformation mechanisms of Cr(VI) in agricultural soils, which facilitates the effective management of Cr-enriched farmland.

Corresponding author:
Jianjun Yang, Chinese Academy of Agricultural Sciences

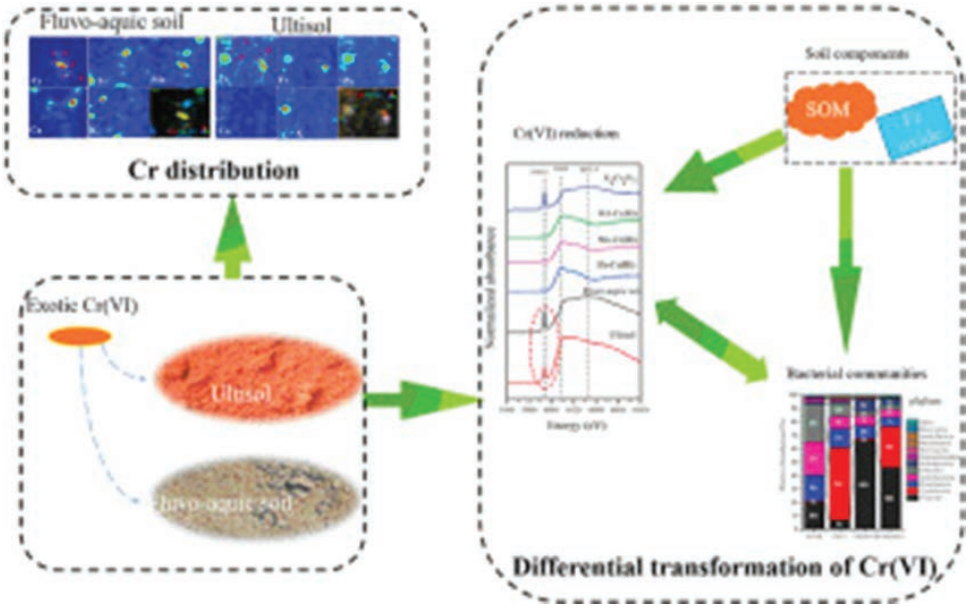

The reduction in exotic Cr(VI) was faster in the Ultisol soil than in the Fluvo-aquic soil.

Tissue specific changes in elements and organic compounds of alfalfa (Medicago sativa L.) cultivars differing in salt tolerance under salt stress

Bhattarai, Surendra, Na Liu, Chithra Karunakaran, Karen K. Tanino, Yong-Bi Fu, Bruce Coulman, Tom Warkentin, and Bill Biligetu. "Tissue specific changes in elements and organic compounds of alfalfa (Medicago sativa L.) cultivars differing in salt tolerance under salt stress." *Journal of Plant Physiology* 264 (2021): 153485.

X-ray fluorescence spectroscopy and mapping combined with mid-infrared spectroscopy techniques were used to understand the physiological changes of salt tolerant and susceptible alfalfa cultivars by revealing the accumulation of organic compounds and elemental distributions in different tissues of alfalfa plants.

IDEAS, Mid-IR,VESPERS

Soil salinity is a global concern and often the primary factor contributing to land degradation, limiting crop growth and production. Alfalfa (*Medicago sativa L.*) is a low input high value forage legume with a wide adaptation. Examining the tissue-specific responses to salt stress will be important to understanding physiological changes of alfalfa. The responses of two alfalfa cultivars (salt tolerant 'Halo', salt intolerant 'Vernal') were studied for 12 weeks in five gradients of salt stress in a sand based hydroponic system in the greenhouse. The accumulation and localization of elements and organic compounds in different tissues of alfalfa under salt stress were evaluated using synchrotron beamlines. The pattern of chlorine accumulation for 'Halo' was: root > stem ~ leaf at 8 dSm^{-1}, and root ~ leaf > stem at 12 dSm^{-1}, potentially preventing toxic ion accumulation in leaf tissues. In contrast, for 'Vernal', it was leaf > stem ~ root at 8 dSm^{-1} and leaf > root ~ stem at 12 dSm^{-1}. The distribution of chlorine in 'Halo' was relatively uniform in the leaf surface and vascular bundles of the stem. Amide concentration in the leaf and stem tissues was greater for 'Halo' than 'Vernal' at all salt gradients. This study determined that low ion accumulation in the shoot was a common strategy in salt tolerant alfalfa up to 8 dSm^{-1} of salt stress, which was then replaced by shoot tissue tolerance at 12 dSm^{-1}.

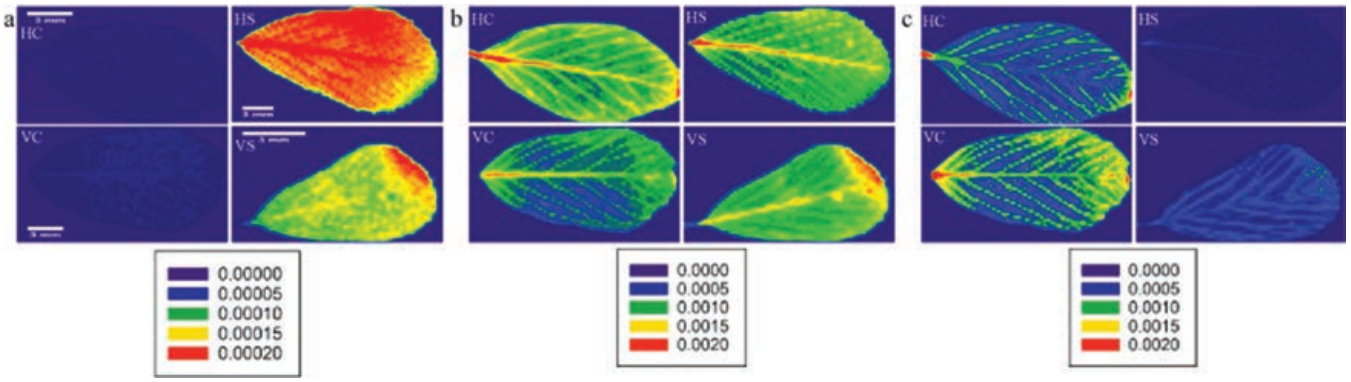

Distribution of chlorine (a), potassium (b), calcium (c) ions in leaf tissues of two alfalfa cultivars as revealed by synchrotron based XRF spectroscopy at IDEAS beamline in the Canadian Light Source. (**HC.** Halo control at 0 dS m^{-1} **HS.** Halo stressed at 12 dS m^{-1} EC **VC.** Vernal control at o dS m^{-1} VS. Vernal stressed at 12 dS m^{-1} EC; Index bar represents integrated absorption peak area).

Corresponding author:
Bill Biligetu, University of Saskatchewan

Bibenzyl synthesis in *Cannabis sativa* L.

Boddington, Kelly F., Eric Soubeyrand, Kristen Van Gelder, José A. Casaretto, Colby Perrin, Taylor JB Forrester, Cameron Parry et al. "Bibenzyl synthesis in Cannabis sativa L." *The Plant Journal* 109, no. 3 (2022): 693-707.

Macromolecular crystallography was used to characterize specialized metabolites synthesized from Cannabis known as the bibenzyls.

CMCF

This study focuses on the biosynthesis of a suite of specialized metabolites from Cannabis that are known as the 'bibenzyls'. In planta, bibenzyls accumulate in response to fungal infection and various other biotic stressors; however, it is their widely recognized anti-inflammatory properties in various animal cell models that have garnered recent therapeutic interest. In this work, it is proposed that these compounds are synthesized via a branch point from the core phenylpropanoid pathway in Cannabis, in a three-step sequence. First, various hydroxycinnamic acids are esterified to acyl-coenzyme A (CoA) by a member of the 4-coumarate-CoA ligase family (Cs4CL4). Next, these CoA esters are reduced by two double-bond reductases (CsDBR2 and CsDBR3) that form their corresponding dihydro-CoA derivatives from preferred substrates. Finally, the bibenzyl backbone is completed by a polyketide synthase that specifically condenses malonyl-CoA with these dihydro-hydroxycinnamoyl-CoA derivatives to form two bibenzyl scaffolds: dihydropiceatannol and dihydroresveratrol. Structural determination of this bibenzyl synthase enzyme (CsBBS2) indicates that a narrowing of the hydrophobic pocket surrounding the active site evolved to sterically favor the non-canonical and more flexible dihydro-hydroxycinnamoyl-CoA substrates in comparison with their oxidized relatives. Accordingly, three point mutations that were introduced into CsBBS2 proved sufficient to restore some enzymatic activity with an oxidized substrate, in vitro. Together, the identification of this set of Cannabis enzymes provides a valuable contribution to the growing parts prospecting inventory that supports the rational metabolic engineering of natural product therapeutics.

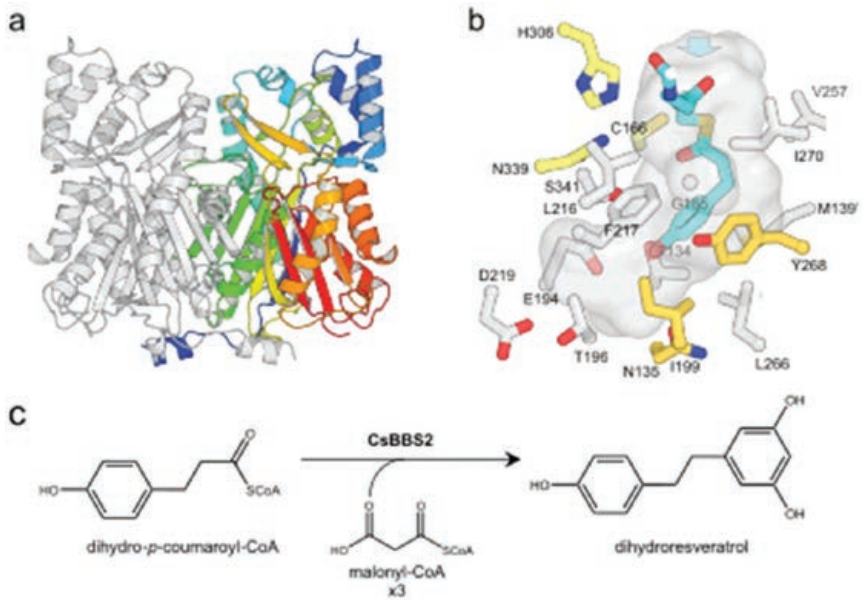

Structure of *Cs*BBS2 and schematic of its catalyzed reaction. (a) Structure of the dimer. One chain is shown in white, the second in a gradient from blue (N-terminus) to red (C-terminus). (b) Model of the *Cs*BBS2 + dihydro-p-coumaroyl-CoA complex. Note that the saturated side chain needs to twist to fit in the constricted binding site. (c) The reaction catalyzed by *Cs*BBS2 in the proposed biosynthetic pathway for bibenzyls in Cannabis sativa. This work was sponsored by Canurta.

Corresponding author:
Tariq A. Akhtar, University of Guelph

ENVIRONMENT

Removal of arsenic and metals from groundwater impacted by mine waste using zero-valent iron and organic carbon

Angai, Joanne U., Carol J. Ptacek, Eva Pakostova, Jeff G. Bain, Brent R. Verbuyst, and David W. Blowes. "Removal of arsenic and metals from groundwater impacted by mine waste using zero-valent iron and organic carbon: Laboratory column experiments." *Journal of Hazardous Materials* 424 (2022): 127295.

SXRMB, CLS@APS

Acid mine drainage and the associated contaminants, including As and metals, are ongoing environmental issues. Passive remediation technologies have the potential to remove As from mine waste effluents. A series of laboratory column experiments was conducted to evaluate the effectiveness of varying mixtures of organic carbon (OC), zero-valent iron (ZVI), and limestone for the treatment of As, metals, SO_4^{2-}, and acidity in groundwater from an abandoned gold mine. The onset of bacterially-mediated SO_4^{2-} reduction was indicated by a decrease in Eh, a decline in aqueous SO_4^{2-} concentrations coupled with enrichment of $\delta^{34}S$, and the presence of sulfate-reducing bacteria and H_2S. Removal of As was observed within the first 3 cm of reactive material, to values below 10 µg L^{-1}, representing >99.9% removal. An increase in pH from 3.5 to circumneutral values and removal of metals including Al, Cu, and Zn was also observed. Synchrotron results suggest As was removed through precipitation of As-crystalline phases such as realgar and orpiment, or through adsorption as As(V) on ferrihydrite. The results indicate the potential for a mixture of OC and ZVI to remove As from acidic, mine-impacted water.

uXRF mapping above the As K-edge on column secondary precipitates showed localized spots of arsenic rather than homogeneously distributed arsenic. As K-edge uXANES identified the presence of multiple As oxidation states with As(V) being predominant in in Fe-S secondary precipitates.

Sulfur uXRF targeted regions of interest identified in the optical and SEM images. S K-edge uXANES measurements identified that the majority of sulfur was present in reduced species.

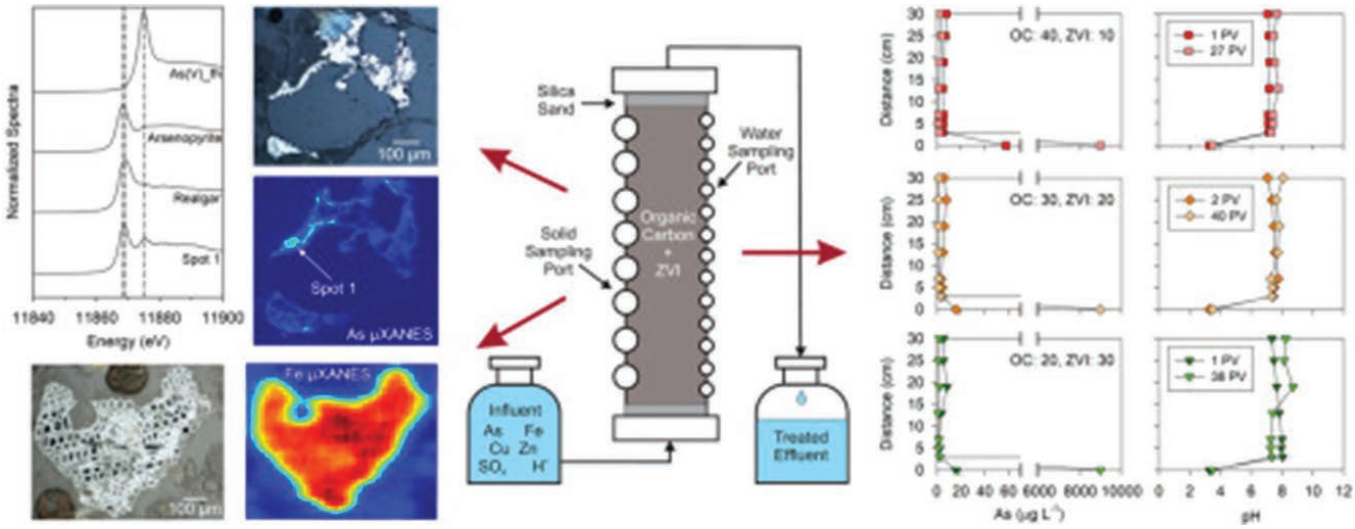

Corresponding author:
Carol Ptacek, University of Waterloo

Organic stabilization of extracellular elemental sulfur in a Sulfurovum-rich biofilm: A new role for extracellular polymeric substances

Cron, Brandi, Jennifer L. Macalady, and Julie Cosmidis. "Organic stabilization of extracellular elemental sulfur in a Sulfurovum-rich biofilm: A new role for extracellular polymeric substances." *Frontiers in Microbiology* 12 (2021).

STXM was used to identify sulfur(0) and associated organic material in biofilms produced by sulfur-oxidizing bacteria.

SM

This work characterizes the role of extracellular polymeric substance (EPS) in the formation and preservation of elemental sulfur biominerals produced by sulfur-oxidizing bacteria. The authors characterized elemental sulfur particles produced within a Sulfurovum-rich biofilm in the Frasassi Cave System (Italy). The particles adopt spherical and bipyramidal morphologies, and display both stable (α-S8) and metastable (β-S8) crystal structures. Elemental sulfur is embedded within a dense matrix of EPS, and the particles are surrounded by organic envelopes rich in amide and carboxylic groups. Organic encapsulation and the presence of metastable crystal structures are consistent with elemental sulfur organomineralization, i.e., the formation and stabilization of elemental sulfur in the presence of organics, a mechanism that has previously been observed in laboratory studies. This research provides new evidence for the important role of microbial EPS in mineral formation in the environment. The authors hypothesize that the extracellular organics are used by sulfur-oxidizing bacteria for the stabilization of elemental sulfur minerals outside of the cell wall as a store of chemical energy. The stabilization of energy sources (in the form of a solid electron acceptor) in biofilms is a potential new role for microbial EPS that requires further investigation.

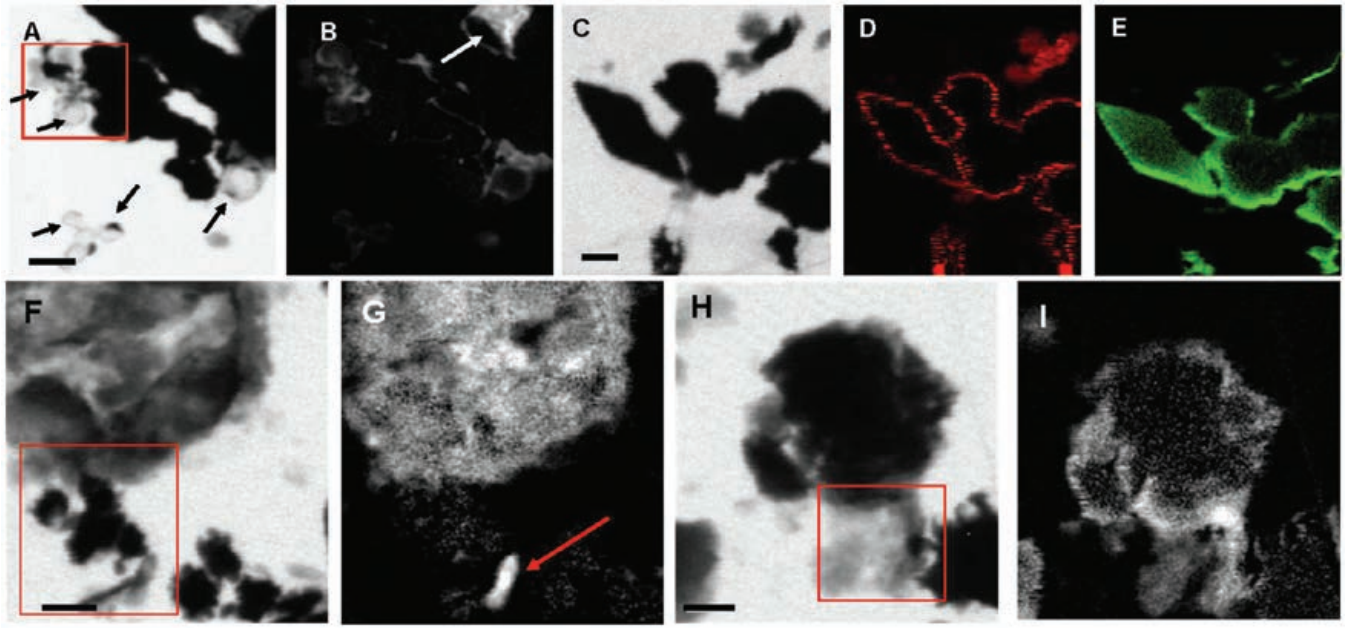

Corresponding author:
Julie Cosmidis, The Pennsylvania State University, University of Oxford

STXM images and maps of Sulfurovum-dominated streamer biofilm. **(A–B)** Sample PC1647. **(A)** image collected at 288.1 eV. Black areas are S(0) particles. The empty spherical envelopes of vaporized S(0) globules are visible (black arrows). **(B)** Corresponding carbon map. The white arrow shows the carbon enveloped around a partially vaporized S(0) particle (a chain of S(0) bipyramids). (C–I) Sample PC1718. **(C)** Image collected at 288.2 eV. **(D)** Carbon map. **(E)** Sulfur map. **(F)** Image collected at 300 eV. **(G)** Carbon map. The arrow points to a rod-shaped microbial cell. **(H–I)** Image collected at 300 eV. **(I)** Carbon map. The boxes in **(A)**, **(F)**, and **(H)** and the arrow in **(B)** indicate where XANES analyses shown in Figure 8 were performed. Scale bars: 1 µm.

Impact of dry intrusion events on the composition and mixing state of particles during the winter Aerosol and Cloud Experiment in the Eastern North Atlantic

Tomlin, Jay M., Kevin A. Jankowski, Daniel P. Veghte, Swarup China, Peiwen Wang, Matthew Fraund, Johannes Weis et al. "Impact of dry intrusion events on the composition and mixing state of particles during the winter Aerosol and Cloud Experiment in the Eastern North Atlantic (ACE-ENA)." *Atmospheric Chemistry and Physics* 21, no. 24 (2021): 18123-18146.

STXM and carbon K-edge NEXAFS/XANES was used to examine carbonaceous particles from clouds to assess the long range transport of continental emissions.

SM

Long-range transport of continental emissions has a far-reaching influence over remote regions, resulting in substantial change in the size, morphology, and composition of the local aerosol population and cloud condensation nuclei (CCN) budget. Here, the authors investigate the physicochemical properties of atmospheric particles collected on board a research aircraft flown over the Azores during the winter 2018 Aerosol and Cloud Experiment in the Eastern North Atlantic (ACE-ENA) campaign. Particles were collected within the marine boundary layer (MBL) and free troposphere (FT) after long-range atmospheric transport episodes facilitated by dry intrusion (DI) events. Chemical and physical properties of individual particles were investigated using complementary capabilities of computer-controlled scanning electron microscopy and x-ray spectromicroscopy to probe particle external and internal mixing state characteristics. Furthermore, real-time measurements of aerosol size distribution, cloud condensation nuclei (CCN) concentration, and back-trajectory calculations were utilized to help bring into context the findings from offline spectromicroscopy analysis. While carbonaceous particles were found to be the dominant particle type in the region, changes in the percent contribution of organics across the particle population (i.e., external mixing) shifted from 68% to 43% in the MBL and from 92% to 46% in FT samples during DI events. This change in carbonaceous contribution is counterbalanced by the increase in inorganics from 32% to 57% in the MBL and 8% to 55% in FT. The quantification of the organic volume fraction (OVF) of individual particles derived from X-ray spectromicroscopy, which relates to the multi-component internal composition of individual particles, showed a factor of 2.06 ± 0.16 and 1.11 ± 0.04 increase in the MBL and FT, respectively, among DI samples. The authors show that supplying particle OVF into the κ-Köhler equation can be used as a good approximation of field-measured in situ CCN concentrations. We also report changes in the κ values in the MBL from $\kappa_{MBL,\ non\text{-}DI}$=0.48 to $\kappa_{MBL,\ DI}$=0.41, while changes in the FT result in $\kappa_{FT,\ non\text{-}DI}$=0.36 to $\kappa_{FT,\ DI}$=0.33, which is consistent with enhancements in OVF followed by the DI episodes. The observations suggest that entrainment of particles from long-range continental sources alters the mixing state population and CCN properties of aerosol in the region. The work presented here provides field observation data that can inform atmospheric models that simulate sources and particle composition in the eastern North Atlantic.

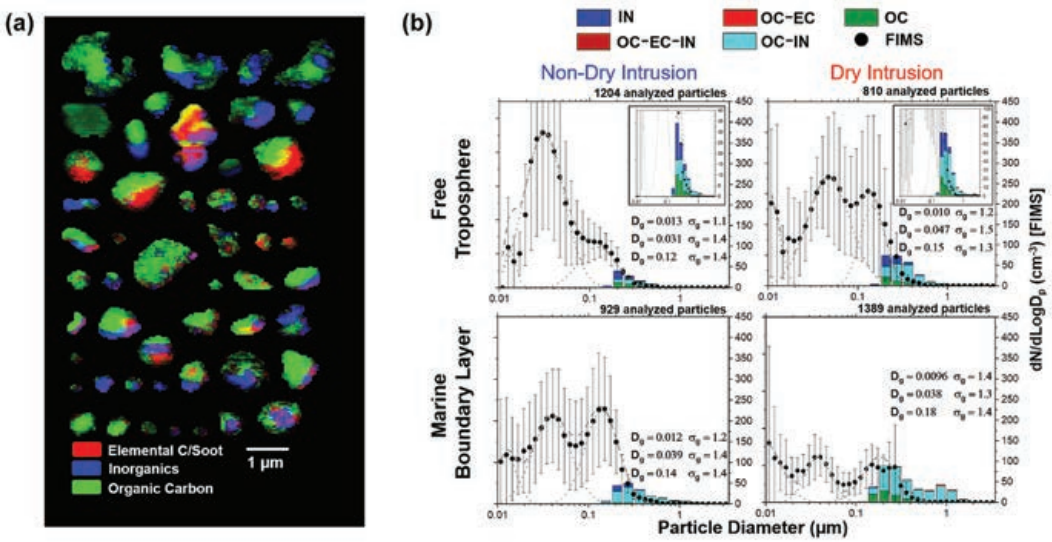

(a) Carbon speciation map of a subset of particles acquired by STXM from DI periods. Note that components can overlap, and each pixel can contain a different combination of the individual components: EC + IN constituents as purple; OC + EC as yellow; OC + IN as cyan. (b) Size distribution of analyzed particles identified via STXM/NEXAFS shown as an 8-bin per decade histogram to compare particle multi-component internal mixing state between atmospheric transport events. FIMS particle size distribution is overlaid to facilitate a visual comparison from the same atmospheric episodes. Abbreviations are as follows: IN – inorganics, OC – organic carbon (i.e., COOH), EC – elemental carbon (i.e., sp2 C=C carbon).

Corresponding author:
Alexander Laskin, Purdue University

Role of ester sulfate and organic disulfide inmercury methylation in peatland soils

Pierce, Caroline E., Olha S. Furman, Sarah L. Nicholas, Jill Coleman Wasik, Caitlin M. Gionfriddo, Ann M. Wymore, Stephen D. Sebestyen et al. "Role of ester sulfate and organic disulfide inmercury methylation in peatland soils." *Environmental science & technology* (2022).

Sulfur K-edge XANES was used to investigate the role of organic sulfur species in Hg methylation in peatland soils. The impacts of climate change may lead to greater toxic methylmercury (MeHg) generation.

SXRMB

The authors examined the composition and spatial correlation of sulfur and mercury pools in peatland soil profiles by measuring sulfur speciation by 1s X-ray absorption near-edge structure spectrocopy and mercury concentrations by cold vapor atomic fluorescence spectroscopy. Also investigated were the methylation/demethylation rate constants and the presence of *hgc*AB genes with depth. Methylmercury (MeHg) concentration and organic disulfide were spatially correlated and had a significant positive correlation ($p < 0.05$). This finding is consistent with these species being products of dissimilatory sulfate reduction. Conversely, a significant negative correlation between organic monosulfides and MeHg was observed, which is consistent with a reduction in Hg(II) bioavailability via complexation reactions. Finally, a significant positive correlation between ester sulfate and instantaneous methylation rate constants was observed, which is consistent with ester sulfate being a substrate for mercury methylation via dissimilatory sulfate reduction. The team's findings point to the importance of organic sulfur species in mercury methylation processes, as substrates and products, as well as potential inhibitors of Hg(II) bioavailability. For a peatland system with sub-μmol L^{-1} porewater concentrations of sulfate and hydrogen sulfide, our findings indicate that the solid-phase sulfur pools, which have a much larger sulfur concentration range, may be accessible to microbial activity or exchanging with the porewater.

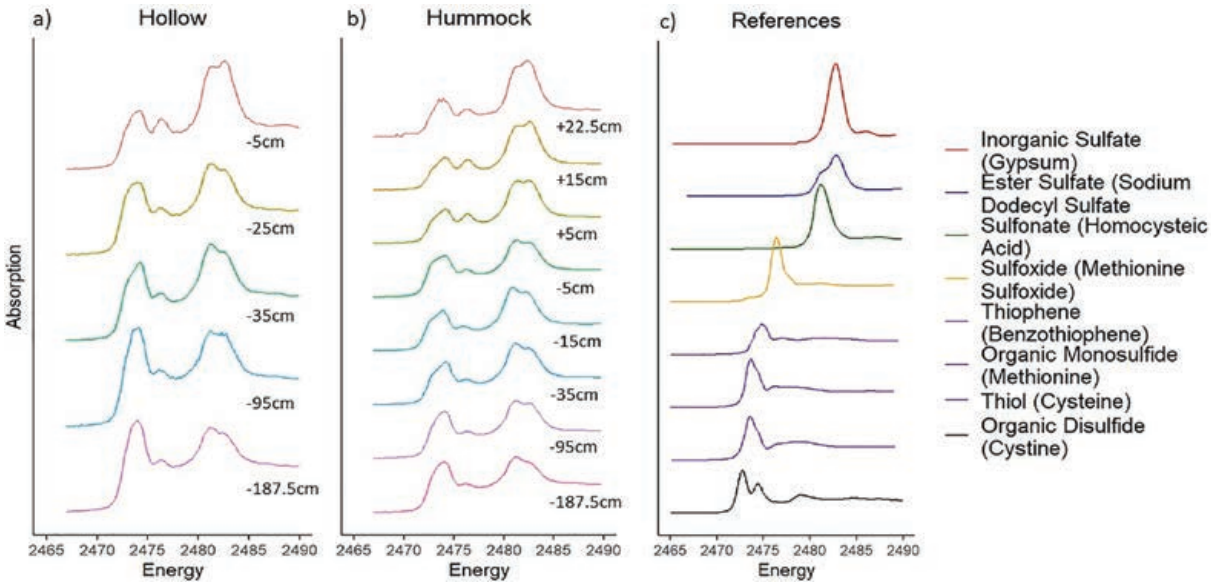

Sulfur 1s XANES spectra from hollow **(a)**, hummock **(b)**, and references that were detected in the samples **(c)**. References are color-coded according to bin type–thiophenes, organic monosulfides, and thiols are binned together.

Almost all sulfur detected in the S1 bog peat with sulfur XANES spectroscopy was in an organic form. Reduced organic sulfur species (having valence states of ≤+1) comprised 42–72% of total sulfur over the full depth profile (+20 to −200 cm) which is consistent with past studies of boreal peatlands. The oxidized sulfur species (valence states ≥ +2) decreased with depth ($p < 0.05$), while reduced sulfur species (valence states ≤ +1) increased with depth ($p < 0.05$). The lowest percentages of reduced sulfur species were observed in surface samples from both hollows (−5 cm, 48% on average) and hummocks (+15 cm, 42% on average).

Corresponding author:
Brandy Toner, University of Minnesota

Persistence of uranium in old and cold subpermafrost groundwater indicated by linking ^{234}U-^{235}U-^{238}U, groundwater ages, and hydrogeochemistry

Skierszkan, Elliott K., John W. Dockrey, Jordi Helsen, Laura-Lee Findlater, Clément P. Bataille, Ghislain de Laplante, Joyce M. McBeth, K. Ulrich Mayer, and Roger D. Beckie. "Persistence of uranium in old and cold subpermafrost groundwater indicated by linking 234U-235U-238U, groundwater ages, and hydrogeochemistry." *ACS Earth and Space Chemistry* 5, no. 12 (2021): 3474-3487.

uXRF mapping and U L3-edge XANES were used to assess the geochemical controls on uranium mobility at a prospective subarctic gold deposit in the Yukon.

VESPERS

Uranium (U) contamination in groundwater from geogenic sources affects water quality globally. Here, we use a multifaceted isotopic and geochemical approach to elucidate U sources and controls on geogenic U release to groundwater and surface water at a prospective subarctic gold deposit in Yukon, that is characterized by permafrost, fractured bedrock, and cold (<2 °C) groundwater. X-ray absorption spectroscopy, sequential extractions, and micro X-ray fluorescence mapping show extensive subsurface oxidation and solid-phase U present in its hexavalent and mobile form. Limited $^{238}U/^{235}U$ isotope fractionation and predominance of U(VI) in rocks suggest U(VI) sorption–desorption is the main driver of U mobilization. Groundwater U concentrations are appreciable (median 38 µg/L, range 1.2–535 µg/L) and are explained by high-alkalinity, Ca-rich groundwater produced from oxidative weathering of sulfide and carbonate-mineralized structures around the deposit. Minor $^{238}U/^{235}U$ isotope fractionation in groundwater indicates that limited U(VI) reduction occurs beneath permafrost despite groundwater redox conditions below Fe(III) and S(VI) reduction, and groundwater ages inferred from ^{3}H and ^{14}C to be on the order of thousands of years. The complexation of U as uranyl–calcium–carbonate complexes and the resilience of these complexes to U(VI) reduction contributes to high U(VI) mobility under cold groundwater conditions. This study provides insight into processes and time scales of U transport in subarctic groundwater at a pivotal time when hydrogeochemical changes may be anticipated in cold regions worldwide due to permafrost degradation.

Corresponding author:
Elliott Skierszkan, University of Saskatchewan

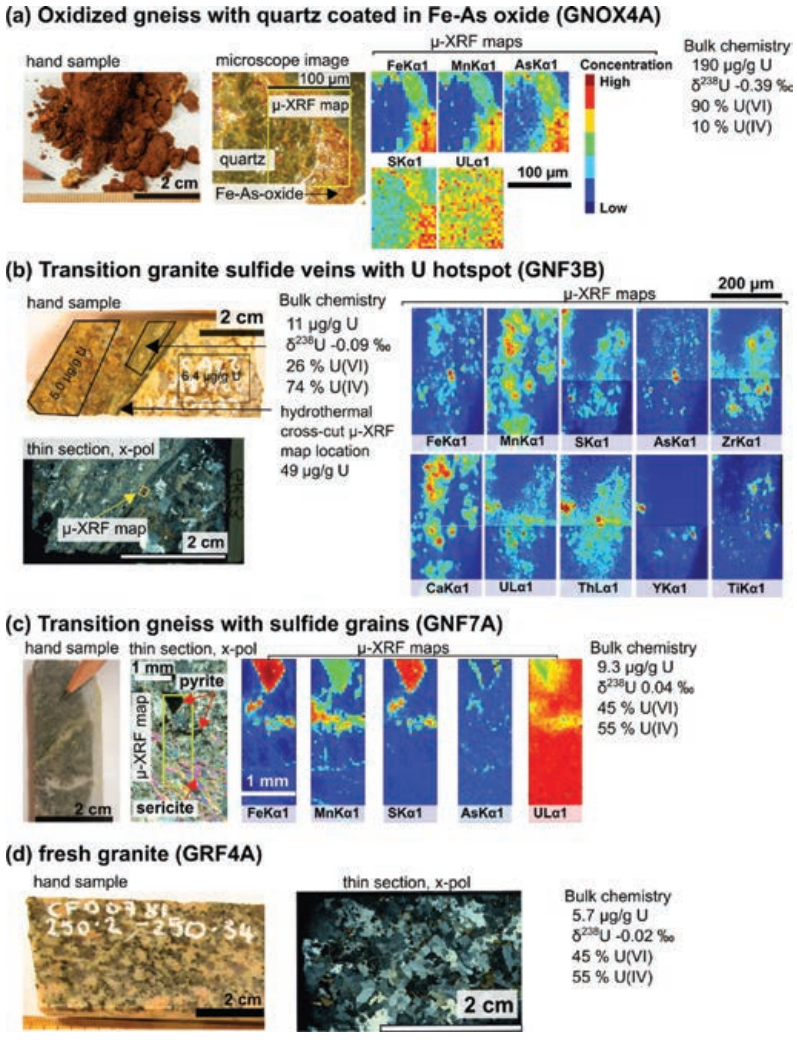

Selection of rock-sample photos from each weathering facies that includes photos of hand-samples, thin-sections, µ-XRF maps of key elements, and bulk geochemical and U isotopic composition. (a) Intensely oxidized gneiss sample with high U abundance and disseminated sorbed U(VI). (b) Transition granite sample cross-cut by a U-rich vein with a majority of U(IV) colocated with Th and Y and spatially distinct from Fe–Mn–As-sulfides. (c) Transition gneiss sample, with hydrothermal alteration and pyrite and a mixture of U(VI) and U(IV). (d) Fresh granite sample with a mixture of U(VI) and U(IV).

HEALTH

Improved SARS-CoV-2 Mpro inhibitors based on feline antiviral drug GC376

Vuong, Wayne, Conrad Fischer, Muhammad Bashir Khan, Marco J. van Belkum, Tess Lamer, Kurtis D. Willoughby, Jimmy Lu et al. "Improved SARS-CoV-2 Mpro inhibitors based on feline antiviral drug GC376: structural enhancements, increased solubility, and micellar studies." *European journal of medicinal chemistry* 222 (2021): 113584.

Macromolecular crystallography was used to solve the crystal structure of the virus that causes COVID-19's main protease with a nanomolar inhibitor.

CMCF

Replication of SARS-CoV-2, the coronavirus causing COVID-19, requires a main protease (M^{pro}) to cleave viral proteins. Consequently, M^{pro} is a target for antiviral agents. The research group and others previously demonstrated that GC376, a bisulfite prodrug with efficacy as an anti-coronaviral agent in animals, is an effective inhibitor of M^{pro} in SARS-CoV-2. Here, we report structure-activity studies of improved GC376 derivatives with nanomolar affinities and therapeutic indices >200. Crystallographic structures of inhibitor-M^{pro} complexes reveal that an alternative binding pocket in M^{pro}, S4, accommodates the P3 position. Alternative binding is induced by polar P3 groups or a nearby methyl. NMR and solubility studies with GC376 show that it exists as a mixture of stereoisomers and forms colloids in aqueous media at higher concentrations, a property not previously reported. Replacement of its Na^+ counter ion with choline greatly increases solubility. The physical, biochemical, crystallographic, and cellular data reveal new avenues for Mpro inhibitor design.

Corresponding author:
John Vederas, University of Alberta

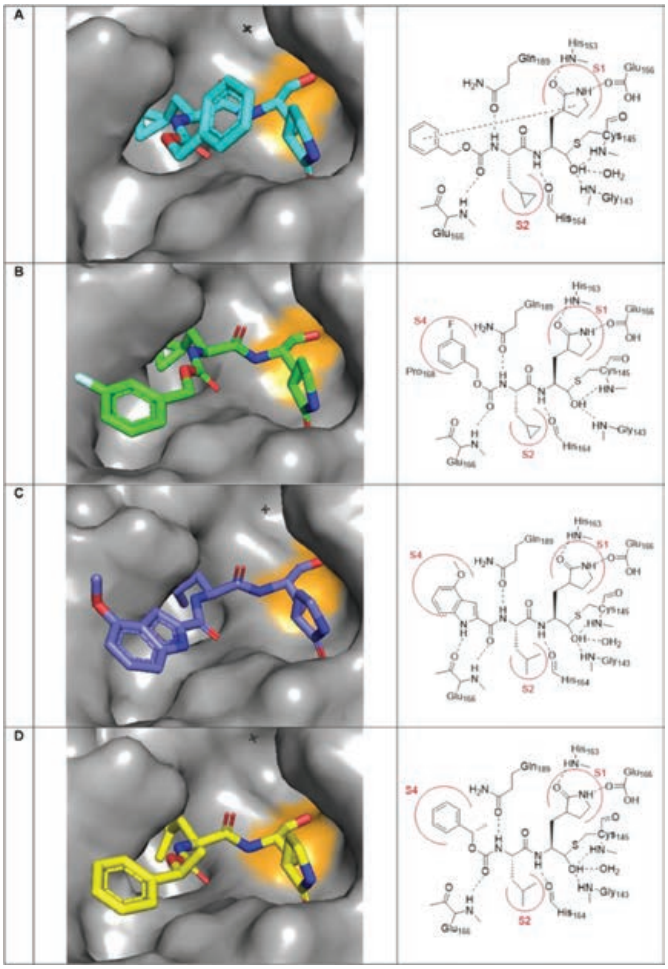

Crystal structures and schematic depictions of inhibitors bound to SARS-CoV-2 M^{pro}. (A) 1a bound to the active site of SARS-CoV-2 M^{pro}. The benzyl ring at the P3 position of the inhibitor can be seen interacting with the S3 surface depression, similarly to the binding mode of GC373 (PDB 7LCS). **(B) 1i** bound to the active site of SARS-CoV-2 M^{pro}. The presence of a fluorine atom at the 3-position on the benzyl ring directs the aromatic moiety into the S4 binding pocket (PDB 7LCO). **(C) 1f** bound to the active site of SARS-CoV-2 M^{pro}. Substitution of the benzyloxy group with a 4-methoxyindole prompts binding of the P3 portion of the inhibitor to the S4 pocket of the enzyme. This is a result of favorable interactions between the indole nitrogen and the carbonyl of Glu166 as well as that of the methoxy group with the binding pocket itself (PDB 7LDL). **(D) 1g** bound to the active site of SARS-CoV-2 M^{pro}. The phenyl ring of (S)-methyl benzyl group can be seen being directed towards the S4 site of the enzyme via the presence of the additional methyl group (PDB 7LCT).

Three-dimensional tonotopic mapping of the human cochlea based on synchrotron radiation phase-contrast imaging

Li, Hao, Luke Helpard, Jonas Ekeroot, Seyed Alireza Rohani, Ning Zhu, Helge Rask-Andersen, Hanif M. Ladak, and Sumit Agrawal. "Three-dimensional tonotopic mapping of the human cochlea based on synchrotron radiation phase-contrast imaging." *Scientific reports* 11, no. 1 (2021): 1-8.

This study uses synchrotron radiation - phase contrast imaging at BMIT to obtain accurate tonotopic maps of the human basilar organ of Corti and the spiral ganglion.

BMIT

The human cochlea transforms sound waves into electrical signals in the acoustic nerve fibers with high acuity. This transformation occurs via vibrating anisotropic membranes (basilar and tectorial membranes) and frequency-specific hair cell receptors. Frequency-positions can be mapped within the cochlea to create a tonotopic chart which fits an almost-exponential function with lowest frequencies positioned apically and highest frequencies positioned at the cochlear base (Bekesy 1960, Greenwood 1961). To date, models of frequency positions have been based on a two-dimensional analysis with inaccurate representations of the cochlear hook region. In the present study, the first three-dimensional frequency analysis of the cochlea using dendritic mapping to obtain accurate tonotopic maps of the human basilar membrane/organ of Corti and the spiral ganglion was performed. A novel imaging technique, synchrotron radiation phase-contrast imaging, was used and a spiral ganglion frequency function was estimated by nonlinear least squares fitting a Greenwood-like function ($F = A(10ax - K)$) to the data. The three-dimensional tonotopic data presented herein has large implications for validating electrode position and creating customized frequency maps for cochlear implant recipients.

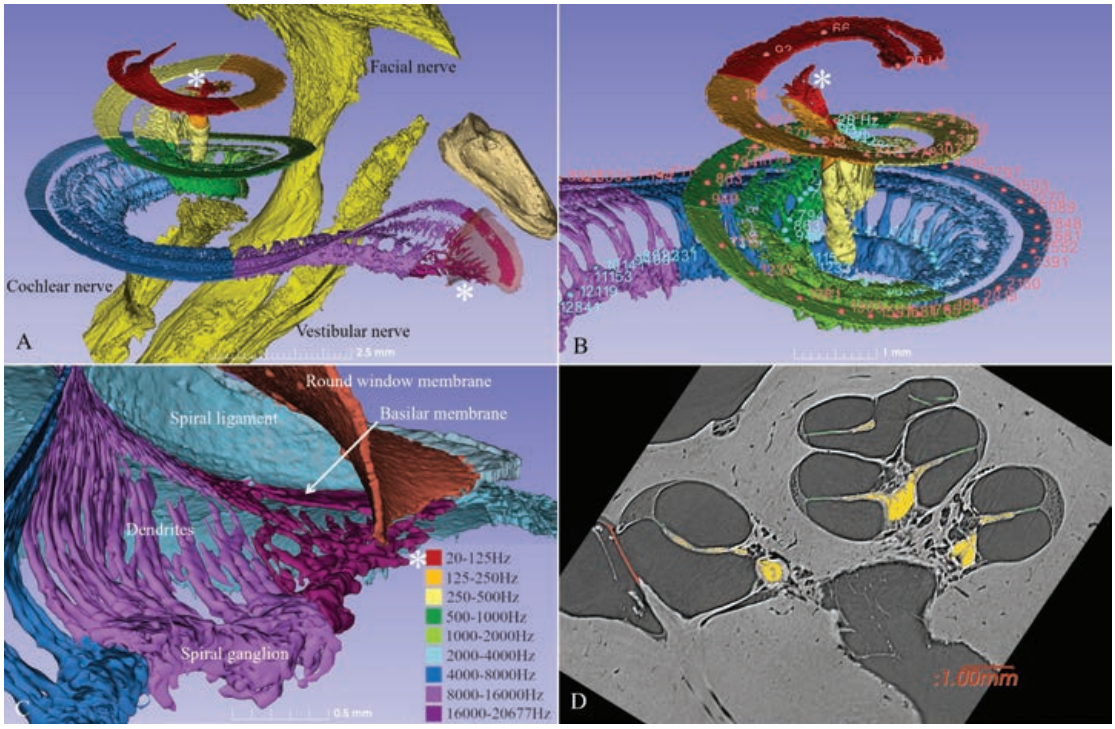

Corresponding authors: Hao Li & Helge Rask-Andersen, Uppsala University Hospital

(A) SR-PCI data of a left human cochlea. 3D Slicer (www.slicer.org, version 4.10.1)13 was used to create a detailed 3D representation including intra-cochlear soft tissue. The basilar membrane and spiral ganglion were segmented, and the frequency coordinates were calculated using Greenwood's formula14 and dendrite tracing. (B,C) For the spiral ganglion, the dendrites were traced from the basilar membrane to make a corresponding frequency map (shown with color scale). Note the angle of dendritic connections are not radial to the mid-modiolar axis in the apical and basal region (denoted by *). (D) Representative tomographic X-ray section showing the segmented round window (red), neural elements (yellow) and basilar membrane (green). GIMP 2 (www.gimp.org) was used to create the figures.

Assessment of hemodialysis clinical practices using polyaryl ether sulfone-polyvinylpyrrolidone clinical membrane

Westphalen, Heloisa, Amira Abdelrasoul, Ahmed Shoker, and Ning Zhu. "Assessment of hemodialysis clinical practices using polyaryl ether sulfone-polyvinylpyrrolidone (PAES: PVP) clinical membrane: Modeling of in vitro fibrinogen adsorption, in situ synchrotron-based imaging, and clinical inflammatory biomarkers investigations." *Separation and Purification Technology* 259 (2021): 118136.

Synchrotron micro-CT allowed the analysis of fouling layer-by-layer within the PAES PVP membrane.

BMIT

Protein adsorption in highly undesirable in hemodialysis (HD) since it leads to activation biochemical cascades and membrane fouling. The present study aims to obtain an in-depth understanding of the influence of clinical practice on in-vitro adsorption of fibrinogen (FB) and inflammatory biomarkers released in patients' uremic blood during and after HD. A mathematical model to predict human serum FB adsorption to Polyaryl Ether Sulfone-Polyvinylpyrrolidone (PAES: PVP) HD hemodialysis membrane currently used in Canadian hospitals was obtained function of feed flow rate, dialysate flow rate and treatment time. Advanced imaging and spectroscopy techniques were applied to assess the occurrence of FB adsorption. A UV/vis spectroscopic was utilized to measure quantitatively the FB adsorption during simulated HD session. In-situ Synchrotron-based X-ray microtomography (SR-μCT) is an innovative technique and was used in this study to evaluate the in vitro adsorption of conjugated human serum FB in each membrane layer. In-situ SR-μCT showed more severe fouling between intermediate and lower layers of the investigated region. Furthermore, the clinical data was used to correlate the adsorption of FB to inflammatory and thrombotic responses experienced by HD patients. Samples were collected from dialysis patients to ascertain the extent of inflammatory biomarkers released, before, during and after dialysis. Collected blood samples were analyzed using Luminex assays for the inflammatory biomarkers of Serpin/ Antithrombin-III, Properdin, C5a, 1L-1α, 1L-1β, TNF-α, IL6, and vWF. The results showed that the hydrodynamic conditions affect both the concentration of FB adsorbed and the time of saturation, and the results presented demonstrate how the clinical operating conditions can be manipulated to control protein adsorption during hemodialysis. In addition, the inflammatory biomarker released during the in vitro incubation of the membrane in uremic blood was compared to the ones released during dialysis at the same duration was compared to examine the influence of hydrodynamics conditions. The clinical study demonstrated how the hydrodynamic conditions influence complement activation, inflammatory and thrombotic responses. Overall, patients treated at lower flow rate demonstrated a more inflammatory profile and stronger tendencies to coagulation and clotting.

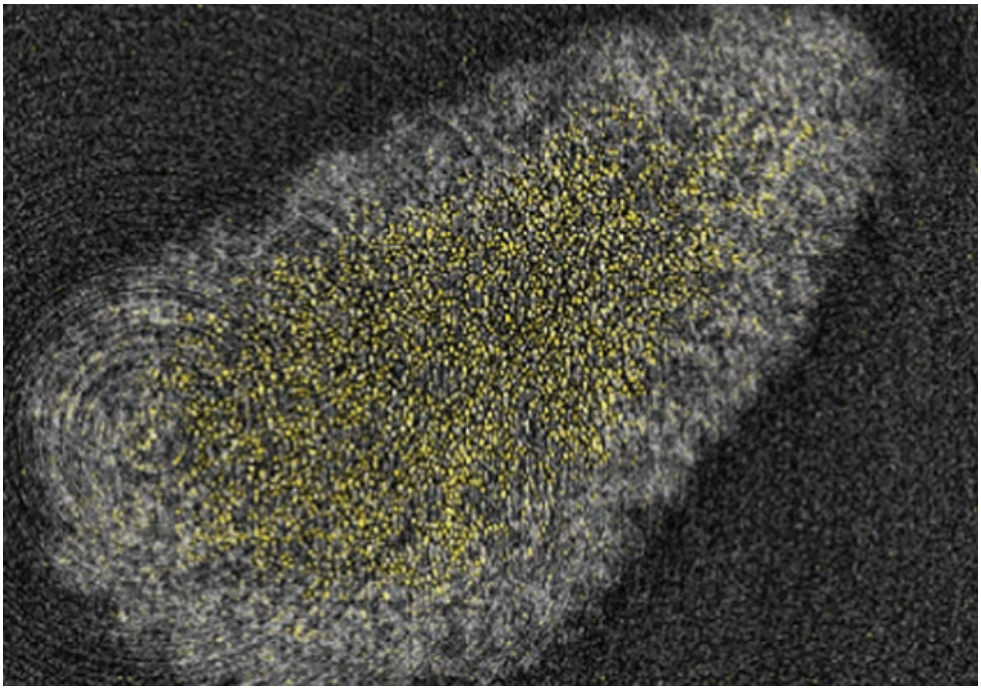

SR-μCT image of gold nanoparticle conjugated to human serum fibrinogen (FB-AuNP) bound to one of PAES-PVP hemodialysis membrane layers.

Corresponding author:
Amira Abdelrasoul,
University of Saskatchewan

A Slam-dependent hemophore contributes to heme acquisition in the bacterial pathogen Acinetobacter baumannii

Bateman, Thomas J., Megha Shah, Timothy Pham Ho, Hyejin Esther Shin, Chuxi Pan, Greg Harris, Jamie E. Fegan et al. "A Slam-dependent hemophore contributes to heme acquisition in the bacterial pathogen Acinetobacter baumannii." *Nature communications* 12, no. 1 (2021): 1-13.

CLS was used to determine the crystal structure of HphA to gain insight into its role in heme uptake.

CMCF

Nutrient acquisition systems are often crucial for pathogen growth and survival during infection, and represent attractive therapeutic targets. Here, we study the protein machinery required for heme uptake in the opportunistic pathogen Acinetobacter baumannii. We show that the hemO locus, which includes a gene encoding the heme-degrading enzyme, is required for high-affinity heme acquisition from hemoglobin and serum albumin. The hemO locus includes a gene coding for a heme scavenger (HphA), which is secreted by a Slam protein. Furthermore, heme uptake is dependent on a TonB-dependent receptor (HphR), which is important for survival and/or dissemination into the vasculature in a mouse model of pulmonary infection. Our results indicate that A. baumannii uses a two-component receptor system for the acquisition of heme from host heme reservoirs.

Corresponding author:
Trevor Moraes, University of Toronto

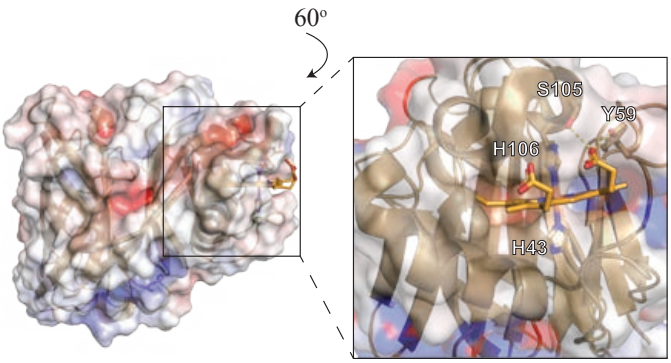

Cartoon model of HphA with an electrostatic surface map. A closer view of the heme binding site shown on the right highlights important heme interaction residues including the iron coorination residues (H43, H106) aand residues that hydrogen bond to the porphyrin carboxyl group (Y59, S105).

Hepatocyte growth factor administration increases bone soluble phosphate and alters bone chemical structure in diabetic hypertensive rats

Awad, Kamal, Natasha G. Boyes, Ramlah Iqbal, Mohamed Ahmed, Adel Mohamed, Pranesh Aswath, Corey R. Tomczak, and Venu Varanasi. "Hepatocyte growth factor administration increases bone soluble phosphate and alters bone chemical structure in diabetic hypertensive rats." *Journal of Materials Research* 36, no. 19 (2021): 3936-3951.

XANES was used to characterize the chemical structure of the three study groups: untreated diabetic control, untreated diabetic hypertensive, and HGF-treated diabetic hypertensive rat bones.

SGM, VLS-PGM, SXRMB

Hepatocyte growth factor (HGF) is a novel potential therapy for improving bone health in patients with type II diabetes and hypertension, but its effect on the bone molecular structure is not revealed yet. Here, X-ray absorption near edge structure (XANES) spectroscopy was used to explore the effects elicited by HGF on the bone chemical structure. This study assessed local calcium (Ca) and phosphorus (P) coordination of diabetic hypertensive rat bones, each with and without HGF treatment. Results revealed that HGF has significant effects on Ca and P coordination chemistry as confirmed by presence of more soluble phosphates in the HGT-treated groups. Data indicated that treated bones have a poorly developed phosphate structure as evidenced by drastic drop in post-edge shoulder in P L2, 3-edge compared to diabetic hypertensive and diabetic control bone. Presence of soluble Ca and P, products of bone resorption, with HGF treatment suggests unbalanced bone resorption and formation.

Corresponding author:
Venu Varanasi, University of Texas at Arlington

Industry

Using automation to keep the data flowing at the CLS

New in-situ capabilities at Brockhouse

Dr. Jon Makar, a Senior Research Officer with the National Research Council Canada, collaborated with the CLS industry group to investigate the effect of carbon dioxide on ordinary Portland cement (OPC) hydration. The team used the BXDS high energy wiggler beamline to study in-situ how carbon dioxide is incorporated in hydrating OPC over long time periods (20 to 24 hours). OPC is produced by heating limestone and clay in kilns, followed by intergrinding with calcium sulfate and limestone. It is the binding material that holds concrete together and is therefore a key construction material in Canada and around the world. Cement production accounts for about 1.5% of Canadian greenhouse gas emissions. Sequestering carbon dioxide in concrete could be a significant way of reducing our carbon footprint.

The high flux, energy and resolution of the Brockhouse high energy wiggler beamline makes it an excellent tool for understanding the real time dynamics of cement setting. For this preliminary in-situ experiment, BXDS Associate Scientist Adam Leontowich modified an existing gas flow cell on the beamline, making it possible to observe what effect carbon dioxide flow has on the phase composition of cement while it sets. Senior Industrial Scientist Joel Reid facilitated data collection and provides analytical expertise to the project.

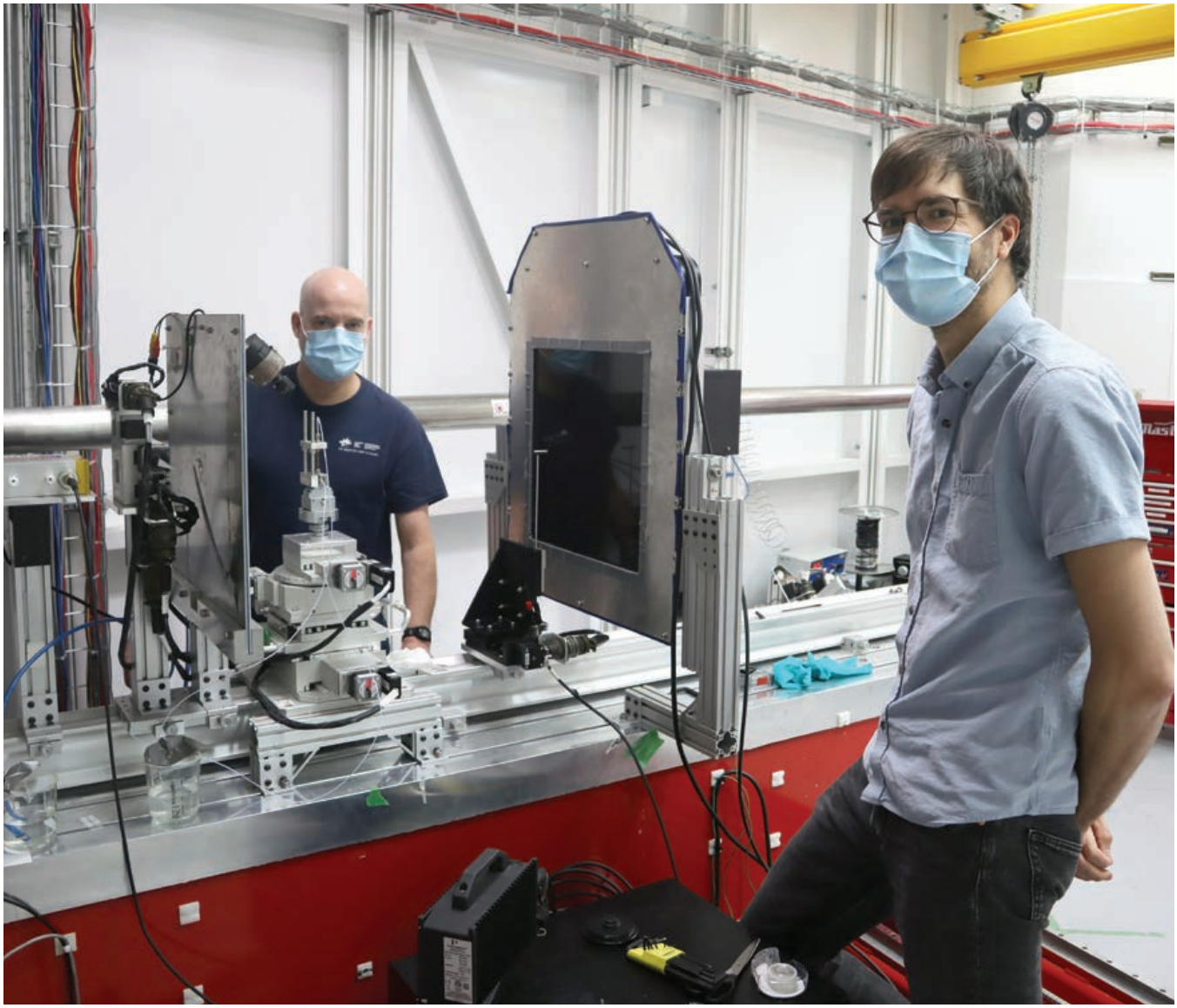

Joel Reid and Adam Leontowich at the High-Energy Wiggler Beamline of BXDS

Industry-academic collaboration for phytoremediation

Chile is the largest copper producer in the world, providing more than a million metric tons of the industrially-important metal each year. University of British Columbia researcher Estefanía Milla-Moreno, along with her collaborators (Dr. Rob Guy and Dr. Raju Soolayanakanahally) is working with the CLS Industry group to understand and refine how plants can be used to sustainably remediate copper mine sites.

The plants being studied grow unusually well in high-metal-content soils like those at mine sites. They are also native Chilean plants, and their use in phytoremediation can help provide refuge for wildlife. By shedding light on the element pathways at play, the research can help optimize and guide plant choices for mine sites.

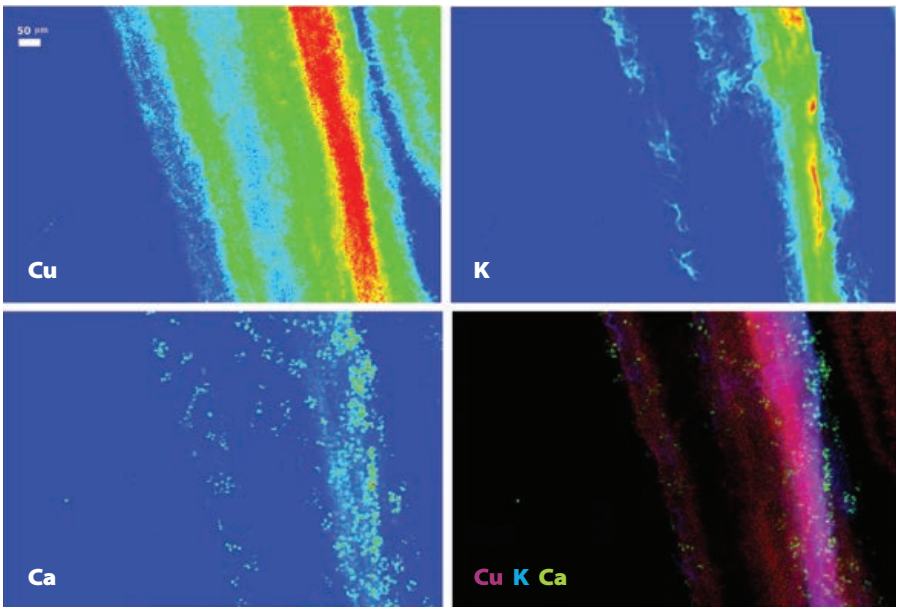

Using the BioXAS-Imaging beamline, Milla-Moreno was able to map several elements of interest within the plants, non-destructively. This precision enables her to understand the specific pathways involved in the plants' stress tolerance and the phytoremediation potential for various metals. In particular, identifying shared pathways for various metals and identifying unexpected metal uptake-interactions has been a great advantage of the technique.

"That has been also a great opportunity for me, to get to know and to get to think about how these other elements that we never thought of could also play a role in this multi-stress response," says Milla-Moreno.

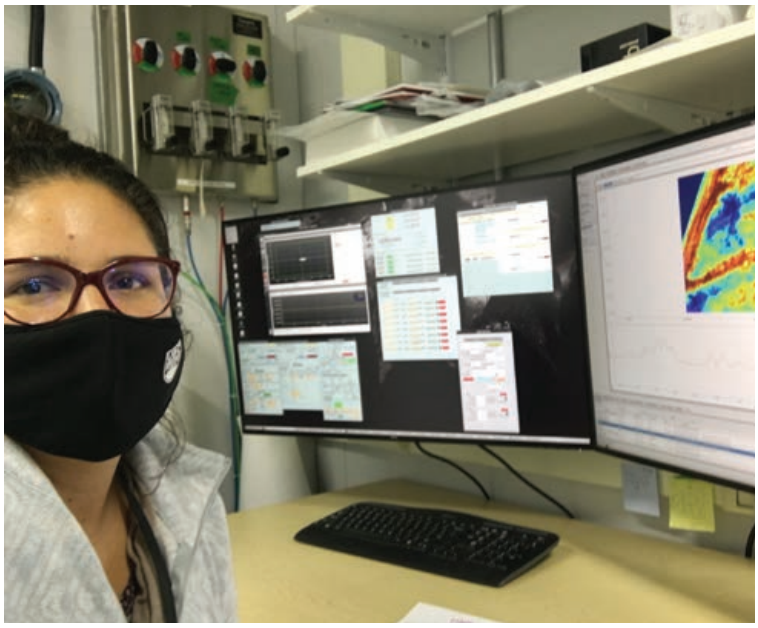

Estefanía Milla-Moreno

Distribution of elements of interest in leaf beamline setup and configuration

- Micro-mode
- Energy 15000 eV
- Focused beam size 5 microns

Milla-Moreno, Estefanía, Robert Dean Guy, and Raju Y. Soolanayakanahally. "Enlightening the Pathway of Phytoremediation: Ecophysiology and X-ray Fluorescence Visualization of Two Chilean Hardwoods Exposed to Excess Copper." *Toxics* 10, no. 5 (2022): 237.

CLS Education: *Partnerships & Collaborations*

Staying connected while a pandemic kept us isolated was a key part of the activities of the Education Team during this last year. Our collaborators continued to work with us to provide virtual experiences for students, create resources for teachers, and develop new programs we are excited to offer in the coming months.

NSERC

During Science Literacy Week, the communications team from NSERC and the education team from CLS collaborated to bring together an unprecedented and remarkable team of Indigenous scientists and their Elder or Traditional Knowledge Keeper advisors. This spectacular dream team is working on a project to support Indigenous science and languages, although we are not ready yet to reveal the project… stay tuned!

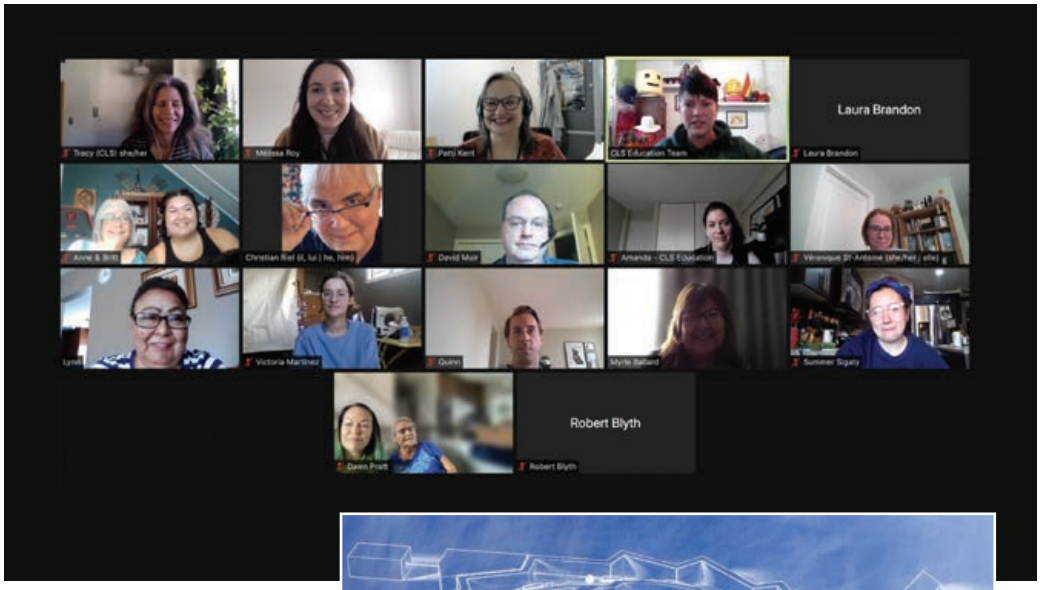

Nutrients for Life

Nutrients for Life, a Canadian science outreach organization, is a leader in "teaching teachers" with science-based, curriculum-aligned plant nutrient resources, programs and initiatives. Together we offered the CLS LiSSE program as PD for teachers and as an experience for students to demonstrate the role of nutrients in plant production and to promote solutions for sustainable agriculture and environmental stewardship.

International Workshop for Teachers in the Middle East

This January CLS, physics teachers from Iran, Israel, Pakistan, and Turkey (that had attended one of our workshops), the SESAME synchrotron in Jordan, and Lightsources for Africa, Asia, the Americas, Middle East, and the Pacific (LAAAMP) showed teachers from worked together to show teachers from Turkey, Jordan, Iran, Israel, Mexico, Pakistan, USA, El Salvador, and India how research conducted at a synchrotron can help them teach curricular content.

SESAME

LAAAMP

Fermilab & The Nature Conservancy's Nachusa Grasslands

Fermilab is the U.S. Department of Energy's premier particle physics and accelerator laboratory. The site includes several research laboratories and a herd of bison. Nachusa Grasslands is a preserve, protected by The Nature Conservancy, a global environmental nonprofit tackling climate change, conserving lands, waters and oceans, providing food and water sustainably, and helping make cities more sustainable. Nachusa Grasslands also has a free-range bison herd. We have been working with education teams from both Fermilab and Nachusa Grasslands to collect hair samples for baseline data in our Bison Project. In addition, we have been exploring ways to walk a path of reconciliation with Indigenous Peoples each in our respective regions.

The Nature Conservancy
Protecting nature. Preserving life.

Health & Sciences Academy at Bishop James Mahoney High School in Saskatoon

This program offers students high school and post-secondary credits through partnerships with institutions providing hands-on, real world experiences that support curricular outcomes. Our partnership uses the CLS as context to teach the Saskatchewan Physical Sciences 20 course using research examples, a beamline experiment, and curricular components to teach physics and chemistry.

Mistik Askiwin Dendrochronology (MAD) Lab

MAD LAB
Mistik Askîwin
Dendrochronology Lab

The MAD Lab, in the College of Agriculture and Bioresources at the University of Saskatchewan, was formed to establish extensive tree-ring chronologies and investigate tree-ring related research questions in Canada.

These chronologies form the foundation of various projects, from researching annually-resolved proxy climatic records, to dating historic structures. Together, the MAD Lab and CLS Education have created a citizen-science opportunity for high school students. The TREE (Trans-Canadian Research & Environmental Education) program enables synchrotron investigation of environmental effects on trembling aspen.

Federation of Sovereign Indigenous Nations (FSIN)

CLS and FSIN have had a memorandum of understanding establishing our partnerships over the last five years. Our collaboration focuses on supporting budding Indigenous scientists through sponsorship of the FSIN Science Fair and has also included professional development for science teachers on reserves and classroom visits to demonstrate light and optics activities.

PUBLICATIONS

PEER-REVIEWED

Abdelrasoul, Amira; Doan, Huu; Lohi, Ali; Zhu, Ning (2021). Synchrotron based Micro Tomography (SR-μCT), Experimental, and Computational Studies to Investigate the Influences of Cross Flow Air Injection in Ultrafiltration Process. *Journal of Environmental Chemical Engineering* 9(1), 104611. 10.1016/j.jece.2020.104611.

Akaki, Tatsuo; Bessho, Yuki; Ito, Takashi; Fujioka, Shingo; Ubukata, Minoru et al. (2021). Fragment-based lead discovery to identify novel inhibitors that target the ATP binding site of pyruvate dehydrogenase kinases. *Bioorganic and Medicinal Chemistry* 44, 116283. 10.1016/j.bmc.2021.116283. [PDB: 7ebb]

Alabi, Wahab O.; Wang, Hui; Adesanmi, Bukola M.; Shakouri, Mohsen; Hu, Yongfeng et al. (2021). Support composition effect on the structures, metallic sites formation, and performance of Ni-Co-Mg-Al-O composite for CO2 reforming of CH4. *Journal of CO2 Utilization* 43, 101355. 10.1016/j.jcou.2020.101355.

Al-Attas, Tareq A.; Marei, Nedal N.; Yong, Xue; Yasri, Nael G.; Thangadurai, Venkataraman et al. (2021). Ligand-Engineered Metal–Organic Frameworks for Electrochemical Reduction of Carbon Dioxide to Carbon Monoxide. *ACS Catalysis* 11(12), 7350-7357. 10.1021/acscatal.1c01506.

Alexander, James; Van Loon, Lisa; Banerjee, Neil (2021). Combined Geochemical and Mineralogical Investigation of Gold Mineralized Quartz Veins at the Vertigo Target, White Gold District, Yukon, Canada. *Microscopy and Microanalysis* 27(S1), 1856-1858. 10.1017/s1431927621006784.

Allen, Meghan; Blyth, Rob; Cubbon, Grant; Ribeiro, Sandra; Weist, Erin et al. (2021). Operating the Canadian Light Source during the Pandemic: Safety, Innovations, and Perseverance. *Synchrotron Radiation News* 34(1-3), 21-23. .1080/08940886.2021.1902720.

Amin, M. Ruhul; Elzer, Eugenia; Schnick, Wolfgang; Moewes, Alexander (2021). Unraveling the Energy Levels of Eu2+ Ions in MBe20N14:Eu2+ (M = Sr, Ba) Phosphors. Journal of *Physical Chemistry* C 125(22), 11828-11837. 10.1021/acs.jpcc.1c01085.

Andronowski, Janna M.; Cole, Mary E.; Hieronymus, Tobin L.; Davis, Reed A.; Usher, Logan R. et al. (2021). Intraskeletal consistency in patterns of vascularity within bat limb bones. *Anatomical Record* 305(2), 462– 476. 10.1002/ar.24694.

Arul, K Thanigai; Chang, Han-Wei; Shiu, Hung-Wei; Dong, Chung-Li; Pong, Way-Faung et al. (2021). A review of energy materials studied by in situ/operando synchrotron x-ray spectro-microscopy. Journal Physics D: *Applied Physics* 54(34), 343001. 10.1088/1361-6463/ac017f.

Aryee, Emma; Essilfie-Dughan, Joseph; Dalai, Ajay K.; Adjaye, John (2021). Comparative Studies of Carbon Nanomaterial and γ-Alumina as Supports for the Ni–Mo Catalyst in Hydrotreating of Gas Oils. *Energy Fuels* 35(7), 6153-6166. 10.1021/acs.energyfuels.0c02394.

Awad, Kamal; Boyes, Natasha G.; Iqbal, Ramlah; Ahmed, Mohamed; Mohamed, Adel et al. (2021). Hepatocyte growth factor administration increases bone soluble phosphate and alters bone chemical structure in diabetic hypertensive rats. *Journal of Materials Research* 36(19), 3936-3951. 10.1557/s43578-021-00300-8.

Azargohar, Ramin; Nanda, Sonil; Borugadda, Venu Babu; Cheng, He; Bond, Toby et al. (2021). Steam and supercritical water gasification of densified canola meal fuel pellets. International *Journal of Hydrogen Energy*. 10.1016/j.ijhydene.2021.09.134.

Bai, Bing; Belovodskiy, Alexandr; Hena, Mostofa; Kandadai, Appan Srinivas; Joyce, Michael A. et al. (2021). Peptidomimetic α-Acyloxymethylketone Warheads with Six-Membered Lactam P1 Glutamine Mimic: SARS-CoV-2 3CL Protease Inhibition, Coronavirus Antiviral Activity, and in Vitro Biological Stability. *Journal of Medicinal Chemistry* 65(4). 10.1021/acs.jmedchem.1c00616.

Bai, Ruijun; Zhang, Miaoxin; Zhang, Xin; Zhao, Shijing; Chen, Weifeng et al. (2021). A Multidimensional Topotactic Host Composite Anode Toward Transparent Flexible Potassium-Ion Microcapacitors. *ACS applied materials interfaces* 14(1). 10.1021/acsami.1c20609.

Bai, Yang; Santos, David A.; Rezaei, Shahed; Stein, Peter; Banerjee, Sarbajit et al. (2021). A chemo-mechanical damage model at large deformation: numerical and experimental studies on polycrystalline energy materials. International *Journal of Solids and Structures* 228, 111099. 10.1016/j.ijsolstr.2021.111099.

Balakrishnan, Manojkumar; Shrestha, Pranay; Lee, ChungHyuk; Ge, Nan; Fahy, Kieran F. et al. (2021). Degradation Characteristics of Electrospun Gas Diffusion Layers with Custom Pore Structures for Polymer Electrolyte Membrane Fuel Cells. *ACS applied materials interfaces* 13(2), 2414–2427. 10.1021/acsami.0c15324.

Bao, Yanping; Bolan, Nanthi S.; Lai, Jinhao; Wang, Yishun; Jin, Xiaohu et al. (2021). Interactions between organic matter and Fe (hydr) oxides and their influences on immobilization and remobilization of metal(loid)s: A review. *Critical Reviews in Environmental Science and Technology*, 1-22. .1080/10643389.2021.1974766.

Bao, Zhongwen; Al, Tom; Couillard, Martin; Poirier, Glenn; Bain, Jeff et al. (2021). A cross scale investigation of galena oxidation and controls on mobilization of lead in mine waste rock. *Journal of Hazardous Materials* 412, 125130. 10.1016/j.jhazmat.2021.125130.

Bateman, Thomas J.; Shah, Megha; Ho, Timothy Pham; Shin, Hyejin Esther; Pan, Chuxi et al. (2021). A Slam-dependent hemophore contributes to heme acquisition in the bacterial pathogen Acinetobacter baumannii. *Nature Communications* 12(1). 10.1038/s41467-021-26545-9. [PDB: 7re4, 7rea, 7red]

Bauer, Robert P.C.; Ravichandran, Aravind; Tse, John S.; Appathurai, Narayan; King, Graham et al. (2021). In Situ X-Ray Diffraction Study on Hydrate Formation at Low Temperature in a High Vacuum. *Journal of Physical Chemistry* C 125(48). 10.1021/acs.jpcc.1c08108.

Baumann, Karen; Eckhardt, Kai-Uwe; Acksel, Andre; Gros, Peter; Glaser, Karin et al. (2021). Contribution of biological soil crusts to soil organic matter composition and stability in temperate forests. *Soil Biology and Biochemistry* 160, 108315. 10.1016/j.soilbio.2021.108315.

Becher, Johannes; Weber, Sebastian; Ferreira Sanchez, Dario; Doronkin, Dmitry E.; Garrevoet, Jan et al. (2021). Sample Environment for Operando Hard X-ray Tomography—An Enabling Technology for Multimodal Characterization in Heterogeneous Catalysis. *Catalysts* 11(4), 459. 10.3390/catal11040459.

Belbessai, Salma; Achouri, Ines Esma; Benyoussef, El Hadi; Gitzhofer, François; Abatzoglou, Nicolas et al. (2021). Toluene steam reforming using nickel-based catalysts made from mining residues. *Catalysis Today* 365, 111-121. 10.1016/j.cattod.2020.07.087.

Berejnov, Viatcheslav; Rubinstein, Boris; Melo, Lis G. A.; Hitchcock, Adam P. (2021). Calculating absorption dose when X-ray irradiation modifies material quantity and chemistry. *Journal of Synchrotron Radiation* 28(3). 10.1107/s1600577521001703.

Beshore, Douglas C.; Adam, Gregory C.; Barnard, Richard J. O.; Burlein, Christine; Gallicchio, Steven N. et al. (2021). Redefining the Histone Deacetylase Inhibitor Pharmacophore: High Potency with No Zinc Cofactor Interaction. ACS *Medicinal Chemistry Letters* 12(4), 540-547. 10.1021/acsmedchemlett.1c00074. [PDB: 7ltg]

Bhagavathula, K. B.; Meredith, C. S.; Ouellet, S.; Satapathy, S. S.; Romanyk, D. L. et al. (2021). Density, Microstructure, and Strain-Rate Effects on the Compressive Response of Polyurethane Foams. *Experimental Mechanics* 62(3). 10.1007/s11340-021-00772-z.

Bhattarai, Surendra; Liu, Na; Karunakaran, Chithra; Tanino, Karen K.; Fu, Yong-Bi et al. (2021). Tissue specific changes in elements and organic compounds of alfalfa (Medicago sativa L.) cultivars differing in salt tolerance under salt stress. *Journal of Plant Physiology* 264, 153485. 10.1016/j.jplph.2021.153485.

Boddington, Kelly F.; Soubeyrand, Eric; Van Gelder, Kristen; Casaretto, José A.; Perrin, Colby et al. (2021). Bibenzyl synthesis in Cannabis sativa L.. *Plant Journal* 109(3). 10.1111/tpj.15588. [PDB: 7sgy]

Boschini, F.; Minola, M.; Sutarto, R.; Schierle, E.; Bluschke, M. et al. (2021). Dynamic electron correlations with charge order wavelength along all directions in the copper oxide plane. *Nature Communications* 12(1). 10.1038/s41467-020-20824-7.

Boyko, Teak D.; Zerr, Andreas; Moewes, Alexander (2021). Tuning the Electronic Band Gap of Oxygen-Bearing Cubic Zirconium Nitride: c-Zr3−x(N1−xOx)4. *ACS Applied Electronic Materials* 3(11). 10.1021/acsaelm.1c00632.

Boyle, T. J.; Walker, M.; Ruiz, A.; Schierle, E.; Zhao, Z. et al. (2021). Large response of charge stripes to uniaxial stress in La1.475Nd0.4Sr0.125CuO4. *Physical Review Research* 3(2). 10.1103/physrevresearch.3.l022004.

Brinkman, Don; Van Loon, Lisa L.; Banerjee, Neil R. (2021). 3D Non-Destructive Identification of Fossil Fish from the Late Cretaceous of Alberta, Canada using Synchrotron Micro Computed Tomography. *Microscopy Today* 29(2), 26-31. 10.1017/s155192952100047x.

Carriere, C.; Dillmann, P.; Gin, S.; Neff, D.; Gentaz, L. et al. (2021). The fate of Si and Fe while nuclear glass alters with steel and clay. npj *Materials Degradation* 5(1). 10.1038/s41529-021-00160-x.

Casimiro-Garcia, Agustin; Allais, Christophe; Brennan, Agnes; Choi, Chulho; Dower, Gabriela et al. (2021). Discovery of a Series of Pyrimidine Carboxamides as Inhibitors of Vanin-1. *Journal of Medicinal Chemistry* 65(1), 757-784. 10.1021/acs.jmedchem.1c01849. [PDB: 7sly]

Caveney, N. A.; Serapio-Palacios, A.; Woodward, S. E.; Bozorgmehr, T.; Caballero, G. et al. (2021). Structural and Cellular Insights into the l, d -Transpeptidase YcbB as a Therapeutic Target in Citrobacter rodentium, Salmonella Typhimurium, and Salmonella Typhi Infections. *Antimicrobial Agents and Chemotherapy* 65(2). 10.1128/aac.01592-20. [PDB: 7kgm]

Ceausu-Velcescu, Adina; Pracna, Petr; Margules, Laurent; Predoi-Cross, Adriana (2021). Rotational spectrum of chloroform, "grass-roots among the forest of trees": The v2 = 1, v3 = 2, v5 = 1, and v6 = 3 vibrational states of CH35Cl3. *Journal of Quantitative Spectroscopy and Radiative Transfer* 276, 107937. 10.1016/j.jqsrt.2021.107937.

Chen, Hsiang-Sheng; Benedetti, Tania M.; Lian, Jiaxin; Cheong, Soshan; O'Mara, Peter B. et al. (2021). Role of the Secondary Metal in Ordered and Disordered Pt–M Intermetallic Nanoparticles: An Example of Pt3Sn Nanocubes for the Electrocatalytic Methanol Oxidation. *ACS Catalysis* 11(4), 2235-2243. 10.1021/acscatal.0c05370.

Chen, Jay; Ghazani, Saeed M.; Stobbs, Jarvis A.; Marangoni, Alejandro G. (2021). Tempering of cocoa butter and chocolate using minor lipidic components. *Nature Communications* 12(1), 5018. 10.1038/s41467-021-25206-1.

Chen, Jiatang; Finfrock, Y. Zou; Wang, Zhiqiang; Sham, Tsun-Kong (2021). Strain and ligand effects in Pt-Ni alloys studied by valence-to-core X-ray emission spectroscopy. *Scientific Reports* 11(1). 10.1038/s41598-021-93068-0.

Chen, Jiatang; Finfrock, Y. Zou; Wang, Zhiqiang; Sham, Tsun-Kong (2021). High Energy Resolution Fluorescence Detection of the Pt L3,2-Edge Whitelines of Pt-Based Bimetallic Systems: Implications for the Pt 5d5/2,3/2 Density of States. *Journal of Physical Chemistry* C 125(4), 2327-2333. 10.1021/acs.jpcc.0c10596.

Chen, Shuo; Cade-Menun, Barbara J.; Bainard, Luke D.; St. Luce, Mervin; Hu, Yongfeng et al. (2021). The influence of long-term N and P fertilization on soil P forms and cycling in a wheat/fallow cropping system. *Geoderma* 404, 115274. 10.1016/j.geoderma.2021.115274.

Chen, Shuo; Wu, Jia-Le; Liang, Ying; Tang, Yi-Gang; Song, Hua-Xin et al. (2021). Arsenic Trioxide Rescues Structural p53 Mutations through a Cryptic Allosteric Site. *Cancer Cell* 39(2). 10.1016/j.ccell.2020.11.013. [PDB: 7dhz]

Chen, Wenjie; Li, Xintong; Hu, Zhenhai; Hu, Ze; Yue, Li et al. (2021). Spin-orbit phase behavior of Na2Co2TeO6 at low temperatures. *Physical Review* B 103(18). 10.1103/physrevb.103.l180404.

Chen, Xu; Guo, Jiangang; Deng, Jun; Wang, Ran; Zhao, Shijing et al. (2021). Highly Active Sites in Quaternary LnPdAsO (Ln = La, Ce, Pr) with Excellent Catalytic Activity for Hydrogen Evolution Reaction. *ACS Applied Energy Materials* 4(5), 4302-4307. 10.1021/acsaem.1c00434.

Chen, Yu Seby; Kozlov, Guennadi; Moeller, Brandon E.; Rohaim, Ahmed; Fakih, Rayan et al. (2021). Crystal structure of an archaeal CorB magnesium transporter. *Nature Communications* 12(1). 10.1038/s41467-021-24282-7. [PDB: 7m1t, 7m1u]

Chen, Zhangsen; Zhang, Gaixia; Wen, Yuren; Chen, Ning; Chen, Weifeng et al. (2021). Atomically Dispersed Fe-Co Bimetallic Catalysts for the Promoted Electroreduction of Carbon Dioxide. *Nano-Micro Letters* 14(1). 10.1007/s40820-021-00746-9.

Chen, Zhaowei; Tsytsarev, Vassiliy; Finfrock, Y. Zou; Antipova, Olga A.; Cai, Zhonghou et al. (2021). Wireless Optogenetic Modulation of Cortical Neurons Enabled by Radioluminescent Nanoparticles. *ACS Nano* 15(3), 5201-5208. 10.1021/acsnano.0c10436.

Chung, Ivy Yeuk Wah; Li, Lei; Cygler, Miroslaw (2021). Legionella effector LegA15/AnkH contains an unrecognized cysteine protease-like domain and displays structural similarity to LegA3/AnkD, but differs in host cell localization. Acta Crystallographica Section D: *Structural Biology* 77(12). 10.1107/s2059798321010469. [PDB: 7kj6]

Chung, Ivy Y. W.; Li, Lei; Tyurin, Oleg; Gagarinova, Alla; Wibawa, Raissa et al. (2021). Structural and functional study of Legionella pneumophila effector RavA. *Protein Science* 30(5). 10.1002/pro.4057. [PDB: 6wo6]

Collier, Breanna; Krueger, Kristopher; Miller, Isaac; Zhao, Jianbao; Billinghurst, Brant E. et al. (2021). The Synchrotron-based Far-infrared Spectrum of Glycolaldehyde. *Astrophysical Journal. Supplement Series* 253(2), 40. 10.3847/1538-4365/abde40.

Corona-Gomez, J.; Jack, T.A.; Feng, R.; Yang, Q. (2021). Wear and corrosion characteristics of nano-crystalline tantalum nitride coatings deposited on CoCrMo alloy for hip joint applications. *Materials Characterization* 182, 111516. 10.1016/j.matchar.2021.111516.

Courchesne, Brittaney; Schindler, Michael; Mykytczuk, Nadia C. S. (2021). Relationships Between the Microbial Composition and the Geochemistry and Mineralogy of the Cobalt-Bearing Legacy Mine Tailings in Northeastern Ontario. *Frontiers in Microbiology* 12. 10.3389/fmicb.2021.660190.

Cron, Brandi; Macalady, Jennifer L.; Cosmidis, Julie (2021). Organic Stabilization of Extracellular Elemental Sulfur in a Sulfurovum-Rich Biofilm: A New Role for Extracellular Polymeric Substances? *Frontiers in Microbiology* 12. 10.3389/fmicb.2021.720101.

Dai, Hongliu; Dong, Jing; Wu, Mingjie; Hu, Qingmin; Wang, Dongniu et al. (2021). Cobalt-Phthalocyanine-Derived Molecular Isolation Layer for Highly Stable Lithium Anode. *Angewandte Chemie - International Edition* 60(36), 19852-19859. 10.1002/anie.202106027.

Dai, Hongliu; Dong, Jing; Wu, Mingjie; Hu, Qingmin; Wang, Dongniu et al. (2021). Cobalt-Phthalocyanine-Derived Molecular Isolation Layer for Highly Stable Lithium Anode. *Angewandte Chemie* 133(36). 10.1002/ange.202106027.

Dam, Than T. N.; Angert, Alon; Krom, Michael D.; Bigio, Laura; Hu, Yongfeng et al. (2021). X-ray Spectroscopic Quantification of Phosphorus Transformation in Saharan Dust during Trans-Atlantic Dust Transport. *Environmental Science Technology* 55(18), 12694-12703. 10.1021/acs.est.1c01573.

Davies, Christopher W.; Stowe, Irma; Phung, Qui T.; Ho, Hoangdung; Bakalarski, Corey E. et al. (2021). Discovery of a caspase cleavage motif antibody reveals insights into noncanonical inflammasome function. *Proceedings of the National Academy of Sciences of the United States of America* 118(12), e2018024118. 10.1073/pnas.2018024118. [PDB: 7jwq]

de Boer, Tristan; Häusler, Jonas; Strobel, Philipp; Boyko, Teak D.; Rudel, Stefan S. et al. (2021). Detecting a Hierarchy of Deep-Level Defects in the Model Semiconductor ZnSiN2. *Journal of Physical Chemistry* C 125(51). 10.1021/acs.jpcc.1c08115.

de Boer, Tristan; Zatsepin, Dmitry; Raikov, Dmitry; Kurmaev, Ernst; Zatsepin, Anatoly F. et al. (2021). Electronic Properties of Carbyne Chains: Experiment and Theory. *Journal of Physical Chemistry* C 125(15), 8268-8273. 10.1021/acs.jpcc.0c11323.

Deng, Sixu; Sun, Qian; Li, Minsi; Adair, Keegan; Yu, Chuang et al. (2021). Insight into cathode surface to boost the performance of solid-state batteries. *Energy Storage Materials* 35. 10.1016/j.ensm.2020.12.003.

Dodangodage, Randika; Bernath, Peter F.; Zhao, Jianbao; Billinghurst, Brant (2021). Absorption cross sections in the CH stretching region for propene broadened by helium and nitrogen. *Journal of Quantitative Spectroscopy and Radiative Transfer,* 107738. 10.1016/j.jqsrt.2021.107738.

Dragomir, Mirela; Arčon, Iztok; Dube, Paul A.; Beam, Jeremiah C.; Grosvenor, Andrew P. et al. (2021). Family of anisotropic spin glasses Ba1−xLa1+xMnO4+δ. *Physical Review Materials* 5(7). 10.1103/physrevmaterials.5.074403.

Dragovich, Peter S.; Pillow, Thomas H.; Blake, Robert A.; Sadowsky, Jack D.; Adaligil, Emel et al. (2021). Antibody-Mediated Delivery of Chimeric BRD4 Degraders. Part 2: Improvement of In Vitro Antiproliferation Activity and In Vivo Antitumor Efficacy. *Journal of Medicinal Chemistry* 64(5). 10.1021/acs.jmedchem.0c01846. [PDB: 7khl]

Duan, Chunyang; Zhao, Dong; Wang, Xiang; Ren, Bei; Li, Mengqi et al. (2021). Highly Textured Assembly of Engineered Si Nanowires for Artificial Synapses Model. *ACS Applied Electronic Materials* 3(3), 1375-1383. 10.1021/acsaelm.1c00004.

Dydula, Christopher; Johns, Paul C. (2021). Development and assessment of an x-ray tube-based multi-beam x-ray scatter projection imaging system. *Review of Scientific Instruments* 92(11), 115106. 10.1063/5.0055900.

Ehsani, Masoume; Zhu, Ning; Doan, Huu; Lohi, Ali; Abdelrasoul, Amira et al. (2021). In-situ synchrotron X-ray imaging of ultrasound (US)-generated bubbles: Influence of US frequency on microbubble cavitation for membrane fouling remediation. *Ultrasonics Sonochemistry* 77, 105697. 10.1016/j.ultsonch.2021.105697.

Elghali, Abdellatif; Benzaazoua, Mostafa; Bouzahzah, Hassan; Abdelmoula, Mustapha; Dynes, James J. et al. (2021). Role of secondary minerals in the acid generating potential of weathered mine tailings: Crystal-chemistry characterization and closed mine site management involvement. *Science of the Total Environment* 784, 147105. 10.1016/j.scitotenv.2021.147105.

Elikem, Essouassi; Persico, Arantxa P.; Bulmer, David; Siciliano, Steven D.; Mussone, Paolo et al. (2021). A sustainable colloidal material with sorption and nutrient-supply capabilities for in situ groundwater bioremediation. *Journal of Environmental Quality* 50(6), 1440-1451. 10.1002/jeq2.20293.

Ereño-Orbea, June; Liu, Xianglei; Sicard, Taylor; Kucharska, Iga; Li, Wei et al. (2021). Structural details of monoclonal antibody m971 recognition of the membrane-proximal domain of CD22. *Journal of Biological Chemistry* 297(2), 100966. 10.1016/j.jbc.2021.100966. [PDB: 7o4y, 7o52]

Esselman, Brian J.; Zdanovskaia, Maria A.; Adkins, Taylor K.; Billinghurst, Brant E.; Zhao, Jianbao et al. (2021). Millimeter-wave and infrared spectroscopy of thiazole (c-C3H3NS) in its ground state and lowest-energy vibrationally excited states (v18, v17, and v13). *Journal of Molecular Spectroscopy* 379, 111493. 10.1016/j.jms.2021.111493.

Feng, Yu; Xu, Yong; Xie, Xianjun; Gan, Yiqun; Su, Chunli et al. (2021). The dual role of oxygen in redox-mediated removal of aqueous arsenic(III/V) by Fe-modified biochar. *Bioresource Technology* 340, 125674. 10.1016/j.biortech.2021.125674.

Freibert, Sven-A.; Boniecki, Michal T.; Stümpfig, Claudia; Schulz, Vinzent; Krapoth, Nils et al. (2021). N-terminal tyrosine of ISCU2 triggers [2Fe-2S] cluster synthesis by ISCU2 dimerization. *Nature Communications* 12(1). 10.1038/s41467-021-27122-w.

Furber, Kendra L.; Lacombe, R. J. Scott; Caine, Sally; Thangaraj, Merlin P.; Read, Stuart et al. (2021). Biochemical Alterations in White Matter Tracts of the Aging Mouse Brain Revealed by FTIR Spectroscopy Imaging. *Neurochemical Research* 47(3). 10.1007/s11064-021-03491-y.

Fu, Xiaogang; Gao, Rui; Jiang, Gaopeng; Li, Matthew; Li, Shuang et al. (2021). Evolution of atomic-scale dispersion of FeNx in hierarchically porous 3D air electrode to boost the interfacial electrocatalysis of oxygen reduction in PEMFC. *Nano Energy* 83, 105734. 10.1016/j.nanoen.2020.105734.

Fu, Xiaogang; Jiang, Gaopeng; Wen, Guobin; Gao, Rui; Li, Shuang et al. (2021). Densely accessible Fe-Nx active sites decorated mesoporous-carbon-spheres for oxygen reduction towards high performance aluminum-air flow batteries. *Applied Catalysis B: Environmental* 293, 120176. 10.1016/j.apcatb.2021.120176.

Gan, Tao; Yang, Jingxiu; Morris, David; Chu, Xuefeng; Zhang, Peng et al. (2021). Electron donation of non-oxide supports boosts O2 activation on nano-platinum catalysts. *Nature Communications* 12(1). 10.1038/s41467-021-22946-y.

Garcia-Martin, Susana; King, Graham; Urones-Garrote, Esteban; Woodward, Patrick M. (2021). Coupled Compositional and Displacive Modulations in KLaMnWO6 Revealed by Atomic Resolution Imaging. *Journal of the American Chemical Society* 143(45). 10.1021/jacs.1c07426.

Gavai, Ashvinikumar V.; Norris, Derek; Delucca, George; Tortolani, David; Tokarski, John S. et al. (2021). Discovery and Preclinical Pharmacology of an Oral Bromodomain and Extra-Terminal (BET) Inhibitor Using Scaffold-Hopping and Structure-Guided Drug Design. *Journal of Medicinal Chemistry* 64(19). 10.1021/acs.jmedchem.1c00625. [PDB: 5s9r]

Gerak, Chloe A.N.; Cho, Sophia Y.; Kolesnikov, Maxim; Okon, Mark; Murphy, Michael E.P. et al. (2021). Biophysical characterization of the ETV6 PNT domain polymerization interfaces. *Journal of Biological Chemistry* 296, 100284. 10.1016/j.jbc.2021.100284. [PDB: 7ju2]

Ghavami, Mehraneh; Soltan, Jafar; Chen, Ning (2021). Enhancing Catalytic Ozonation of Acetone and Toluene in Air Using MnOx/Al2O3 Catalysts at Room Temperature. Industrial Engineering *Chemistry Research* 60(33). 10.1021/acs.iecr.1c02288.

Gianoncelli, Alessandra; Kourousias, George; Schöder, Sebastian; Santostefano, Antonella; L'Héronde, Maëva et al. (2021). Synchrotron X-ray Microprobes: An Application on Ancient Ceramics. *Applied Sciences* (Switzerland) 11(17), 8052. 10.3390/app11178052.

Gimat, Alice; Michelin, Anne; Belhadj, Oulfa; Pellizzi, Eleonora; Massiani, Pascale et al. (2021). Paper sizing with gelatine: from the macro- to the nano-scale. *Cellulose* 28(4), 2419-2432. 10.1007/s10570-020-03655-z.

Gimat, Alice; Michelin, Anne; Massiani, Pascale; Rouchon, Véronique (2021). Beneficial effect of gelatin on iron gall ink corrosion. *Heritage Science* 9(1). 10.1186/s40494-021-00593-2.

Golkar, Tolou; Bassenden, Angelia V.; Maiti, Krishnagopal; Arya, Dev P.; Schmeing, T. Martin et al. (2021). Structural basis for plazomicin antibiotic action and resistance. *Communications Biology* 4(1). 10.1038/s42003-021-02261-4. [PDB: 6vou, 7lh5]

Green, R. J.; Zabolotnyy, V.; Zwiebler, M.; Liao, Z.; Macke, S. et al. (2021). Intrinsic versus extrinsic orbital and electronic reconstructions at complex oxide interfaces. *Physical Review Materials* 5(6). 10.1103/physrevmaterials.5.065004.

Grochulski, Pawel; Labiuk, Shaunivan (2021). Review of health research at the Canadian Light Source. Nuclear Instruments and Methods in Physics Research. Section B: Beam Interactions with *Materials and Atoms* 499, 70-76. 10.1016/j.nimb.2021.05.003.

Guin, Satya N.; Xu, Qiunan; Kumar, Nitesh; Kung, Hsiang-Hsi; Dufresne, Sydney et al. (2021). 2D-Berry-Curvature-Driven Large Anomalous Hall Effect in Layered Topological Nodal-Line MnAlGe. *Advanced Materials* 33(21), 2006301. 10.1002/adma.202006301.

Guldiken, Burcu; Konieczny, Dellaney; Wang, Ning; Hou, Anfu; House, James D. et al. (2021). Effect of variety and environment on the physicochemical, functional, and nutritional properties of navy bean flours. *European Food Research and Technology* 247(7). 10.1007/s00217-021-03745-7.

Guldiken, Burcu; Stobbs, Jarvis; Nickerson, Michael (2021). Heat induced gelation of pulse protein networks. *Food Chemistry* 350, 129158. 10.1016/j.foodchem.2021.129158.

Guo, Amin; Zhang, Jianhua; Wang, Yufei; Fan, Jiadong; He, Bo et al. (2021). Nanoscale Detection of Subcellular Nanoparticles by X-Ray Diffraction Imaging for Precise Quantitative Analysis of Whole Cancer Cells. *Analytical Chemistry* 93(12), 5201-5210. 10.1021/acs.analchem.0c05282.

Guo, Rui; Wang, Dongniu; Zuin, Lucia; Gallant, Betar M. (2021). Reactivity and Evolution of Ionic Phases in the Lithium Solid–Electrolyte Interphase. *ACS Energy Letters* 6(3), 877-885. 10.1021/acsenergylett.1c00117.

Guo, Shuaiqi; Vance, Tyler D. R.; Zahiri, Hossein; Eves, Robert; Stevens, Corey et al. (2021). Structural Basis of Ligand Selectivity by a Bacterial Adhesin Lectin Involved in Multispecies Biofilm Formation. *mBio* 12(2). 10.1128/mbio.00130-21. [PDB: 6x7j, 6x7t, 6x7y, 6x7z, 6x8a, 6x8d, 6x8y, 6x95, 6x9m, 6x9p, 6xa5, 6xaq]

Guo, Ying; Zhang, Shaoce; Zhang, Rong; Wang, Donghong; Zhu, Daming et al. (2021). Electrochemical Nitrate Production via Nitrogen Oxidation with Atomically Dispersed Fe on N-Doped Carbon Nanosheets. *ACS Nano* 16(1), 655-663. 10.1021/acsnano.1c08109.

Gupta, Naman K.; McMahon, Christopher; Sutarto, Ronny; Shi, Tianyu; Gong, Rantong et al. (2021). Vanishing nematic order beyond the pseudogap phase in overdoped cuprate superconductors. *Proceedings of the National Academy of Sciences of the United States of America* 118(34), e2106881118. 10.1073/pnas.2106881118.

Gu, Zhengxiang; Shen, Hao; Chen, Zheng; Yang, Yaoyue; Yang, Chao et al. (2021). Efficient Electrocatalytic CO2 Reduction to C2+ Alcohols at Defect-Site-Rich Cu Surface. *Joule* 5(2), 429-440. 10.1016/j.joule.2020.12.011.

He, Mengxue; Li, Xia; Li, Weihan; Zheng, Matthew; Wang, Jiajun et al. (2021). Immobilization and kinetic promotion of polysulfides by molybdenum carbide in lithium-sulfur batteries. *Chemical Engineering Journal* 411, 128563. 10.1016/j.cej.2021.128563.

Higgins, Melanie A.; Tegl, Gregor; MacDonald, Spencer S.; Arnal, Gregory; Brumer, Harry et al. (2021). N-Glycan Degradation Pathways in Gut- and Soil-Dwelling Actinobacteria Share Common Core Genes. *ACS Chemical Biology* 16(4). 10.1021/acschembio.0c00995. [PDB: 7lqx, 7lr1]

Hill, Matthew D.; Quesnelle, Claude; Tokarski, John; Fang, Haiquan; Fanslau, Carolynn et al. (2021). Development of BET inhibitors as potential treatments for cancer: A new carboline chemotype. *Bioorganic and Medicinal Chemistry Letters* 51, 128376. 10.1016/j.bmcl.2021.128376. [PDB: 7mce]

Hitchcock, Adam P.; Zhang, Chunyang; Eraky, Haytham; Shahcheraghi, Ladan; Ismail, Fatma et al. (2021). In-situ and Operando Studies with Soft X-Ray Transmission Spectromicroscopy. *Microscopy and Microanalysis* 27(S2), 59-60. 10.1017/s1431927621013295.

Huang, Ji; Fraser, Marie E. (2021). Second distinct conformation of the phosphohistidine loop in succinyl-CoA synthetase. Acta Crystallographica Section D: *Structural Biology* 77(3), 357-368. 10.1107/s2059798321000334. [PDB: 7jj0, 7jkr]

Huang, Jing; Huang, Gordon; Xin, Xiaying; Halstead, David; Gaetz, Katelyn et al. (2021). Characterization of canola growth and in-vivo element fate in Canadian prairie under the interferences of tillage and residue treatment. *Journal of Cleaner Production* 320, 128707. 10.1016/j.jclepro.2021.128707.

Hu, Carol H.; Neissel Valente, Meriah W.; Halpern, O. Scott; Jusuf, Sutjano; Khan, Javed A. et al. (2021). Small molecule and macrocyclic pyrazole derived inhibitors of myeloperoxidase (MPO). *Bioorganic and Medicinal Chemistry Letters* 42, 128010. 10.1016/j.bmcl.2021.128010. [PDB: 7lag, 7lan]

Hussain, Syed I.; Phillips, Lori A.; Hu, Yongfeng; Frey, Steven K.; Geuder,

David S. et al. (2021). Differences in phosphorus biogeochemistry and mediating microorganisms in the matrix and macropores of an agricultural clay loam soil. *Soil Biology and Biochemistry* 161, 108365. 10.1016/j.soilbio.2021.108365.

Hu, Yanyun; Salvador, James R.; Chen, Ning; Alatas, Ahmet; Kim, Young-June et al. (2021). Anharmonicity in partially filled skutterudites YbxCo4Sb12. *Journal of Applied Physics* 130(18), 185105. 10.1063/5.0064849.

Jalilehvand, Farideh; Enriquez Garcia, Alejandra; Niksirat, Pantea; Finfrock, Y. Zou; Gelfand, Benjamin S. et al. (2021). Binding of histidine and human serum albumin to dirhodium(II) tetraacetate. *Journal of Inorganic Biochemistry* 224, 111556. 10.1016/j.jinorgbio.2021.111556.

Jiang, Juan; Lee, Alex Taekyung; Lee, Sangjae; Lau, Claudia; Li, Min et al. (2021). Electronic properties of epitaxial La1−xSrxRhO3 thin films. *Physical Review B* 103(19). 10.1103/physrevb.103.195153.

Jiang, Junjie; Tsounis, Constantine; Gallington, Leighanne C.; Hu, Yongfeng; Scott, Robert W. J. et al. (2021). Disordered TiOx–SiOx Nanocatalysts Using Bioinspired Synthetic Routes. *ACS Applied Energy Materials* 4(8), 7691-7701. 10.1021/acsaem.1c01025.

Jiang, Yingying; Tan, Shuo; Hu, Jianping; Chen, Xin; Chen, Feng et al. (2021). Amorphous calcium magnesium phosphate nanocomposites with superior osteogenic activity for bone regeneration. *Regenerative Biomaterials* 8(6), rbab068. 10.1093/rb/rbab068.

Joly, Maxime; Deng, Tianyang; Morhart, Tyler A.; Wells, Garth; Achenbach, Sven et al. (2021). Scanning Aperture Approach for Spatially Selective ATR-FTIR Spectroscopy: Application to Microfluidics. *Analytical Chemistry* 93(42). 10.1021/acs.analchem.1c01614.

Keylor, Mitchell H.; Gulati, Anmol; Kattar, Solomon D.; Johnson, Rebecca E.; Chau, Ryan W. et al. (2021). Structure-Guided Discovery of Aminoquinazolines as Brain-Penetrant and Selective LRRK2 Inhibitors. *Journal of Medicinal Chemistry* 65(1), 838-856. 10.1021/acs.jmedchem.1c01968. [PDB: 7suh]

Kim, Chang-Yong; Slusar, Tetiana; Cho, Jinchul; Kim, Hyun-Tak (2021). Mott Switching and Structural Transition in the Metal Phase of VO2 Nanodomain. *ACS Applied Electronic Materials* 3(2), 605-610. 10.1021/acsaelm.0c00983.

Kim, Seon Hwa; Lahlali, Rachid; Karunakaran, Chithra; Vujanovic, Vladimir (2021). Specific Mycoparasite-Fusarium Graminearum Molecular Signatures in Germinating Seeds Disabled Fusarium Head Blight Pathogen's Infection. *International Journal of Molecular Sciences* 22(5), 2461. 10.3390/ijms22052461.

Köble, Kerstin; Eifert, László; Bevilacqua, Nico; Fahy, Kieran F.; Bazylak, Aimy et al. (2021). Synchrotron X-Ray radiography of vanadium redox flow batteries – Time and spatial resolved electrolyte flow in porous carbon electrodes. *Journal of Power Sources* 492, 229660. 10.1016/j.jpowsour.2021.229660.

Krause, Kevin; Lee, ChungHyuk; Lee, Jason K.; Fahy, Kieran F.; Shafaque, Hisan W. et al. (2021). Unstable Cathode Potential in Alkaline Flow Cells for CO2 Electroreduction Driven by Gas Evolution. *ACS Sustainable Chemistry and Engineering* 9(16), 5570–5579. 10.1021/acssuschemeng.0c08993.

Kuduk, Scott D.; Stoops, Bart; Alexander, Richard; Lam, Angela M.; Espiritu, Christine et al. (2021). Identification of a new class of HBV capsid assembly modulator. *Bioorganic and Medicinal Chemistry Letters* 39, 127848. 10.1016/j.bmcl.2021.127848. [PDB: 7k5m]

Kumar, Amit; Paul, Marilyn; Panda, Manoranjan; Jayaram, Shruthi; Kalidindi, Narasimharaju et al. (2021). Molecular mechanism of interspecies differences in the binding affinity of TD139 to Galectin-3. *Glycobiology* 31(10). 10.1093/glycob/cwab072. [PDB: 7cxa]

Langston, Steven P.; Grossman, Stephen; England, Dylan; Afroze, Roushan; Bence, Neil et al. (2021). Discovery of TAK-981, a First-in-Class Inhibitor of SUMO-Activating Enzyme for the Treatment of Cancer. *Journal of Medicinal Chemistry* 64(5). 10.1021/acs.jmedchem.0c01491. [PDB: 6xog, 6xoh]

Leontowich, Adam F. G.; Gomez, Ariel; Diaz Moreno, Beatriz; Muir, David; Spasyuk, Denis et al. (2021). The lower energy diffraction and scattering side-bounce beamline for materials science at the Canadian Light Source. *Journal of Synchrotron Radiation* 28(3). 10.1107/s1600577521002496.

Liang, Yue; Zhang, Yichi; Fábri, Csaba; Ma, Jiarui; Zhao, Jianbao et al. (2021). High-resolution FTIR spectroscopy of benzaldehyde in the far-infrared region: probing the rotational barrier. *Physical Chemistry Chemical Physics* 23(14). 10.1039/d1cp00188d.

Liang, Zhifu; Jiang, Daochuan; Wang, Xiang; Shakouri, Mohsen; Zhang, Ting et al. (2021). Molecular Engineering to Tune the Ligand Environment of Atomically Dispersed Nickel for Efficient Alcohol Electrochemical Oxidation. *Advanced Functional Materials* 31(51), 2106349. 10.1002/adfm.202106349.

Li, Chaojie; Zhao, Yan; Zhang, Yongguang; Luo, Dan; Liu, Jiabing et al. (2021). A new defect-rich and ultrathin ZnCo layered double hydroxide/carbon nanotubes architecture to facilitate catalytic conversion of polysulfides for high-performance Li-S batteries. *Chemical Engineering Journal* 417, 129248. 10.1016/j.cej.2021.129248.

Li, Chen; Zhang, Yuzhou; Zhu, Ning; Emady, Heather N.; Zhang, Lifeng et al. (2021). Experimental investigation of wet pharmaceutical granulation using in-situ synchrotron X-ray imaging. *Powder Technology* 378, 65-75. 10.1016/j.powtec.2020.09.063.

Li, Fengmiao; Zou, Yuting; Han, Myung-Geun; Foyevtsova, Kateryna; Shin, Hyungki et al. (2021). Single-crystalline epitaxial TiO film: A metal and superconductor, similar to Ti metal. *Science advances* 7(2), eabd4248. 10.1126/sciadv.abd4248.

Li, Franco K.K.; Gale, Robert T.; Petrotchenko, Evgeniy V.; Borchers, Christoph H.; Brown, Eric D. et al. (2021). Crystallographic analysis of TarI and TarJ, a cytidylyltransferase and reductase pair for CDP-ribitol synthesis in Staphylococcus aureus wall teichoic acid biogenesis. *Journal of Structural Biology* 213(2), 107733. 10.1016/j.jsb.2021.107733. [PDB: 6xh9, 6xhk, 6xhp, 6xhq, 6xhr, 6xhs, 6xht]

Li, Hao; Helpard, Luke; Ekeroot, Jonas; Rohani, Seyed Alireza; Zhu, Ning et al. (2021). Three-dimensional tonotopic mapping of the human cochlea based on synchrotron radiation phase-contrast imaging. *Scientific Reports* 11(1), 4437. 10.1038/s41598-021-83225-w.

Li, Jiarui; Green, Robert J.; Zhang, Zhen; Sutarto, Ronny; Sadowski, Jerzy T. et al. (2021). Sudden Collapse of Magnetic Order in Oxygen-Deficient Nickelate Films. *Physical Review Letters* 126(18). 10.1103/physrevlett.126.187602.

Li, Jinhua; Liu, Peiyu; Tamaxia, Alima; Zhang, Heng; Liu, Yan et al. (2021). Diverse Intracellular Inclusion Types Within Magnetotactic Bacteria: Implications for Biogeochemical Cycling in Aquatic Environments. *Journal of Geophysical Research Biogeosciences* 126(7). 10.1029/2021jg006310.

Li, Junjie; Banis, Mohammad Norouzi; Ren, Zhouhong; Adair, Keegan R.; Doyle-Davis, Kieran et al. (2021). Unveiling the Nature of Pt Single-Atom Catalyst during Electrocatalytic Hydrogen Evolution and Oxygen Reduction Reactions. *Small* 17(11), 2007245. 10.1002/smll.202007245.

Li, Junjie; Jiang, Ya-fei; Wang, Qi; Xu, Cong-Qiao; Wu, Duojie et al. (2021). A general strategy for preparing pyrrolic-N4 type single-atom catalysts via pre-located isolated atoms. *Nature Communications* 12(1). 10.1038/s41467-021-27143-5.

Li, Jun; Ozden, Adnan; Wan, Mingyu; Hu, Yongfeng; Li, Fengwang et al. (2021). Silica-copper catalyst interfaces enable carbon-carbon coupling towards ethylene electrosynthesis. *Nature Communications* 12(1), 2808. 10.1038/s41467-021-23023-0.

Li, Minsi; Li, Weihan; Chen, Ning; Liang, Jianwen; Liu, Yanyu et al. (2021). Revealing Dopant Local Structure of Se-Doped Black Phosphorus. *Chemistry of Materials* 33(6), 2029-2036. 10.1021/acs.chemmater.0c04072.

Li, Minsi; Li, Weihan; Hu, Yongfeng; Yakovenko, Andrey A.; Ren, Yang et al. (2021). New Insights into the High-Performance Black Phosphorus Anode for Lithium-Ion Batteries. *Advanced Materials* 33(35), 2101259. 10.1002/adma.202101259.

Lin, Chang Sheng-Huei; Chan, Anson C.K.; Vermeulen, Jenny; Brockerman, Jacob; Soni, Arvind S. et al. (2021). Peptidoglycan binding by a pocket on the accessory NTF2-domain of Pgp2 directs helical cell shape of Campylobacter jejuni. *Journal of Biological Chemistry* 296, 100528. 10.1016/j.jbc.2021.100528. [PDB: 6xj7]

Liu, Chong; Day, Ryan P.; Li, Fengmiao; Roemer, Ryan L.; Zhdanovich, Sergey et al. (2021). High-order replica bands in monolayer FeSe/SrTiO3 revealed by polarization-dependent photoemission spectroscopy. *Nature Communications* 12(1). 10.1038/s41467-021-24783-5.

LIU, Min; WANG, Yong-gang; CHEN, Gui-feng; SHI, Quan; HU, Yong-feng et al. (2021). Effects of iron catalyst and atmosphere on sulfur transformation during pressurized low-temperature pyrolysis of Baishihu coal. *Journal of Fuel Chemistry and Technology* 49(4), 436-443. 10.1016/s1872-5813(21)60058-0.

Liu, Na; Hu, Qing; Wang, Chao; Tong, Lizhi; Weng, Chih-Huang et al. (2021). Hexachloroethane dechlorination in sulfide-containing aqueous solutions catalyzed by nitrogen-doped carbon materials. *Environmental Pollution* 281, 116915. 10.1016/j.envpol.2021.116915.

Liu, Shao-Qing; Gao, Min-Rui; Feng, Ren-Fei; Gong, Lu; Zeng, Hongbo et al. (2021). Electronic Delocalization of Bismuth Oxide Induced by Sulfur Doping for Efficient CO2 Electroreduction to Formate. *ACS Catalysis* 11(12), 7604-7612. 10.1021/acscatal.1c01899.

Liu, Weifeng; Maben, Zachary; Wang, Carole; Lindquist, Kevin C.; Li, Manqing et al. (2021). Structural delineation and phase-dependent activation of the costimulatory CD27:CD70 complex. *Journal of Biological Chemistry* 297(4), 101102. 10.1016/j.jbc.2021.101102. [PDB: 7kx0]

Liu, Yannan; Chen, Chuanshuang; Valdez, Jesus; Motta Meira, Debora; He, Wanting et al. (2021). Phase-enabled metal-organic framework homojunction for highly selective CO2 photoreduction. *Nature Communications* 12(1). 10.1038/s41467-021-21401-2.

Liu, Yuan; Chen, Ning; Li, Weidong; Sun, Mingzi; Wu, Tong et al. (2021). Engineering the synergistic effect of carbon dots-stabilized atomic and subnanometric ruthenium as highly efficient electrocatalysts for robust hydrogen evolution. *SmartMat*. 10.1002/smm2.1067.

Liu, Yuwei; Li, Yan; Li, Yanzhang; Chen, Ning; Ding, Hongrui et al. (2021). Photo-stimulated anoxic reduction of birnessite (δ-MnO2) by citrate and its fine structural responses: Insights on a proton-promoted photoelectron transfer process. *Chemical Geology* 561, 120029. 10.1016/j.chemgeo.2020.120029.

Li, Wenshuai; Liu, Xiao-Ming; Hu, Yan; Teng, Fang-Zhen; Hu, Yong-Feng et al. (2021). Potassium isotopic fractionation in a humid and an arid soil–plant system in Hawai'i. *Geoderma* 400, 115219. 10.1016/j.geoderma.2021.115219.

Li, Wenshuai; Liu, Xiao-Ming; Wang, Kun; Fodrie, F. Joel; Yoshimura, Toshihiro et al. (2021). Potassium phases and isotopic composition in modern marine biogenic carbonates. Geochimica et *Cosmochimica Acta* 304, 364-380. 10.1016/j.gca.2021.04.018.

Li, Xiaoling; Zhang, Ke; Chang, Liping; Wang, Hui (2021). Review of researches on H2S splitting cycle for hydrogen production via low-temperature route. *Chemical Engineering Science: X* 11, 100107. 10.1016/j.cesx.2021.100107.

Li, Zhaoqiang; Yang, Jingyi; Ge, Xiaoli; Deng, Ya-Ping; Jiang, Gaopeng et al. (2021). Self-assembly of colloidal MOFs derived yolk-shelled microcages as flexible air cathode for rechargeable Zn-air batteries. *Nano Energy* 89, 106314. 10.1016/j.nanoen.2021.106314.

Lozano-Gorrín, Antonio D.; Wright, Bradley; Dube, Paul A.; Marjerrison, Casey A.; Yuan, Fang et al. (2021). Magnetism in Mixed Valence, Defect, Cubic Perovskites: BaIn1−xFexO2.5+δ, x = 0.25, 0.50, and 0.75. Local and Average Structures. *ACS Omega* 6(8). 10.1021/acsomega.1c00416.

Luo, Dan; Li, Chaojie; Zhang, Yongguang; Ma, Qianyi; Ma, Chuyin et al. (2021). Design of Quasi-MOF Nanospheres as a Dynamic Electrocatalyst toward Accelerated Sulfur Reduction Reaction for High-Performance Lithium–Sulfur Batteries. *Advanced Materials* 34(2), 2105541. 10.1002/adma.202105541.

Luo, Dan; Zheng, Lei; Zhang, Zhen; Li, Matthew; Chen, Zhongwei et al. (2021). Constructing multifunctional solid electrolyte interface via in-situ polymerization for dendrite-free and low N/P ratio lithium metal batteries. *Nature Communications* 12(1). 10.1038/s41467-020-20339-1.

MacIver, Michael R.; Hamza, Hassan; Pawlik, Marek (2021). Effect of suspension conductivity and fines concentration on coarse particle settling in oil sands tailings. *Canadian Journal of Chemical Engineering*. 10.1002/cjce.23935.

Majewski, Dorothy D.; Okon, Mark; Heinkel, Florian; Robb, Craig S.; Vuckovic, Marija et al. (2021). Characterization of the Pilotin-Secretin Complex from the Salmonella enterica Type III Secretion System Using Hybrid Structural Methods. *Structure* 29(2). 10.1016/j.str.2020.08.006. [PDB: 6xfj]

Mane, Jonathan Y.; Michaelian, Kirk H.; Stoyanov, Stanislav R.; Billinghurst, Brant E.; Zhao, Jianbao et al. (2021). Computational and infrared spectroscopic investigations of N-substituted carbazoles. *Physical Chemistry Chemical Physics* 23(14). 10.1039/d0cp03879b.

Marouane, Bouchra; Chen, Ning; Obst, Martin; Peiffer, Stefan (2021). Competing Sorption of Se(IV) and Se(VI) on Schwertmannite. *Minerals* 11(7), 764. 10.3390/min11070764.

Mokoloko, Lerato L; Matsoso, Boitumelo J; Forbes, Roy P.; Barrett, Dean H.; Moreno, Beatriz D. et al. (2021). Evolution of large-area reduced graphene oxide nanosheets from carbon dots via thermal treatment. *Carbon Trends 4,* 100074. 10.1016/j.cartre.2021.100074.

Mollahosseini, Arash; Min Lee, Kyu; Abdelrasoul, Amira; Doan, Huu; Zhu, Ning et al. (2021). Innovative in situ investigations using synchrotron-based micro tomography and molecular dynamics simulation for fouling assessment in ceramic membranes for dairy and food industry. *International Journal of Applied Ceramic Technology* 18(6). 10.1111/ijac.13824.

Morhart, Tyler A.; Tu, Kaiyang; Read, Stuart T.; Rosendahl, Scott M.; Wells, Garth et al. (2021). Surface enhanced infrared spectroelectrochemistry using a microband electrode. *Canadian Journal of Chemistry*. 10.1139/cjc-2021-0183.

Morris, David J.; Zhang, Peng (2021). In situ X-ray Absorption Spectroscopy of Platinum Electrocatalysts. *Chemistry - Methods* 1(3), 162-172. 10.1002/cmtd.202000069.

Moustafa, Ahmed; Evans, Alex; Hofstetter, Simmon; Boutros, Jenny; Pourrezaei, Parastoo et al. (2021). Operando Studies of Iodine Species in an Advanced Oxidative Water Treatment Reactor. *ACS ES T Water* 1(11). 10.1021/acsestwater.1c00149.

Mukherjee, Alivia; Borugadda, Venu Babu; Dynes, James J.; Niu, Catherine; Dalai, Ajay K. et al. (2021). Carbon dioxide capture from flue gas in biochar produced from spent coffee grounds: Effect of surface chemistry and porous structure. *Journal of Environmental Chemical Engineering* 9(5), 106049. 10.1016/j.jece.2021.106049.

Mukhopadhyay, Indranath; Billinghurst, B.E. (2021). Very high-resolution synchrotron radiation far-infrared (FIR) spectrum of methanol D2 (CHD2OH) millimeter-wave (MMW) measurements involving highly excited torsional vibrational rotational states, and identification of optically pumped FIR laser lines. *Infrared Physics and Technology* 113, 103563. 10.1016/j.infrared.2020.103563.

Müller-Stöver, Dorette; Thompson, Rhys; Lu, Changyong; Thomsen, Tobias Pape; Glæsner, Nadia et al. (2021). Increasing plant phosphorus availability in thermally treated sewage sludge by post-process oxidation and particle size management. *Waste Management 120*, 716-724. 10.1016/j.wasman.2020.10.034.

Mulligan, Vikram Khipple; Workman, Sean; Sun, Tianjun; Rettie, Stephen; Li, Xinting et al. (2021). Computationally designed peptide macrocycle inhibitors of New Delhi metallo-β-lactamase 1. *Proceedings of the National Academy of Sciences of the United States of America* 118(12), e2012800118. 10.1073/pnas.2012800118. [PDB: 6xbe, 6xbf]

Munira, Sirajum; Dynes, James J.; Islam, Mofizul; Khan, Fahad; Adesanya, Theresa et al. (2021). Relative proportions of organic carbon functional groups in biochars as influenced by spectral data collection and processing. *Chemosphere* 283, 131023. 10.1016/j.chemosphere.2021.131023.

Munir, Rahim; Cieplechowicz, Edward; Lamarche, Renaud Miclette; Chernikov, Roman; Trudel, Simon et al. (2021). Air-Processed Organic Photovoltaics for Outdoor and Indoor Use Based upon a Tin Oxide-Perylene Diimide Electron Transporting Bilayer. *Advanced Materials Interfaces* 9(3), 2101918. 10.1002/admi.202101918.

Murphy, Michael W.; Bovo, Laura; Bottaro, Gregorio; Armelao, Lidia; Sham, Tsun-Kong et al. (2021). Electronic and relating behavior of Mn-doped ZnO nanostructures: An x-ray absorption spectroscopy study. *AIP Advances* 11(6), 065027. 10.1063/5.0047053.

Mushtaha, Farah N.; Kuehn, Tristan K.; El-Deeb, Omar; Rohani, Seyed A.; Helpard, Luke W. et al. (2021). Design and characterization of a 3D-printed axon-mimetic phantom for diffusion MRI. *Magnetic Resonance in Medicine* 86(5), 2482–2496. 10.1002/mrm.28886.

Naineni, Sai Kiran; Liang, Jason; Hull, Kenneth; Cencic, Regina; Zhu, Mingzhao et al. (2021). Functional mimicry revealed by the crystal structure of an eIF4A:RNA complex bound to the interfacial inhibitor, desmethyl pateamine A. *Cell Chemical Biology* 28(6). 10.1016/j.chembiol.2020.12.006. [PDB: 6xki]

Nasu, Yusuke; Murphy-Royal, Ciaran; Wen, Yurong; Haidey, Jordan N.; Molina, Rosana S. et al. (2021). A genetically encoded fluorescent biosensor for extracellular l-lactate. *Nature Communications* 12(1). 10.1038/s41467-021-27332-2. [PDB: 7e9y]

Naughton, Hannah R.; Keiluweit, Marco; Tfaily, Malak M.; Dynes, James J.; Regier, Tom et al. (2021). Development of energetic and enzymatic limitations on microbial carbon cycling in soils. *Biogeochemistry* 153(2), 191-213. 10.1007/s10533-021-00781-z.

Negassa, Wakene; Eckhardt, Kai-Uwe; Regier, Tom; Leinweber, Peter (2021). Dissolved organic matter concentration, molecular composition, and functional groups in contrasting management practices of peatlands. *Journal of Environmental Quality* 50(6). 10.1002/jeq2.20284.

Nilvebrant, Johan; Ereño-Orbea, June; Gorelik, Maryna; Julian, Mark C.; Tessier, Peter M. et al. (2021). Systematic Engineering of Optimized Autonomous Heavy-Chain Variable Domains. *Journal of Molecular Biology* 433(21), 167241. 10.1016/j.jmb.2021.167241. [PDB: 7ooi]

Nims, Christine; Lafond, Julia; Alleon, Julien; Templeton, Alexis S.; Cosmidis, Julie et al. (2021). Organic biomorphs may be better preserved thanmicroorganisms in early Earth sediments. *Geology*. 10.1130/g48152.1.

Ning, Liqun; Zhu, Ning; Smith, An; Rajaram, Ajay; Hou, Huishu et al. (2021). Noninvasive Three-Dimensional In Situ and In Vivo Characterization of Bioprinted Hydrogel Scaffolds Using the X-ray Propagation-Based Imaging Technique. *ACS applied materials interfaces* 13(22), 25611–25623. 10.1021/acsami.1c02297.

Okbinoglu, Tulin; Kennepohl, Pierre (2021). Nature of S–N Bonding in Sulfonamides and Related Compounds: Insights into π-Bonding Contributions from Sulfur K-Edge X-ray Absorption Spectroscopy. *Journal of Physical Chemistry* A 125(2), 615-620. 10.1021/acs.jpca.0c09768.

Ozden, Adnan; Liu, Yanjiang; Dinh, Cao-Thang; Li, Jun; Ou, Pengfei et al. (2021). Gold Adparticles on Silver Combine Low Overpotential and High Selectivity in Electrochemical CO2 Conversion. *ACS Applied Energy Materials* 4(8), 7504-7512. 10.1021/acsaem.1c01577.

Ozden, Adnan; Wang, Yuhang; Li, Fengwang; Luo, Mingchuan; Sisler, Jared et al. (2021). Cascade CO2 electroreduction enables efficient carbonate-free production of ethylene. *Joule* 5(3), 706-719. 10.1016/j.joule.2021.01.007.

Pan, Yuanming; Li, Dien; Feng, Renfei; Wiens, Eli; Chen, Ning et al. (2021). Uranyl binding mechanism in microcrystalline silicas: A potential missing link for uranium mineralization by direct uranyl co-precipitation and environmental implications. *Geochimica et Cosmochimica Acta* 292, 518-531. 10.1016/j.gca.2020.10.017.

Parashar, Abhinav; Gourgas, Ophélie; Lau, Kirk; Li, Jingjing; Muiznieks, Lisa et al. (2021). Elastin calcification in in vitro models and its prevention by MGP's N-terminal peptide. *Journal of Structural Biology* 213(1), 107637. 10.1016/j.jsb.2020.107637.

Pattammattel, Ajith; Leppert, Valerie J.; Aronstein, Paul; Robinson, Matthew; Mousavi, Amirhosein et al. (2021). Iron speciation in particulate matter (PM2.5) from urban Los Angeles using spectro-microscopy methods. *Atmospheric Environment* 245, 117988. 10.1016/j.atmosenv.2020.117988.

Pei, Yi; Li, Shuang; Chen, Qing; Liang, Ruilin; Li, Matthew et al. (2021). Cationic–anionic redox couple gradient to immunize against irreversible processes of Li-rich layered oxides. *Journal of Materials Chemistry* A 9(4), 2325-2333. 10.1039/d0ta09609a.

Peterson, Ronald C.; Graham, Robert C.; Ervin, Jarel O.; Kozin, Igor S.; Sickman, James O. et al. (2021). Sveite from the Northeastern San Joaquin Valley, California. *Canadian Mineralogist* 59(2). 10.3749/canmin.1900074.

Pham, N. T. Hang; Létourneau, Myriam; Fortier, Marlène; Bégin, Gabriel; Al-Abdul-Wahid, M. Sameer et al. (2021). Perturbing dimer interactions and allosteric communication modulates the immunosuppressive activity of human galectin-7. **Journal of Biological Chemistry** 297(5), 101308. 10.1016/j.jbc.2021.101308. [PDB: 6vtp, 6vtr]

Phue, Wut H.; Bahadi, Mazen; Dynes, James J.; Wang, Jian; Kuppili, Venkata S. C. et al. (2021). Protein–biomolecule interactions play a major role in shaping corona proteome: studies on milk interacted dietary particles. *Nanoscale* 13(31), 13353-13367. 10.1039/d1nr03712a.

Picard, Aude; Gartman, Amy; Girguis, Peter R. (2021). Interactions Between Iron Sulfide Minerals and Organic Carbon: Implications for Biosignature Preservation and Detection. *Astrobiology* 21(5). 10.1089/ast.2020.2276.

Pitumpe Arachchige, Pavithra S.; Hettiarachchi, Ganga M.; Rice, Charles W.; Maurmann, Leila; Dynes, James J. et al. (2021). Chemistry and Associations of Carbon in Water-Stable Soil Aggregates from a Long-Term Temperate Agroecosystem and Implications on Soil Carbon Stabilization. *ACS Agricultural Science Technology* 1(4), 294-302. 10.1021/acsagscitech.0c00074.

Possinger, Angela R.; Zachman, Michael J.; Dynes, James J.; Regier, Tom Z.; Kourkoutis, Lena F. et al. (2021). Co-precipitation induces changes to iron and carbon chemistry and spatial distribution at the nanometer scale. *Geochimica et Cosmochimica Acta* 314. 10.1016/j.gca.2021.09.003.

Prasertanan, Theerawat; Palmer, David R.J.; Sanders, David A.R. (2021). Snapshots along the catalytic path of KabA, a PLP-dependent aminotransferase required for kanosamine biosynthesis in Bacillus cereus UW85. *Journal of Structural Biology* 213(2), 107744. 10.1016/j.jsb.2021.107744. [PDB: 7kz3, 7kz5, 7kz6, 7kzd]

Pravica, Michael; Chernikov, Roman; Ayala-Pineda, Kevin; Zhao, Jianbao; Cifligu, Petrika et al. (2021). Observation of pressure-induced electron transfer in SnC2O4. *Physical Chemistry Chemical Physics* 23(10). 10.1039/d1cp00306b.

Proppe, Andrew H.; Johnston, Andrew; Teale, Sam; Mahata, Arup; Quintero-Bermudez, Rafael et al. (2021). Multication perovskite 2D/3D interfaces form via progressive dimensional reduction. *Nature Communications* 12(1). 10.1038/s41467-021-23616-9.

Qiao, Yusen; Ganguly, Gaurab; Booth, Corwin H.; Branson, Jacob A.; Ditter, Alexander S. et al. (2021). Enhanced 5f-δ bonding in [U(C7H7)2]−: C K-edge XAS, magnetism, and ab initio calculations. *Chemical Communications* 57(75), 9562-9565. 10.1039/d1cc03414f.

Quiroz, Ryan V.; Reutershan, Michael H.; Schneider, Sebastian E.; Sloman, David; Lacey, Brian M. et al. (2021). The Discovery of Two Novel Classes of 5,5-Bicyclic Nucleoside-Derived PRMT5 Inhibitors for the Treatment of Cancer. *Journal of Medicinal Chemistry* 64(7), 3911-3939. 10.1021/acs.jmedchem.0c02083. [PDB: 7kib]

Qureshi, Asif; Bussière, Bruno; Benzaazoua, Mostafa; Lessard, Fannie; Boulanger-Martel, Vincent et al. (2021). Geochemical Assessment of Desulphurized Tailings as Cover Material in Cold Climates. *Minerals* 11(3), 280. 10.3390/min11030280.

Radka, Christopher D.; Aller, Stephen G. (2021). Site 2 of the Yersinia pestis substrate-binding protein YfeA is a dynamic surface metal-binding site. Acta Crystallographica Section F:*Structural Biology Communications* 77(9), 286-293. 10.1107/s2053230x21008086. [PDB: 7me1]

Rahman, K.M.M.; Qin, W.; Szpunar, J.A.; Kozinski, J.; Song, M. et al. (2021). New insight into the role of inclusions in hydrogen-induced degradation of fracture toughness: three-dimensional imaging and modeling. The Philosophical Magazine *A Journal of Theoretical Experimental and Applied Physics* 101(8), 1-21.0.1080/14786435.2021.1876267.

Rahman, Noabur; Hangs, Ryan; Peak, Derek; Schoenau, Jeff (2021). Chemical and molecular scale speciation of copper, zinc, and boron in agricultural soils of the Canadian prairies. *Canadian Journal of Soil Science* 101(4). 10.1139/cjss-2020-0162.

Rakhmatullin, Aydar; Molokeev, Maxim S.; King, Graham; Polovov, Ilya B.; Maksimtsev, Konstantin V. et al. (2021). Polymorphs of Rb3ScF6: X-ray and Neutron Diffraction, *Solid-State NMR, and Density Functional Theory Calculations Study. Inorganic Chemistry* 60(8), 6016-6026. 10.1021/acs.inorgchem.1c00485.

Randell, Nicholas M.; Miclette Lamarche, Renaud; Tintori, Franceso; Chernikov, Roman; Welch, Gregory C. et al. (2021). Photodeposited Polyamorphous CuOx Hole-Transport Layers in Organic Photovoltaics. *ACS Applied Energy Materials* 4(11), 12900-12908. 10.1021/acsaem.1c02577.

Rathinaswamy, Manoj K; Gaieb, Zied; Fleming, Kaelin D; Borsari, Chiara; Harris, Noah J et al. (2021). Disease-related mutations in PI3Kγ disrupt regulatory C-terminal dynamics and reveal a path to selective inhibitors. *eLife* 10. 10.7554/elife.64691. [PDB: 7jwe, 7jwz, 7jx0]

Reid, Joel W. (2021). Powder X-ray diffraction data for dimethylarsinic acid, (CH3)2AsO(OH). *Powder Diffraction* 36(3), 190-195. 10.1017/s0885715621000270.

Reid, Joel W.; Kaduk, James A. (2021). Crystal structure of donepezil hydrochloride form III, C24H29NO3–HCl. *Powder Diffraction* 36(4), 233-240. 10.1017/s0885715621000415.

Rippner, Devin A.; Margenot, Andrew J.; Fakra, Sirine C.; Aguilera, L. Andrea; Li, Chongyang et al. (2021). Microbial response to copper oxide nanoparticles in soils is controlled by land use rather than copper fate. *Environmental Science: Nano* 8(12), 3560-3576. 10.1039/d1en00656h.

Rojas-Buzo, Sergio; Bohigues, Benjamin; Lopes, Christian W.; Meira, Débora M.; Boronat, Mercedes et al. (2021). Tailoring Lewis/Brønsted acid properties of MOF nodes via hydrothermal and solvothermal synthesis: simple approach with exceptional catalytic implications. *Chemical Science* 12(29), 10106-10115. 10.1039/d1sc02833b.

Saadati, Shaghayegh; Eduok, Ubong; Westphalen, Heloisa; Abdelrasoul, Amira; Shoker, Ahmed et al. (2021). Assessment of polyethersulfone and polyacrylonitrile hemodialysis clinical membranes: In situ synchrotron-based imaging of human serum proteins adsorption, interaction analyses, molecular docking and clinical inflammatory biomarkers investigations. *Materials Today Communications* 29, 102928. 10.1016/j.mtcomm.2021.102928.

Saadati, Shaghayegh; Eduok, Ubong; Westphalen, Heloisa; Abdelrasoul, Amira; Shoker, Ahmed et al. (2021). In situ synchrotron imaging of human serum proteins interactions, molecular docking and inflammatory biomarkers of hemocompatible synthesized zwitterionic polymer coated-polyvinylidene fluoride (PVDF) dialysis membranes. *Surfaces and Interfaces* 27, 101505. 10.1016/j.surfin.2021.101505.

Sanchez-Cano, Carlos; Alvarez-Puebla, Ramon A.; Abendroth, John M.; Beck, Tobias; Blick, Robert et al. (2021). X-ray-Based Techniques to Study the Nano–Bio Interface. ACS Nano 15(3), 3754-3807. 10.1021/acsnano.0c09563.

Sarker, Tumpa Rani; Azargohar, Ramin; Dalai, Ajay K.; Meda, Venkatesh (2021). Characteristics of torrefied fuel pellets obtained

from co-pelletization of agriculture residues with pyrolysis oil. *Biomass and Bioenergy* 150, 106139. 10.1016/j.biombioe.2021.106139.

Satishkumar, Nidhi; Alexander, J Andrew N; Poon, Raymond; Buggeln, Emma; Argudín, Maria A et al. (2021). PBP4-mediated β-lactam resistance among clinical strains of Staphylococcus aureus. *Journal of Antimicrobial Chemotherapy* 76(9). 10.1093/jac/dkab201. [PDB: 7kcv]

Schenkel, Laurie B.; Molina, Jennifer R.; Swinger, Kerren K.; Abo, Ryan; Blackwell, Danielle J. et al. (2021). A potent and selective PARP14 inhibitor decreases protumor macrophage gene expression and elicits inflammatory responses in tumor explants. *Cell Chemical Biology* 28(8). 10.1016/j.chembiol.2021.02.010. [PDB: 6we2]

Schoen, Martin A. W.; Calderon, Oliver; Randell, Nicholas M.; Jimenez-Villegas, Santiago; Daly, Katelynn M. et al. (2021). Local structural changes in polyamorphous (Ni,Fe)Ox electrocatalysts suggest a dual-site oxygen evolution reaction mechanism. *Journal of Materials Chemistry* A, 13252-13262. 10.1039/d1ta02104d.

Scholl, Connor L.; Tsuda, Sakae; Graham, Laurie A.; Davies, Peter L. (2021). Crystal waters on the nine polyproline type II helical bundle springtail antifreeze protein from Granisotoma rainieri match the ice lattice. *FEBS Journal* 288(14). 10.1111/febs.15717. [PDB: 7jjv]

Schulte, Christie A.; Deaton, David N.; Diaz, Elsie; Do, Young; Gampe, Robert T. et al. (2021). A knowledge-based, structural-aided discovery of a novel class of 2-phenylimidazo[1,2-a]pyridine-6-carboxamide H-PGDS inhibitors. *Bioorganic and Medicinal Chemistry Letters* 47, 128113. 10.1016/j.bmcl.2021.128113. [PDB: 7jr6]

Shafaque, Hisan W.; Lee, Jason K.; Krause, Kevin; Lee, ChungHyuk; Fahy, Kieran F. et al. (2021). Temperature enhances the ohmic and mass transport behaviour in membrane electrode assembly carbon dioxide electrolyzers. *Energy Conversion and Management* 243, 114302. 10.1016/j.enconman.2021.114302.

Shah, Megha; Taylor, Véronique L.; Bona, Diane; Tsao, Yvonne; Stanley, Sabrina Y. et al. (2021). A phage-encoded anti-activator inhibits quorum sensing in Pseudomonas aeruginosa. *Molecular Cell* 81(3), 571-583.e6. 10.1016/j.molcel.2020.12.011. [PDB: 6v7u, 6v7v]

Sharma, Shalini; Zintler, Alexander; Günzing, Damian; Lill, Johanna; Meira, Debora Motta et al. (2021). Epitaxy Induced Highly Ordered Sm2Co17–SmCo5 Nanoscale Thin-Film Magnets. *ACS applied materials interfaces* 13(27), 32415-32423. 10.1021/acsami.1c04780.

Shin, Jeonghee; Park, Sehee; Trinh, Tung X.; Kwon, Sook Jin; Bae, Jiwon et al. (2021). Scanning transmission X-ray microscopy study of subcellular granules in human platelets at the carbon K- and calcium L2,3-edges. *Platelets* 33(4), 1-8.10.1080/09537104.2021.1981846.

Siebers, Nina; Wang, Liming; Funk, Theresa; von Tucher, Sabine; Merbach, Ines et al. (2021). Subsoils—a sink for excess fertilizer P but a minor contribution to P plant nutrition: evidence from long-term fertilization trials. *Environmental Sciences Europe* 33(1), 60. 10.1186/s12302-021-00496-w.

Singh, Harishchandra; Shu, Qifeng; King, Graham; Liang, Ziqing; Wang, Zhifeng et al. (2021). Structure and viscosity of CaO–Al2 O3 –B O3 – BaO slags with varying mass ratio of BaO to CaO. *Journal of the American Ceramic Society* 104(9). 10.1111/jace.17877.

Situm, Arthur; Guo, Xiaoxuan; Barlow, Burke C.; Guo, Bao; Burgess, Ian J. et al. (2021). A Study of the Corrosion of Polymethyl Methacrylate Coated Rebar Using Glancing Angle X-Ray Absorption Near Edge Spectroscopy. *Corrosion* 77(12), 1291-1298. 10.5006/3912.

Skierszkan, Elliott K.; Dockrey, John W.; Helsen, Jordi; Findlater, Laura-Lee; Bataille, Clément P. et al. (2021). Persistence of Uranium in Old and Cold Subpermafrost Groundwater Indicated by Linking 234U-235U-238U, Groundwater Ages, and Hydrogeochemistry. *ACS Earth and Space Chemistry* 5(12), 3474-3487. 10.1021/acsearthspacechem.1c00307.

Smith, Lianna J.D.; Paktunc, Dogan; Blowes, David W. (2021). Trace elements in sulfides and release to porewater from sulfide oxidation in a historical waste-rock pile, Ontario, Canada. *Applied Geochemistry* 126, 104899. 10.1016/j.apgeochem.2021.104899.

Stark, Alison; Filice, Fraser; Noël, James J.; Martin, Ronald R.; Sham, Tsun-Kong et al. (2021). Retrieving Tarnished Daguerreotype Content Using X-ray Fluorescence Imaging—Recent Observations on the Effect of Chemical and Electrochemical Cleaning Methods. *Heritage* 4(3), 1605-1615. 10.3390/heritage4030089.

Stevenson, James; Ngo, Maria; Brandt, Alicia; Weadge, Joel T.; Suits, Michael D. L. et al. (2021). Analysis of Two SusE-Like Enzymes From Bacteroides thetaiotaomicron Reveals a Potential Degradative Capacity for This Protein Family. *Frontiers in Microbiology* 12. 10.3389/fmicb.2021.645765. [PDB: 7m1a, 7m1b]

Su, Chunli; Wang, Sheng; Zhou, Ziyi; Wang, Hongjie; Xie, Xianjun et al. (2021). Chemical processes of Cr(VI) removal by Fe-modified biochar under aerobic and anaerobic conditions and mechanism characterization under aerobic conditions using synchrotron-related techniques. *Science of the Total Environment* 768, 144604. 10.1016/j.scitotenv.2020.144604.

Sudheeshkumar, Veeranmaril; Soong, Charles; Dogel, Stas; Scott, Robert W. J. (2021). Probing the Thermal Stability of (3-Mercaptopropyl)-trimethoxysilane-Protected Au 25 Clusters by In Situ Transmission Electron Microscopy. *Small* 17(27), 2004539. 10.1002/smll.202004539.

Sudheeshkumar, V.; Lavier, Miranda; Lukan, Brianna; Shen, Jing; Semagina, Natalia et al. (2021). Silica-encapsulated palladium clusters for methane combustion catalysis. *Catalysis Today.* 10.1016/j.cattod.2021.11.031.

Sun, Fei; Xiang, Yuxuan; Sun, Qian; Zhong, Guiming; Banis, Mohammad Norouzi et al. (2021). Origin of High Ionic Conductivity of Sc-Doped Sodium-Rich NASICON Solid-State Electrolytes. *Advanced Functional Materials* 31(31), 2102129. 10.1002/adfm.202102129.

Sun, Fei; Xiang, Yuxuan; Sun, Qian; Zhong, Guiming; Banis, Mohammad Norouzi et al. (2021). Insight into Ion Diffusion Dynamics/Mechanisms and Electronic Structure of Highly Conductive Sodium-Rich Na3+xLaxZr2–xSi2PO12 (0 ≤ x ≤ 0.5) Solid-State Electrolytes. *ACS applied materials interfaces* 13(11), 13132-13138. 10.1021/acsami.0c21882.

Sun, Gang; Zhao, Changtai; Yu, Fu-Da; Yu, Ruizhi; Wang, Jian et al. (2021). In-situ surface chemical and structural self-reconstruction strategy enables high performance of Li-rich cathode. *Nano Energy* 79, 105459. 10.1016/j.nanoen.2020.105459.

Sun, Tianxiao; Zhang, Xiangzhi; Xu, Zijian; Wang, Yong; Guo, Zhi et al. (2021). A bidirectional scanning method for scanning transmission X-ray microscopy. Journal of Synchrotron *Radiation* 28(2), 512-517. 10.1107/s1600577520016112.

Su, Rui; Ma, Xu; Lin, Jinru; Yin, Xiuling; Wang, Xin et al. (2021). An alternative method for the treatment of metallurgical arsenic-alkali residue and recovery of high-purity sodium bicarbonate. *Hydrometallurgy* 202, 105590. 10.1016/j.hydromet.2021.105590.

Sylvain, Nicole J.; Salman, Mootaz M.; Pushie, M. Jake; Hou, Huishu; Meher, Vedashree et al. (2021). The effects of trifluoperazine on brain edema, aquaporin-4 expression and metabolic markers during the acute phase of stroke using photothrombotic mouse model. *Biochimica et Biophysica Acta - Biomembranes* 1863(5), 183573. 10.1016/j.bbamem.2021.183573.

Tan, Xuehai; Jiang, Keren; Zhai, Shengli; Zhou, Jigang; Wang, Jian et al. (2021). X-Ray Spectromicroscopy Investigation of Heterogeneous Sodiation in Hard Carbon Nanosheets with Vertically Oriented (002) Planes. *Small* 17(52), 2102109. 10.1002/smll.202102109.

Tomlin, Jay M.; Jankowski, Kevin A.; Veghte, Daniel P.; China, Swarup; Wang, Peiwen et al. (2021). Impact of dry intrusion events on the composition and mixing state of particles during the winter Aerosol and Cloud Experiment in the Eastern North Atlantic (ACE-ENA). *Atmospheric Chemistry and Physics* 21(24), 18123-18146. 10.5194/acp-21-18123-2021.

Ton, Ngoc; Goncin, Una; Panahifar, Arash; Chapman, Dean; Wiebe, Sheldon et al. (2021). Developing a Microbubble-Based Contrast Agent for Synchrotron In-Line Phase Contrast Imaging. *IEEE Transactions on Biomedical Engineering* 68(5), 1527 - 1535. 10.1109/tbme.2020.3040079.

Toplak, Marko; Read, Stuart T.; Sandt, Christophe; Borondics, Ferenc (2021). Quasar: Easy Machine Learning for Biospectroscopy. *Cells* 10(9), 2300. 10.3390/cells10092300.

Tu, Kaiyang; Morhart, Tyler A.; Read, Stuart T.; Rosendahl, Scott M.; Burgess, Ian J. et al. (2021). Probing Heterogeneity in Attenuated Total Reflection Surface-Enhanced Infrared Absorption Spectroscopy (ATR-SEIRAS) Response with Synchrotron Infrared Microspectroscopy. *Applied Spectroscopy* 75(9), 000370282110058. 10.1177/00037028211005817.

Tyvanchuk, Yuriy B.; Fecica, Matthew; Garcia, Griheydi; Mar, Arthur; Oliynyk, Anton O. et al. (2021). Ternary Rare-Earth-Metal Nickel Indides RE23Ni7In4 (RE = Gd, Tb, Dy) with Yb23Cu7Mg4-Type Structure. *Inorganic Chemistry* 60(23), 17900-17910. 10.1021/acs.inorgchem.1c02486.

Udayakantha, Malsha; Handy, Joseph V.; Davidson, Rachel D.; Kaur, Jagjit; Villalpando, Graciela et al. (2021). Halide Replacement with Complete Preservation of Crystal Lattice in Mixed-Anion Lanthanide Oxyhalides. *Angewandte Chemie* 133(28), 15710-15717. 10.1002/ange.202104231.

Udayakantha, Malsha; Handy, Joseph V.; Davidson, Rachel D.; Kaur, Jagjit; Villalpando, Graciela et al. (2021). Halide Replacement with Complete Preservation of Crystal Lattice in Mixed-Anion Lanthanide Oxyhalides. *Angewandte Chemie - International Edition* 60(28). 10.1002/anie.202104231.

Udayakantha, Malsha; Perera, S. Sameera; Davidson, Rachel D.; Zuin, Lucia; Rabuffetti, Federico A. et al. (2021). Structure-Dependent Accessibility of Phonon-Coupled Radiative Relaxation Pathways Probed by X-ray-Excited Optical Luminescence. *Journal of Physical Chemistry Letters* 12(45), 11170-11175. 10.1021/acs.jpclett.1c03103.

Van Loon, Lisa; Alexander, James; Valliant, Mac; Iannicca, Adrienne; Goszczynski, Natalia et al. (2021). Multiple-Scale Synchrotron and Lab Source X-Ray Fluorescence 2D Mapping of Gold Mineralization Styles at the Troilus Gold Project, Frotêt-Evans Greenstone Belt, Quebec, Canada. *Microscopy and Microanalysis* 27(S1), 1544-1547. 10.1017/s1431927621005705.

Vatta, Maritza; Lyons, Bronwyn; Heney, Kayla A.; Lidster, Taylor; Merrill, A. Rod et al. (2021). Mapping the DNA-Binding Motif of Scabin Toxin, a Guanine Modifying Enzyme from Streptomyces scabies. *Toxins* 13(1), 55. 10.3390/toxins13010055. [PDB: 6vuv, 6vv4, 6vvf]

Vickers, Evan T.; Chen, Ziyi; Cherrette, Vivien; Smart, Tyler; Zhang, Peng et al. (2021). Interplay between Perovskite Magic-Sized Clusters and Amino Lead Halide Molecular Clusters. *Research 2021*, 1-7. 10.34133/2021/6047971.

Vogel, Christian; Helfenstein, Julian; Massey, Michael S.; Sekine, Ryo; Kretzschmar, Ruben et al. (2021). Microspectroscopy reveals dust-derived apatite grains in acidic, highly-weathered Hawaiian soils. *Geoderma* 381, 114681. 10.1016/j.geoderma.2020.114681.

Voth, Kevin; Pasricha, Shivani; Chung, Ivy Yeuk Wah; Wibawa, Rachelia R.; Zainudin, Engku Nuraishah Huda E. et al. (2021). Structural and Functional Characterization of Legionella pneumophila Effector MavL. *Biomolecules* 11(12), 1802. 10.3390/biom11121802.

Vuong, Wayne; Fischer, Conrad; Khan, Muhammad Bashir; van Belkum, Marco J.; Lamer, Tess et al. (2021). Improved SARS-CoV-2 Mpro inhibitors based on feline antiviral drug GC376: Structural enhancements, increased solubility, and micellar studies. European *Journal of Medicinal Chemistry* 222, 113584. 10.1016/j.ejmech.2021.113584. [PDB: 7lco, 7ldl]

Vyavhare, Kimaya; Sharma, Vibhu; Sharma, Vinay; Erdemir, Ali; Aswath, Pranesh B. et al. (2021). XANES Study of Tribofilm Formation With Low Phosphorus Additive Mixtures of Phosphonium Ionic Liquid and Borate Ester. *Frontiers in Mechanical Engineering 7*. 10.3389/fmech.2021.671457.

Vyavhare, Kimaya; Timmons, Richard B.; Erdemir, Ali; Aswath, Pranesh B. (2021). Tribological Interaction of Plasma-Functionalized CaCO3 Nanoparticles with Zinc and Ashless Dithiophosphate Additives. *Tribology Letters* 69(2). 10.1007/s11249-021-01423-z.

Vyavhare, Kimaya; Timmons, Richard B.; Erdemir, Ali; Edwards, Brian L.; Aswath, Pranesh B. et al. (2021). Robust Interfacial Tribofilms by Borate- and Polymer-Coated ZnO Nanoparticles Leading to Improved Wear Protection under a Boundary Lubrication Regime. *Langmuir* 37(5), 1743-1759. 10.1021/acs.langmuir.0c02985.

Vyavhare, Kimaya; Timmons, Richard B.; Erdemir, Ali; Edwards, Brian L.; Aswath, Pranesh B. et al. (2021). Tribochemistry of fluorinated ZnO nanoparticles and ZDDP lubricated interface and implications for enhanced anti-wear performance at boundary lubricated contacts. *Wear* 474-475, 203717. 10.1016/j.wear.2021.203717.

Wang, Alana O.; Ptacek, Carol J.; Mack, E. Erin; Blowes, David W. (2021). Impact of multiple drying and rewetting events on biochar amendments for Hg stabilization in floodplain soil from South River, VA. *Chemosphere* 262, 127794. 10.1016/j.chemosphere.2020.127794.

Wang, Changhong; Hwang, Sooyeon; Jiang, Ming; Liang, Jianwen; Sun, Yipeng et al. (2021). Deciphering Interfacial Chemical and Electrochemical Reactions of Sulfide-Based All-Solid-State Batteries. *Advanced Energy Materials* 11(24), 2100210. 10.1002/aenm.202100210.

Wang, Chenjie; Xie, Juan; Chen, Ning; Chen, Weifeng; Bai, Penghui et al. (2021). Non-Noble-Metal Catalyst of Cu/g-C3N4 for Efficient Photocatalytic Hydrogen Evolution. *ACS Applied Energy Materials* 4(12), 13796-13802. 10.1021/acsaem.1c02551.

Wang, Daorui; Deng, Ya-Ping; Zhang, Yongguang; Zhao, Yan; Zhou, Guofu et al. (2021). Defect engineering on three-dimensionally ordered macroporous phosphorus doped Co3O4–δ microspheres as an efficient bifunctional electrocatalyst for Zn-air batteries. *Energy Storage Materials* 41, 427-235. 10.1016/j.ensm.2021.06.017.

Wang, Daorui; Luo, Dan; Zhang, Yongguang; Zhao, Yan; Zhou, Guofu et al. (2021). Deciphering interpenetrated interface of transition metal oxides/phosphates from atomic level for reliable Li/S electrocatalytic behavior. *Nano Energy* 81, 105602. 10.1016/j.nanoen.2020.105602.

Wang, Dongmei; Root, Robert A.; Chorover, Jon (2021). Biochar-templated surface precipitation and inner-sphere complexation effectively removes arsenic from acid mine drainage. *Environmental Science and Pollution Research* 28(33). 10.1007/s11356-021-13869-8.

Wang, Duo; Cao, Liang; Luo, Dan; Gao, Rui; Li, Haibo et al. (2021). Chain mail heterostructured hydrangea-like binary metal sulfides for high efficiency sodium ion battery. *Nano Energy* 87, 106185. 10.1016/j.nanoen.2021.106185.

Wang, Jiayi; Zhao, Yan; Li, Gaoran; Luo, Dan; Liu, Jiabing et al. (2021). Aligned sulfur-deficient ZnS1−x nanotube arrays as efficient catalyzer for high-performance lithium/sulfur batteries. *Nano Energy* 84, 105891. 10.1016/j.nanoen.2021.105891.

Wang, Na; Zhai, Shengli; Ma, Yuanyuan; Tan, Xuehai; Jiang, Keren et al. (2021). Tridentate citrate chelation towards stable fiber zinc-polypyrrole battery with hybrid mechanism. *Energy Storage Materials* 43. 10.1016/j.ensm.2021.10.004.

Wang, Ning; Sun, Qiming; Zhang, Tianjun; Mayoral, Alvaro; Li, Lin et al. (2021). Impregnating Subnanometer Metallic Nanocatalysts into Self-Pillared Zeolite Nanosheets. *Journal of the American Chemical Society* 143(18), 6905-6914. 10.1021/jacs.1c00578.

Wang, Shaofeng; Zeng, Xiangfeng; Lin, Jinru; Yuan, Zidan; Qu, Shan et al. (2021). Molecular Structure of Molybdate Adsorption on Goethite at pH 5–8: A Combined DFT + U, EXAFS, and Ab Initio XANES Study. *Journal of Physical Chemistry* C 125(40), 22052-22063. 10.1021/acs.jpcc.1c05497.

Wang, Shubo; Kistanov, Andrey A.; King, Graham; Ghosh, Sumit; Singh, Harishchandra et al. (2021). In-situ quantification and density functional theory elucidation of phase transformation in carbon steel during quenching and partitioning. *Acta Materialia* 221, 117361. 10.1016/j.actamat.2021.117361.

Wang, Sizhe; Feng, Shaopei; Liang, Jianwen; Su, Qingmei; Zhao, Feipeng et al. (2021). Insight into MoS 2 –MoN Heterostructure to Accelerate Polysulfide Conversion toward High-Energy-Density Lithium–Sulfur Batteries. *Advanced Energy Materials* 11(11), 2003314. 10.1002/aenm.202003314.

Wang, Tong; Luo, Dan; Zhang, Yongguang; Zhang, Zhen; Wang, Jiayi et al. (2021). Hierarchically Porous Ti3C2 MXene with Tunable Active Edges and Unsaturated Coordination Bonds for Superior Lithium–Sulfur Batteries. *ACS Nano* 15(12), 19457-19467. 10.1021/acsnano.1c06213.

Wang, Xin; Luo, Dan; Wang, Jiayi; Sun, Zhenghao; Cui, Guoliang et al. (2021). Strain Engineering of a MXene/CNT Hierarchical Porous Hollow Microsphere Electrocatalyst for a High-Efficiency Lithium Polysulfide Conversion Process. *Angewandte Chemie - International Edition* 60(5). 10.1002/anie.202011493.

Wang, Xue; Ou, Pengfei; Wicks, Joshua; Xie, Yi; Wang, Ying et al. (2021). Gold-in-copper at low *CO coverage enables efficient electromethanation of CO2. *Nature Communications* 12(1). 10.1038/s41467-021-23699-4.

Wang, Xuewan; Wu, Dan; Liu, Suyun; Zhang, Jiujun; Fu, Xian-Zhu et al. (2021). Folic Acid Self-Assembly Enabling Manganese Single-Atom Electrocatalyst for Selective Nitrogen Reduction to Ammonia. *Nano-Micro Letters* 13(1). 10.1007/s40820-021-00651-1.

Wang, Xuewan; Xi, Xiuan; Huo, Ge; Xu, Chenyu; Sui, Pengfei et al. (2021). Co- and N-doped carbon nanotubes with hierarchical pores derived from metal–organic nanotubes for oxygen reduction reaction. *Journal of Energy Chemistry* 53, 49-55. 10.1016/j.jechem.2020.05.020.

Wang, Yajin; Cheng, Wenzheng; Yuan, Pengfei; Yang, Gege; Mu, Shichun et al. (2021). Boosting Nitrogen Reduction to Ammonia on FeN 4 Sites by Atomic Spin Regulation. Advanced Science 8(20), 2102915. 10.1002/advs.202102915.

Wang, Yihao; Yang, Jianjun; Han, Hui; Hu, Yongfeng; Wang, Jian et al. (2021). Differential transformation mechanisms of exotic Cr(VI) in agricultural soils with contrasting physio-chemical and biological properties. *Chemosphere* 279, 130546. 10.1016/j.chemosphere.2021.130546.

Ward, Matthew; Regier, Tom; Vogt, Johannes; Han, Wei-Qiang; Sham, Tsun-Kong et al. (2021). Direct Observation of Optical Band Gap Components in Ga1−xZnxN1−xOx Solid-Solution Nanoparticles. *Journal of Physical Chemistry* C 125(35), 19438-19444. 10.1021/acs.jpcc.1c04016.

Wen, Yunzhou; Chen, Peining; Wang, Lu; Li, Shangyu; Wang, Ziyun et al. (2021). Stabilizing Highly Active Ru Sites by Suppressing Lattice Oxygen Participation in Acidic Water Oxidation. *Journal of the American Chemical Society* 143(17), 6482-6490. 10.1021/jacs.1c00384.

Westphalen, Heloisa; Abdelrasoul, Amira; Shoker, Ahmed; Zhu, Ning (2021). Assessment of hemodialysis clinical practices using polyaryl ether sulfone-polyvinylpyrrolidone (PAES: PVP) clinical membrane: Modeling of in vitro fibrinogen adsorption, in situ synchrotron-based imaging, and clinical inflammatory biomarkers investigations. *Separation and Purification Technology* 259, 118136. 10.1016/j.seppur.2020.118136.

Wigle, Tim J.; Ren, Yue; Molina, Jennifer R.; Blackwell, Danielle J.; Schenkel, Laurie B. et al. (2021). Targeted Degradation of PARP14 Using a Heterobifunctional Small Molecule. *ChemBioChem* 22(12). 10.1002/cbic.202100047. [PDB: 7l9y]

Workman, Sean D.; Day, Jonathan; Farha, Maya A.; El Zahed, Sara S.; Bon, Chris et al. (2021). Structural Insights into the Inhibition of Undecaprenyl Pyrophosphate Synthase from Gram-Positive Bacteria. *Journal of Medicinal Chemistry* 64(18), 13540–13550. 10.1021/acs.jmedchem.1c00941. [PDB: 7jli]

Wu, Dan; Feng, Renfei; Xu, Chenyu; Sui, Peng-Fei; Zhang, Jiujun et al. (2021). Regulating the Electron Localization of Metallic Bismuth for Boosting CO2 Electroreduction. *Nano-Micro Letters* 14(1). 10.1007/s40820-021-00772-7.

Wu, Lizhi; Ren, Zhuangzhuang; He, Yongsheng; Yang, Meng; Yu, Yunkai et al. (2021). Atomically Dispersed Co2+ Sites Incorporated into a Silicalite-1 Zeolite Framework as a High-Performance and Coking-Resistant Catalyst for Propane Nonoxidative Dehydrogenation to Propylene. *ACS applied materials interfaces* 13(41), 48934–48948. 10.1021/acsami.1c15892.

Wu, Mingjie; Zhang, Gaixia; Chen, Ning; Hu, Yongfeng; Regier, Tom et al. (2021). Self-Reconstruction of Co/Co2P Heterojunctions Confined in N-Doped Carbon Nanotubes for Zinc–Air Flow Batteries. *ACS Energy Letters*, 1153-1161. 10.1021/acsenergylett.1c00037.

Wu, Mingjie; Zhang, Gaixia; Tong, Hui; Liu, Xianhu; Du, Lei et al. (2021). Cobalt (II) oxide nanosheets with rich oxygen vacancies as highly efficient bifunctional catalysts for ultra-stable rechargeable Zn-air flow battery. *Nano Energy* 79, 105409. 10.1016/j.nanoen.2020.105409.

Xia, Chuan; Qiu, Yunrui; Xia, Yang; Zhu, Peng; King, Graham et al. (2021). General synthesis of single-atom catalysts with high metal loading using graphene quantum dots. *Nature Chemistry* 13(9). 10.1038/s41557-021-00734-x.

Xiao, Meiling; Zhu, Jianbing; Li, Shuang; Li, Gaoran; Liu, Wenwen et al. (2021). 3d-Orbital Occupancy Regulated Ir-Co Atomic Pair Toward Superior Bifunctional Oxygen Electrocatalysis. *ACS Catalysis* 11(14), 8837-8846. 10.1021/acscatal.1c02165.

Xie, Juan; Wang, Chenjie; Chen, Ning; Chen, Weifeng; Xu, Jiake et al. (2021). Highly active g-C3N4 photocatalysts modified with transition metal cobalt for hydrogen evolution. *Journal of Materials Chemistry* C 9(12), 4378-4384. 10.1039/d0tc05338d.

Xing, Zhenjiang; Xu, Zijian; Zhang, Xiangzhi; Chen, Bo; Guo, Zhi et al. (2021). Virtual depth-scan multi-slice ptychography for improved three-dimensional imaging. *Optics Express* 29(11), 16214. 10.1364/oe.422214.

Xin, Xiaying; Huang, Guohe; Halstead, David; Gaetz, Katelyn; Benmerrouche, Leila et al. (2021). The Optimization of Canola Crop Production through Wheat Residue Management within a Western Canadian Context—A Case Study of Saint-Front, Saskatchewan. *Sustainability* 13(18), 10459. 10.3390/su131810459.

Xin, Xiaying; Huang, Guohe; Zhang, Baiyu; Zhou, Yang (2021). Trophic transfer potential of nTiO2, nZnO, and triclosan in an algae-algae eating fish food chain. *Aquatic Toxicology* 235, 105824. 10.1016/j.aquatox.2021.105824.

Xu, Chenyu; Zhang, Xuhan; Zhu, Meng-Nan; Zhang, Li; Sui, Peng-Fei et al. (2021). Accelerating photoelectric CO2 conversion with a photothermal wavelength-dependent plasmonic local field. *Applied Catalysis B: Environmental* 298, 120533. 10.1016/j.apcatb.2021.120533.

Xu, Shuai; Zhou, Jigang; Wang, Jian; Pathiranage, Sameera; Oncel, Nuri et al. (2021). In Situ Synthesis of Graphene-Coated Silicon Monoxide Anodes from Coal-Derived Humic Acid for High-Performance Lithium-Ion Batteries. *Advanced Functional Materials* 31(32), 2101645. 10.1002/adfm.202101645.

Xu, Yuanmei; Zhang, Wenna; Ma, Heng; Zhou, Guofu; Zhang, Yongguang et al. (2021). Engineering the 3D framework of defective phosphorene-based sulfur cathodes for high-efficiency lithium-sulfur batteries. *Electrochimica Acta* 392, 139025. 10.1016/j.electacta.2021.139025.

Yan, Bei; Wang, Jian; Liu, Jinxia (2021). STXM-XANES and computational investigations of adsorption of per- and polyfluoroalkyl substances on modified clay. *Water Research* 201, 117371. 10.1016/j.watres.2021.117371.

Yang, Gege; Zhu, Jiawei; Yuan, Pengfei; Hu, Yongfeng; Qu, Gan et al. (2021). Regulating Fe-spin state by atomically dispersed Mn-N in Fe-N-C catalysts with high oxygen reduction activity. *Nature Communications* 12(1), 1734. 10.1038/s41467-021-21919-5.

Yang, Liuqing; De-Jager, Cindy Rae; Adsetts, Jonathan Ralph; Chu, Kenneth; Liu, Kehan et al. (2021). Analyzing Near-Infrared Electrochemiluminescence of Graphene Quantum Dots in Aqueous Media. *Analytical Chemistry* 93(36). 10.1021/acs.analchem.1c02441.

Yang, Peng; Wen, Ke; Beyer, Kevin A.; Xu, Wenqian; Wang, Qian et al. (2021). Inhibition of Oxyanions on Redox-driven Transformation of Layered Manganese Oxides. *Environmental Science Technology* 55(5), 3419-3429. 10.1021/acs.est.0c06310.

Yang, Xiaohan; Huang, Guohe; An, Chunjiang; Chen, Xiujuan; Shen, Jian et al. (2021). Removal of arsenic from water through ceramic filter modified by nano-CeO2: A cost-effective approach for remote areas. *Science of the Total Environment* 750, 141510. 10.1016/j.scitotenv.2020.141510.

Yang, Xinru; Liu, Peng; Yao, Meng; Sun, He; Liu, Ruxue et al. (2021). Mechanism and enhancement of Cr(VI) contaminated groundwater remediation by molasses. *Science of the Total Environment* 780, 146580. 10.1016/j.scitotenv.2021.146580.

Yang, Yuhong; Xu, Yuanyuan; Yue, Yuan; Wang, Heng; Cui, Yumeng et al. (2021). Investigate Natural Product Indolmycin and the Synthetically Improved Analogue Toward Antimycobacterial Agents. *ACS Chemical Biology* 17(1), 39-53. 10.1021/acschembio.1c00394. [PDB: 7ent, 7ev3]

Yao, Yonggang; Huang, Zhennan; Hughes, Lauren A.; Gao, Jinlong; Li, Tangyuan et al. (2021). Extreme mixing in nanoscale transition metal alloys. *Matter* 4(7). 10.1016/j.matt.2021.04.014.

Yasri, Nael G.; Al-Attas, Tareq A.; Hu, Jinguang; Kibria, Md Golam (2021). Electropolymerized metal-protoporphyrin electrodes for selective electrochemical reduction of CO2. *Catalysis Science and Technology* 11(4), 1580-1589. 10.1039/d0cy02150d.

Yin, Jianan; Huang, Guohe; An, Chunjiang; Zhang, Peng; Xin, Xiaying et al. (2021). Exploration of nanocellulose washing agent for the green remediation of phenanthrene-contaminated soil. *Journal of Hazardous Materials* 403, 123861. 10.1016/j.jhazmat.2020.123861.

Yin, Xiuling; Zhang, Guoqing; Su, Rui; Zeng, Xiangfeng; Yan, Zelong et al. (2021). Oxidation and incorporation of adsorbed antimonite during iron(II)-catalyzed recrystallization of ferrihydrite. *Science of the Total Environment* 778, 146424. 10.1016/j.scitotenv.2021.146424.

Yoshinaka, Akio; Desgreniers, Serge; Hu, Anguang (2021). Nitroethane at high density: an experimental and computational vibrational study. *Physical Chemistry Chemical Physics* 23(15), 9325-9336. 10.1039/d0cp06557a.

Yuan, Hao; Yuan, Hui; Casagrande, Travis; Shapiro, David; Yu, Young-Sang et al. (2021). 4D Imaging of ZnO-Coated Nanoporous Al2O3 Aerogels by Chemically Sensitive Ptychographic Tomography: Implications for Designer Catalysts. *ACS Applied Nano Materials* 4(1), 621-632. 10.1021/acsanm.0c02924.

Yu, Ruizhi; Banis, Mohammad Norouzi; Wang, Changhong; Wu, Bing; Huang, Yan et al. (2021). Tailoring bulk Li+ ion diffusion kinetics and surface lattice oxygen activity for high-performance lithium-rich manganese-based layered oxides. *Energy Storage Materials* 37, 509-520. 10.1016/j.ensm.2021.02.025.

Zhang, Chunzi; Koughia, Cyril; Zhu, Jianfeng; Feng, Renfei; Gunes, Ozan et al. (2021). Self-assembled single crystal VO2 (A) microbelts by the reduction of V2O5 thin films: synthesis, structure and optical properties. *Journal of Alloys and Compounds* 863, 158728. 10.1016/j.jallcom.2021.158728.

Zhang, Lijie; Zhuang, Linzhou; Liu, Hongli; Zhang, Longzhou; Cai, Rongsheng et al. (2021). Beyond Platinum: Defects Abundant CoP 3 / Ni 2 P Heterostructure for Hydrogen Evolution Electrocatalysis. *Small Science* 1(4), 2000027. 10.1002/smsc.202000027.

Zhang, Maiwen; Liang, Ruilin; Yang, Na; Gao, Rui; Zheng, Yun et al. (2021). Eutectic Etching toward In-Plane Porosity Manipulation of Cl-Terminated MXene for High-Performance Dual-Ion Battery Anode. *Advanced Energy Materials* 12(1), 2102493. 10.1002/aenm.202102493.

Zhang, Shumin; Zhao, Feipeng; Wang, Shuo; Liang, Jianwen; Wang, Jian et al. (2021). Advanced High-Voltage All-Solid-State Li-Ion Batteries Enabled by a Dual-Halogen Solid Electrolyte. *Advanced*

Energy Materials 11(32), 2100836. 10.1002/aenm.202100836.

Zhang, Tianjun; Walsh, Andrew G.; Yu, Jihong; Zhang, Peng (2021). Single-atom alloy catalysts: structural analysis, electronic properties and catalytic activities. *Chemical Society Reviews* 50(1), 569-588. 10.1039/d0cs00844c.

Zhang, Xiaomin; Li, Gaoran; Zhang, Yongguang; Luo, Dan; Yu, Aiping et al. (2021). Amorphizing metal-organic framework towards multifunctional polysulfide barrier for high-performance lithium-sulfur batteries. *Nano Energy* 86, 106094. 10.1016/j.nanoen.2021.106094.

Zhang, Xiaomin; Wang, Jiayi; Wang, Xingbo; Li, Yebao; Zhao, Yan et al. (2021). 3D ordered macroporous amorphous Nb2O5 as anode material for high-performance sodium-ion batteries. *Applied Surface Science* 567, 150862. 10.1016/j.apsusc.2021.150862.

Zhang, Yongguang; Liu, Jiabing; Wang, Jiayi; Zhao, Yan; Luo, Dan et al. (2021). Engineering Oversaturated Fe-N 5 Multifunctional Catalytic Sites for Durable Lithium-Sulfur Batteries. *Angewandte Chemie - International Edition* 60(51), 26622-26629. 10.1002/anie.202108882.

Zhang, Yunhui; Alessi, Daniel S.; Chen, Ning; Luo, Mina; Hao, Weiduo et al. (2021). Lead (Pb) sorption to hydrophobic and hydrophilic zeolites in the presence and absence of MTBE. *Journal of Hazardous Materials* 420, 126528. 10.1016/j.jhazmat.2021.126528.

Zhang, Yuzhou; Hirpara, Viral; Patel, Virat; Li, Chen; Anderson, Ryan et al. (2021). Imaging of desaturation of the frozen gas diffusion layers by synchrotron X-ray radiography. International *Journal of Hydrogen Energy* 46(34), 17897-17908. 10.1016/j.ijhydene.2021.02.197.

Zhang, Zhen; Wen, Guobin; Luo, Dan; Ren, Bohua; Zhu, Yanfei et al. (2021). "Two Ships in a Bottle" Design for Zn–Ag–O Catalyst Enabling Selective and Long-Lasting CO2 Electroreduction. *Journal of the American Chemical Society* 143(18), 6855-6864. 10.1021/jacs.0c12418.

Zhang, Zhifeng; Walsh, Andrew G.; Zhang, Peng (2021). Dynamic Structure of Metal Nanoclusters from Synchrotron X-ray Spectroscopy. *Journal of Physical Chemistry* C 125(11), 5982-5994. 10.1021/acs.jpcc.0c11298.

Zhang, Zhuojun; Zhao, Zhiqi; Liu, Congqiang; Chadwick, Oliver A.; Liang, Chao et al. (2021). Vertical patterns of phosphorus concentration and speciation in three forest soil profiles of contrasting climate. *Geochimica et Cosmochimica* Acta 310, 1-18. 10.1016/j.gca.2021.07.002.

Zhao, Bin; Liu, Jianwen; Feng, Renfei; Wang, Lei; Zhang, Jiujun et al. (2021). Less-Energy Consumed Hydrogen Evolution Coupled with Electrocatalytic Removal of Ethanolamine Pollutant in Saline Water over Ni@Ni 3 S 2 /CNT Nano-Heterostructured Electrocatalysts. *Small Methods* 6(3), 2101195. 10.1002/smtd.202101195.

Zhao, Bin; Liu, Jianwen; Wang, Xuewan; Xu, Chenyu; Sui, Pengfei et al. (2021). CO2-emission-free electrocatalytic CH3OH selective upgrading with high productivity at large current densities for energy saved hydrogen co-generation. *Nano Energy* 80, 105530. 10.1016/j.nanoen.2020.105530.

Zhao, Bin; Liu, Jianwen; Xu, Chenyu; Feng, Renfei; Sui, Pengfei et al. (2021). Interfacial engineering of Cu2Se/Co3Se4 multivalent hetero-nanocrystals for energy-efficient electrocatalytic co-generation of value-added chemicals and hydrogen. *Applied Catalysis B: Environmental* 285, 119800. 10.1016/j.apcatb.2020.119800.

Zhao, Feipeng; Alahakoon, Sandamini H.; Adair, Keegan; Zhang, Shumin; Xia, Wei et al. (2021). An Air-Stable and Li-Metal-Compatible Glass-Ceramic Electrolyte enabling High-Performance All-Solid-State Li Metal Batteries. *Advanced Materials* 33(8), 2006577. 10.1002/adma.202006577.

Zhao, Zhao; Wang, Dandan; Gao, Rui; Wen, Guobin; Feng, Ming et al. (2021). Magnetic-Field-Stimulated Efficient Photocatalytic N 2 Fixation over Defective BaTiO 3 Perovskites. *Angewandte Chemie* 133(21), 12017-12025. 10.1002/ange.202100726.

Zheng, Matthew; Gao, Xuejie; Sun, Yipeng; Adair, Keegan; Li, Minsi et al. (2021). Realizing High-Performance Li-S Batteries through Additive Manufactured and Chemically Enhanced Cathodes. *Small Methods* 5(9), 2100176. 10.1002/smtd.202100176.

Zhou, Qingyan; Cai, Jiajun; Zhang, Zhen; Gao, Rui; Chen, Bo et al. (2021). A Gas-Phase Migration Strategy to Synthesize Atomically Dispersed Mn-N-C Catalysts for Zn–Air Batteries. *Small Methods* 5(6), 2100024. 10.1002/smtd.202100024.

Zhuang, Shuxin; Jia, Deli; Wang, Quanbin; Hu, Yongfeng; Zhang, Minshu et al. (2021). Insight into the inhomogeneous capacity distribution characteristic of LiFePO4 cathode in large-format lithium ion cell. *Ceramics International* 47(7), 9132-9136. 10.1016/j.ceramint.2020.12.037.

Zhu, Lihua; Zhu, Huaze; Shakouri, Mohsen; Zeng, Linghai; Yang, Zhiqing et al. (2021). Mechanistic insights into interfacial nano-synergistic effects in trimetallic Rh-on-NiCo on-CNTs for room temperature solvent-free hydrogenations. *Applied Catalysis B: Environmental* 297, 120404. 10.1016/j.apcatb.2021.120404.

Zhu, Xiaodong; Cao, Ziyi; Wang, Wenjie; Li, Haijing; Dong, Juncai et al. (2021). Superior-Performance Aqueous Zinc-Ion Batteries Based on the In Situ Growth of MnO2 Nanosheets on V2CTX MXene. *ACS Nano* 15(2), 2971-2983. 10.1021/acsnano.0c09205.

Zhu, Yanfang; Xu, Guiyang; Song, Wenqi; Zhao, Yuzhen; He, Zemin et al. (2021). Anchoring single Ni atoms on defected 2D MXene nanosheets as an efficient electrocatalyst for enhanced hydrogen evolution reaction. *Ceramics International* 47(21), 30005-30011. 10.1016/j.ceramint.2021.07.175.

Zhu, Yanfei; Li, Gaoran; Luo, Dan; Wan, Hui; Feng, Ming et al. (2021). Unsaturated coordination polymer frameworks as multifunctional sulfur reservoir for fast and durable lithium-sulfur batteries. *Nano Energy* 79, 105393. 10.1016/j.nanoen.2020.105393.

Zuhaib, Amara; Urquhart, Stephen G. (2021). Internal molecular conformation of organic glasses: A NEXAFS study. *Journal of Chemical Physics* 155(3), 034503. 10.1063/5.0054442.

BOOKS AND CHAPTER

Zhou, Jigang; Wang, Jian (2021). Applications of Soft X-ray Spectromicroscopy in Energy Research from Materials to Batteries. In Jiajun Wang(Ed.), Advanced X-ray Imaging of Electrochemical Energy Materials and Devices. *Singapore: Springer.*, 141-178 10.1007/978-981-16-5328-5_7.

PDB DEPOSITION

Alexander, J.A.N.; Strynadka, N.C.J. (2021). Crystal structure of S. aureus penicillin-binding protein 4 (PBP4) mutant (R200L). Protein Data Bank: 7kcv.

Alexander, J.A.N.; Strynadka, N.C.J. (2021). Crystal structure of S. aureus penicillin-binding protein 4 (PBP4) mutant (R200L) in complex with cefoxitin. Protein Data Bank: 7kcx.

Alexander, J.A.N.; Strynadka, N.C.J. (2021). Crystal structure of S. aureus penicillin-binding protein 4 (PBP4) with cefoxitin. Protein Data Bank: 7kcy.

Alexander, J.A.; Strynadka, N.C. (2021). Crystal structure of S. aureus penicillin-binding protein 4 (PBP4) mutant (R200L) in complex with nafcillin. Protein Data Bank: 7kcw.

Bassenden, A.V.; Berghuis, A.M. (2021). Aminoglycoside N-2'-Acetyltransferase-Ia [AAC(2')-Ia] in complex with acetylated-plazomicin and CoA. Protein Data Bank: 6vou.

Bateman, T.J.; Shah, M.; Moraes, T.F. (2021). Holo Hemophilin from A. baumannii. Protein Data Bank: 7red.

Bateman, T.J.; Shah, M.; Moraes, T.F. (2021). Apo Hemophilin from A. baumannii. Protein Data Bank: 7rea.

Bateman, T.J.; Shah, M.; Moraes, T.F. (2021). Apo Hemophilin from A. baumannii. Protein Data Bank: 7re4.

Boniecki, M.T.; Cygler, M. (2021). Structure of the (NIAU)2 complex with N-terminal mutation of ISCU2 Y35D at 2.5 A resolution. Protein Data Bank: 7rtk.

Boniecki, M.T.; Uhlemann, E.E.; Dmitriev, O.Y. (2021). Structure of iron bound MEMO1. Protein Data Bank: 7kq8.

Burke, J.E.; Rathinaswamy, M.K.; Harris, N.J. (2021). Gedatolisib bound to the PI3Kg catalytic subunit p110 gamma. Protein Data Bank: 7jwe.

Burke, J.E.; Rathinaswamy, M.K.; Harris, N.J. (2021). NVS-PI3-4 bound to the PI3Kg catalytic subunit p110 gamma. Protein Data Bank: 7jx0.

Burke, J.E.; Rathinaswamy, M.K.; Harris, N.J. (2021). IPI-549 bound to the PI3Kg catalytic subunit p110 gamma. Protein Data Bank: 7jwz.

Chen, S.; Lu, M. (2021). Arsenic-bound p53 DNA-binding domain mutant R249S. Protein Data Bank: 7dhz.

Chen, Y.S.; Kozlov, G.; Gehring, K. (2021). Crystal structure of an archaeal CNNM, MtCorB, with C-terminal deletion in complex with Mg2+-ATP. Protein Data Bank: 7m1t.

Chen, Y.S.; Kozlov, G.; Gehring, K. (2021). Crystal structure of an archaeal CNNM, MtCorB, R235L mutant with C-terminal deletion. Protein Data Bank: 7m1u.

Chen; Y.S.; Kozlov; G.; Gehring et al. (2021). Crystal structure of MtCNNM with C-terminal deletion in complex with Mg2+-ATP. Protein Data Bank: 7lj7.

Cleland, C.P.; Mosimann, S.C. (2021). Structure of the PTP-like myo-inositol phosphatase from Desulfovibrio magneticus in complex with myo-inositol hexakisphosphate. Protein Data Bank: 7k6w.

Cleland, C.P.; Van Herk, P.H.; Mosimann, S.C. (2021). Structure of the PTP-like myo-inositol phosphatase from Desulfovibrio magneticus. Protein Data Bank: 7k67.

Cygler, M.; Chung, I.Y.W. (2021). Structure of Legionella Effector LegA15. Protein Data Bank: 7kj6.

Cygler, M.; Chung, I.Y.W. (2021). Structure of RavA (lpp0008) E38A/K39A surface entropy reduction mutant. Protein Data Bank: 6wo6.

Dorsey, B.W.; Swinger, K.K.; Schenkel, L.B.; Church, W.D.; Perl, N.R. et al. (2021). Human PARP14 (ARTD8), catalytic fragment in complex with RBN012042. Protein Data Bank: 7l9y.

Ereno-Orbea, J.; Nilvebrant, J.; Sidhu, S.; Julien, J.P. (2021). Anti-EphA1 JD1 VH domain. Protein Data Bank: 7ooi.

Ereno-Orbea, J.; Sicard, T.; Julien, J.P. (2021). CD22 d6-d7 in complex with Fab m971. Protein Data Bank: 7o52.

Ereno-Orbea, J.; Sicard, T.; Julien, J.P. (2021). m971 Fab in complex with anti-Kappa VHH domain. Protein Data Bank: 7o4y.

Gerak; C.A.N.; Kolesnikov; M.; Murphy et al. (2021). Crystal structure of the monomeric ETV6 PNT domain. Protein Data Bank: 7ju2.

Golkar, T.; Berghuis, A.M.; Schmeing, T.M. (2021). Crystal structure of the Thermus thermophilus 70S ribosome in complex with plazomicin, mRNA and tRNAs. Protein Data Bank: 7lh5.

Guo, S.; Davies, P.L. (2021). Peptide-bound structure of Marinomonas primoryensis peptide-binding domain. Protein Data Bank: 6x5w.

Guo, S.; Davies, P.L. (2021). Peptide-bound structure of Marinomonas primoryensis peptide-binding domain. Protein Data Bank: 6x5v.

Guo, S.; Davies, P.L. (2021). fucose-bound structure of Marinomonas primoryensis PA14 carbohydrate-binding domain. Protein Data Bank: 6x7j.

Guo, S.; Davies, P.L. (2021). Allose-bound structure of Marinomonas primoryensis PA14 carbohydrate-binding domain. Protein Data Bank: 6x7t.

Guo, S.; Davies, P.L. (2021). Alpha-methyl-glucose-bound structure of Marinomonas primoryensis PA14 carbohydrate-binding domain. Protein Data Bank: 6xaq.

Guo, S.; Davies, P.L. (2021). Trehalose-bound structure of Marinomonas primoryensis PA14 carbohydrate-binding domain. Protein Data Bank: 6xa5.

Guo, S.; Davies, P.L. (2021). Ribose-bound structure of Marinomonas primoryensis PA14 carbohydrate-binding domain. Protein Data Bank: 6x8y.

Guo, S.; Davies, P.L. (2021). 3-O-methyl-glucose-bound structure of Marinomonas primoryensis PA14 carbohydrate-binding domain. Protein Data Bank: 6x9m.

Guo, S.; Davies, P.L. (2021). 2-deoxyribose-bound structure of Marinomonas primoryensis PA14 carbohydrate-binding domain. Protein Data Bank: 6x9p.

Guo, S.; Davies, P.L. (2021). N-acetyl-glucosamine-bound structure of Marinomonas primoryensis PA14 carbohydrate-binding domain. Protein Data Bank: 6x7y.

Guo, S.; Davies, P.L. (2021). Inositol-bound structure of Marinomonas primoryensis PA14 carbohydrate-binding domain. Protein Data Bank: 6x7z.

Guo, S.; Davies, P.L. (2021). Arabinose-bound structure of Marinomonas primoryensis PA14 carbohydrate-binding domain. Protein Data Bank: 6x8d.

Guo, S.; Davies, P.L. (2021). Sucrose-bound structure of Marinomonas primoryensis PA14 carbohydrate-binding domain. Protein Data Bank: 6x8a.

Guo, S.; Davies, P.L. (2021). 2-deoxy-glucose-bound structure of Marinomonas primoryensis PA14 carbohydrate-binding domain. Protein Data Bank: 6x95.

Guo, Y.; Dong, A.; Hou, F.; Li, Y.; Zhang, W. et al. (2021). Crystal structure of STAMBPL1 in complex with an engineered binder. Protein Data Bank: 7l97.

Heney; K.; Lyons; B.; Merrill et al. (2021). Scabin (Y129H) toxin from Streptomyces scabies. Protein Data Bank: 6vvf.

Heney; K.; Lyons; B.; Merrill et al. (2021). Scabin (V109G) toxin from Streptomyces scabies. Protein Data Bank: 6vv4.

Higgins, M.A.; Ryan, K.S. (2021). Crystal structure of GH5_18 from Bifidobacterium longum subsp. longum ATCC 55813. Protein Data Bank: 7lr1.

Higgins, M.A.; Ryan, K.S. (2021). Crystal structure of a GH5_18 from Bifidobacterium longum subsp. infantis. Protein Data Bank: 7lqx.

Huang, J.; Fraser, M.E. (2021). GTP-specific succinyl-CoA synthetase complexed with Mg-GMPPNP, phosphohistidine loop pointing towards nucleotide binding site. Protein Data Bank: 7jkr.

Huang, J.; Fraser, M.E. (2021). GTP-specific succinyl-CoA synthetase complexed with Mg-GMPPCP. Protein Data Bank: 7jj0.

Kalthoff, E.; Schmeing, M. (2021). Crystal structure of the M. abscessus LeuRS editing domain in complex with epetraborole-AMP adduct. Protein Data Bank: 7n12.

Khan, J.A. (2021). Crystal structure of myeloperoxidase subform c

(mpo) complex with compound-30 aka 7-[(3~{S},4~{R},6~{R})-4-benzyl-2-oxa-7,13,14-triazatetracyclo[14.3.1.1^{3,6}.1^{11,14}]docosa-1(19),11(21),12,16(20),17-pentaen-10-yl]-3~{H}-triazolo[4,5-b]pyridin-5-amine. Protein Data Bank: 7lan.

Khan, J.A. (2021). Crystal structure of myeloperoxidase subform c (mpo) complex with Compound-14 AKA 7-({1-[(3-phenoxyphenyl) methyl]-1H-pyrazol-4-yl}methyl)-3H-[1,2,3]triazolo[4,5-b]pyridin-5-amine. Protein Data Bank: 7lag.

Khan, M.B.; Lu, J.; Arutyunova, E.; Young, H.S.; Lemieux, M.J. et al. (2021). Improved Feline Drugs as SARS-CoV-2 Mpro Inhibitors: Structure-Activity Studies Micellar Solubilization for Enhanced Bioavailability. Protein Data Bank: 7lco.

Khan, M.B.; Lu, J.; Arutyunova, E.; Young, H.S.; Lemieux, M.J. et al. (2021). Improved Feline Drugs as SARS-CoV-2 Mpro Inhibitors: Structure-Activity Studies Micellar Solubilization for Enhanced Bioavailability. Protein Data Bank: 7ldl.

Kimber, M.S.; Forrester, T.J.B. (2021). Cannabis sativa bibenzyl synthase. Protein Data Bank: 7sgy.

Kimber, M.S.; Stirling, A.J.; Seah, S.Y.K. (2021). Tcur3481-Tcur3483 steroid ACAD. Protein Data Bank: 6wy8.

Klein, D.J.; Beshore, D.C. (2021). STRUCTURE OF HUMAN HDAC2 IN COMPLEX WITH APICIDIN. Protein Data Bank: 7ltg.

Kuatsjah, E.; Chan, A.C.; Katahira, R.; Beckham, G.T.; Murphy, M.E. et al. (2021). Crystal structure of DCA-S bound to Co-LSD4 from Sphingobium sp. strain SYK-6. Protein Data Bank: 6xm7.

Kuatsjah, E.; Chan, A.C.; Katahira, R.; Beckham, G.T.; Murphy, M.E. et al. (2021). Crystal structure of cobalt-bound LSD4 from Sphingobium sp. strain SYK-6. Protein Data Bank: 6xm6.

Kuatsjah, E.; Chan, A.C.; Katahira, R.; Beckham, G.T.; Murphy, M.E. et al. (2021). Crystal structure of lignostilbene bound to Co-LSD4 from Sphingobium sp. strain SYK-6. Protein Data Bank: 6xm8.

Kuduk, S.D.; Stoops, B.; Alexander, R.; Lam, A.M.; Espiritu, C. et al. (2021). CRYSTAL STRUCTURE OF HBV CAPSID Y132A MUTANT IN COMPLEX WITH N-(3-chloro-4-fluorophenyl)-3-phenyl-1,4,6,7-tetrahydro-5H-pyrazolo[4,3-c] pyridine-5-carboxamide AT 2.65A RESOLUTION. Protein Data Bank: 7k5m.

Kumar, A. (2021). Structure of human Galectin-3 CRD in complex with TD-139 belonging to P31 space group.. Protein Data Bank: 7cxa.

Liang; J.; Naineni; S.K.; Pelletier et al. (2021). Crystal structure of eIF4A-I in complex with RNA bound to des-MePateA, a pateamine A analog. Protein Data Bank: 6xki.

Li, F.K.K.; Strynadka, N.C.J. (2021). Crystal structure of S. aureus TarJ in complex with NADPH. Protein Data Bank: 6xhk.

Li, F.K.K.; Strynadka, N.C.J. (2021). Crystal structure of S. aureus TarI in complex with CDP-ribitol (space group P1211). Protein Data Bank: 6xht.

Li, F.K.K.; Strynadka, N.C.J. (2021). Crystal structure of S. aureus TarI (space group P1211). Protein Data Bank: 6xhr.

Li, F.K.K.; Strynadka, N.C.J. (2021). Crystal structure of S. aureus TarI in complex with CTP (space group P1211). Protein Data Bank: 6xhs.

Li, F.K.K.; Strynadka, N.C.J. (2021). Crystal structure of S. aureus TarI (space group C121). Protein Data Bank: 6xhp.

Li, F.K.K.; Strynadka, N.C.J. (2021). Crystal structure of S. aureus TarI in complex with CDP-ribitol (space group C121). Protein Data Bank: 6xhq.

Li, F.K.K.; Strynadka, N.C.J. (2021). Crystal structure of S. aureus TarJ. Protein Data Bank: 6xh9.

Lin, C.S.; Chan, A.C.; Murphy, M.E. (2021). Crystal structure of the helical cell shape determining protein Pgp2 (K307A mutant) from Campylobacter jejuni. Protein Data Bank: 6xj7.

Li; Z.; Rini; J.M. (2021). SARS-CoV-2 RBD in complex with Fab 15033. Protein Data Bank: 7klg.

Li; Z.; Rini; J.M. (2021). SARS-CoV-2 RBD in complex with Fab 15033-7. Protein Data Bank: 7klh.

Lyons; B.; Lidster; T.; Merrill et al. (2021). Scabin (S117A) toxin from Streptomyces scabies. Protein Data Bank: 6vuv.

Lyons; B.; Lidster; T.; Merrill et al. (2021). Scabin (N110A) toxin from Streptomyces scabies. Protein Data Bank: 6vpa.

Maben, Z.; Liu, W.; Mosyak, L.; Chaparro-Riggers, J. (2021). Crystal structure of the CD27:CD70 co-stimulatory complex. Protein Data Bank: 7kx0.

Mao, Z.W.; Xia, W.; Tao, X. (2021). The crystal structure of SARS-CoV-2 3CLpro with Zinc. Protein Data Bank: 7d64.

Murray, B.W.; Rogers, E.; Zhai, D.; Deng, W.; Chen, X. et al. (2021). Crystal structure of TrkA kinase with repotrectinib. Protein Data Bank: 7vko.

Murray, J.M. (2021). BRD4-BD1 Compound6 (methyl 4-(3,5-difluoropyridin-2-yl)-10-methyl-7-((methylsulfonyl)methyl)-11-oxo-3,4,10,11-tetrahydro-1H-1,4,10-triazadibenzo[cd,f] azulene-6-carboxylate). Protein Data Bank: 7khl.

Nolte, R.T.; Somers, D.O.; Gampe, R.T. (2021). H-PDGS complexed with a 2-phenylimidazo[1,2-a]pyridine-6-carboxamide inhibitors. Protein Data Bank: 7jr6.

Orita, T.; Doi, S.; Iwanaga, T.; Adachi, T. (2021). Crystal structure of human pyruvate dehydrogenase kinase 4 in complex with compound 2. Protein Data Bank: 7ebb.

Orth, P. (2021). Structure of human plasma factor XIIa in complex with (2S)-4-(5-chloro-1,3-benzoxazol-2-yl)-1-(N,3-dicyclohexyl-D-alanyl)-N-[(thiophen-2-yl)methyl]piperazine-2-carboxamide (compound 7). Protein Data Bank: 6x0s.

Palte, R.L.; Hayes, R.P. (2021). PRMT5:MEP50 Complexed with 5,5-Bicyclic Inhibitor Compound 4. Protein Data Bank: 7kib.

Park, J. (2021). Crystal structure of human ribokinase in complex with AMPCP. Protein Data Bank: 6wjz.

Payandeh, J.; Ho, H. (2021). Fab CJ11 in complex IL-1beta peptide liberated by Caspase cleavage. Protein Data Bank: 7jwq.

Pham, N.T.H.; Calmettes, C.; Doucet, N. (2021). Crystal structure of G16S human Galectin-7 mutant in complex with lactose. Protein Data Bank: 6vts.

Pham, N.T.H.; Calmettes, C.; Doucet, N. (2021). Crystal structure of G16C human Galectin-7 mutant in complex with lactose. Protein Data Bank: 6vtq.

Pham, N.T.H.; Calmettes, C.; Doucet, N. (2021). Crystal structure of G16S human Galectin-7 mutant. Protein Data Bank: 6vtr.

Pham, N.T.H.; Calmettes, C.; Doucet, N. (2021). Crystal structure of G16C human Galectin-7 mutant. Protein Data Bank: 6vtp.

Pham, N.T.H.; Calmettes, C.; Doucet, N. (2021). Crystal structure of human Galectin-7 in complex with 4-O-beta-D-Galactopyranosyl-D-glucose. Protein Data Bank: 6vto.

Prasertanan, T.; Palmer, D.R.J.; Sanders, D.A.R. (2021). Crystal structure of KabA from Bacillus cereus UW85 in complex with the internal aldimine. Protein Data Bank: 7kz3.

Prasertanan, T.; Palmer, D.R.J.; Sanders, D.A.R. (2021). Crystal structure of KabA from Bacillus cereus UW85 in complex with the plp external aldimine adduct with kanosamine-6-phosphate. Protein Data Bank: 7kz5.

Prasertanan, T.; Palmer, D.R.J.; Sanders, D.A.R. (2021). Crystal structure of KabA from Bacillus cereus UW85 with bound cofactor PMP. Protein Data Bank: 7kz6.

Prasertanan, T.; Palmer, D.R.J.; Sanders, D.A.R. (2021). Crystal structure of KabA from Bacillus cereus UW85 in complex with the reduced internal aldimine and with bound Glutarate. Protein Data Bank: 7kzd.

Radka, C.D.; Aller, S.G. (2021). YfeA oligomer crystal 1, form 1. Protein Data Bank: 7me1.

Rasool, S.; Veyron, S.; Trempe, J.F. (2021). Crystal structure of the cytosolic domain of Tribolium castaneum PINK1 phosphorylated at Ser205 in complex with ADP analog. Protein Data Bank: 7mp9.

Rasool, S.; Veyron, S.; Trempe, J.F. (2021). Crystal structure of the cytosolic domain of Tribolium castaneum PINK1 in the non-phosphorylated state. Protein Data Bank: 7mp8.

Rutbeek, N.R.; Prehna, G. (2021). Prx in complex with ComR DNA-binding domain. Protein Data Bank: 7n1n.

Sahtout, N.; Kuttiyatveetil, J.R.A.; Sanders, D.A.R. (2021). Structure of thioredoxin reductase from the thermophilic eubacterium Thermosipho africanus TCF52B. Protein Data Bank: 7jyp.

Saran, S.; Majdi Yazdi, M.; Sanders, D.A.R. (2021). Dihydrodipicolinate synthase (DHDPS) from C.jejuni, E88D mutant with pyruvate bound in the active site and L-lysine bound at the allosteric site. Protein Data Bank: 7ko3.

Saran, S.; Majdi Yazdi, M.; Sanders, D.A.R. (2021). Dihydrodipicolinate synthase (DHDPS) from C.jejuni, E88D mutant with pyruvate bound in the active site. Protein Data Bank: 7ko1.

Saran, S.; Majdi Yazdi, M.; Sanders, D.A.R. (2021). Dihydrodipicolinate synthase (DHDPS) from C.jejuni, H59N mutant with pyruvate bound in the active site and R,R-bislysine bound at the allosteric site. Protein Data Bank: 7km1.

Saran, S.; Majdi Yazdi, M.; Sanders, D.A.R. (2021). Dihydrodipicolinate synthase (DHDPS) from C.jejuni, N84D mutant with pyruvate bound in the active site and R,R-bislysine bound at the allosteric site. Protein Data Bank: 7kkt.

Saran, S.; Majdi Yazdi, M.; Sanders, D.A.R. (2021). Dihydrodipicolinate synthase (DHDPS) from C.jejuni, N84D mutant with pyruvate bound in the active site and L-lysine bound at the allosteric site. Protein Data Bank: 7kkg.

Saran, S.; Majdi Yazdi, M.; Sanders, D.A.R. (2021). Dihydrodipicolinate synthase (DHDPS) from C.jejuni, N84A mutant with pyruvate bound in the active site and R,R-bislysine bound at the allosteric site. Protein Data Bank: 7kkd.

Saran, S.; Majdi Yazdi, M.; Sanders, D.A.R. (2021). Dihydrodipicolinate synthase (DHDPS) from C.jejuni, N84A mutant with pyruvate bound in the active site and L-lysine bound at the allosteric site. Protein Data Bank: 7kk1.

Saran, S.; Majdi Yazdi, M.; Sanders, D.A.R. (2021). Dihydrodipicolinate synthase (DHDPS) from C.jejuni, H56W mutant with pyruvate bound in the active site and R,R-bislysine bound at the allosteric site. Protein Data Bank: 7kh4.

Saran, S.; Majdi Yazdi, M.; Sanders, D.A.R. (2021). Dihydrodipicolinate synthase (DHDPS) from C.jejuni, H56W mutant with pyruvate bound in the active site and L-lysine bound at the allosteric site. Protein Data Bank: 7kg9.

Saran, S.; Majdi Yazdi, M.; Sanders, D.A.R. (2021). Dihydrodipicolinate synthase (DHDPS) from C.jejuni, H56W mutant with pyruvate bound in the active site. Protein Data Bank: 7kg5.

Saran, S.; Majdi Yazdi, M.; Sanders, D.A.R. (2021). Dihydrodipicolinate synthase (DHDPS) from C.jejuni, H59K mutant with pyruvate bound in the active site and L-histidine bound at the allosteric site. Protein Data Bank: 7kg2.

Saran, S.; Sanders, D.A.R. (2021). Dihydrodipicolinate synthase (DHDPS) from C.jejuni with pyruvate bound in the active site in P1211 space group. Protein Data Bank: 7l4b.

Saran, S.; Sanders, D.A.R. (2021). Dihydrodipicolinate synthase (DHDPS) from C.jejuni, Y110F mutant with pyruvate bound in the active site and L-lysine bound at the allosteric site in C2221 space group. Protein Data Bank: 7kz2.

Saran, S.; Sanders, D.A.R. (2021). Dihydrodipicolinate synthase (DHDPS) from C.jejuni with pyruvate bound in the active site and R,R-bislysine bound at the allosteric site in C2221 space group. Protein Data Bank: 7kxh.

Saran, S.; Sanders, D.A.R. (2021). Dihydrodipicolinate synthase (DHDPS) from C.jejuni with pyruvate bound in the active site and L-histidine bound at the allosteric site. Protein Data Bank: 7kxg.

Saran, S.; Sanders, D.A.R. (2021). Dihydrodipicolinate synthase (DHDPS) from C.jejuni, Y110F mutant with pyruvate bound in the active in C2221 space group. Protein Data Bank: 7kx1.

Saran, S.; Sanders, D.A.R. (2021). Dihydrodipicolinate synthase (DHDPS) from C.jejuni with pyruvate bound in the active site and L-lysine bound at the allosteric site in C2221 space group. Protein Data Bank: 7kwp.

Saran, S.; Sanders, D.A.R. (2021). Dihydrodipicolinate synthase from C. jejuni with pyruvate bound to the active site in C2221 space group. Protein Data Bank: 7kwn.

Saran, S.; Sanders, D.A.R. (2021). Dihydrodipicolinate synthase (DHDPS) from C.jejuni, H56N mutant with pyruvate bound in the active site and R,R-bislysine bound at the allosteric site. Protein Data Bank: 7kwf.

Saran, S.; Sanders, D.A.R. (2021). Dihydrodipicolinate synthase (DHDPS) from C.jejuni, H56N mutant with pyruvate bound in the active site and L-lysine bound at the allosteric site. Protein Data Bank: 7kuz

Saran, S.; Sanders, D.A.R. (2021). Dihydrodipicolinate synthase (DHDPS) from C.jejuni, H56N mutant with pyruvate bound in the active site. Protein Data Bank: 7ku6.

Saran, S.; Sanders, D.A.R. (2021). Dihydrodipicolinate synthase (DHDPS) from C.jejuni, H56A mutant with pyruvate bound in the active site and R,R-bislysine bound at the allosteric site. Protein Data Bank: 7kto.

Saran, S.; Sanders, D.A.R. (2021). Dihydrodipicolinate synthase (DHDPS) from C.jejuni, H56A mutant with pyruvate bound in the active site. Protein Data Bank: 7kr8.

Saran, S.; Sanders, D.A.R. (2021). Dihydrodipicolinate synthase (DHDPS) from C.jejuni, H56A mutant with pyruvate bound in the active site and L-lysine at the allosteric site. Protein Data Bank: 7kr7.

Saran, S.; Sanders, D.A.R. (2021). Dihydrodipicolinate synthase (DHDPS) from C.jejuni, E88Q mutant with pyruvate bound in the active site and R,R-bislysine at the allosteric site. Protein Data Bank: 7kpe.

Saran, S.; Sanders, D.A.R. (2021). Dihydrodipicolinate synthase (DHDPS) from C.jejuni, E88Q mutant with pyruvate bound in the active site and L-lysine bound at the allosteric site. Protein Data Bank: 7kpc.

Saran, S.; Sanders, D.A.R. (2021). Dihydrodipicolinate synthase (DHDPS) from C.jejuni, E88Q

mutant with pyruvate bound in the active site. Protein Data Bank: 7koc.

Saran, S.; Sanders, D.A.R. (2021). Dihydrodipicolinate synthase (DHDPS) from C.jejuni, E88A mutant with pyruvate bound in the active site and R,R-bislysine at the allosteric site. Protein Data Bank: 7knz.

Saran, S.; Sanders, D.A.R. (2021). Dihydrodipicolinate synthase (DHDPS) from C.jejuni, E88A mutant with pyruvate bound in the active site and L-lysine bound at the allosteric site. Protein Data Bank: 7kn9.

Saran, S.; Sanders, D.A.R. (2021). Dihydrodipicolinate synthase (DHDPS) from C.jejuni, E88A mutant with pyruvate bound in the active site. Protein Data Bank: 7kn2.

Saran, S.; Sanders, D.A.R. (2021). Dihydrodipicolinate synthase (DHDPS) from C.jejuni, H59N mutant with pyruvate bound in the active site and L-lysine bound at the allosteric site. Protein Data Bank: 7kly.

Saran, S.; Sanders, D.A.R. (2021). Dihydrodipicolinate synthase (DHDPS) from C.jejuni, H59N mutant with pyruvate bound in the active site. Protein Data Bank: 7klt.

Saran, S.; Sanders, D.A.R. (2021). Dihydrodipicolinate synthase (DHDPS) from C.jejuni, H59A mutant with pyruvate bound in the active site and L-lysine bound at the allosteric site. Protein Data Bank: 7kls.

Saran, S.; Sanders, D.A.R. (2021). Dihydrodipicolinate synthase (DHDPS) from C.jejuni, H59K mutant with pyruvate bound in the active site. Protein Data Bank: 7kel.

Scholl; C.L.; Tsuda; S.; Graham et al. (2021). Crystal waters on the nine polyproline type II helical bundle springtail antifreeze protein from Granisotoma rainieri match the ice lattice. Protein Data Bank: 7jjv.

Sharon, I.; Stille, J.; Tjutrins, J.; Wang, G.; Venegas, F.A. et al. (2021). Crystal Structure of SARS-CoV-2 Main Protease (3CLpro/Mpro) Covalently Bound to Compound C7. Protein Data Bank: 7mlf.

Sheriff, S. (2021). CRYSTAL STRUCTURE OF THE FIRST BROMODOMAIN OF HUMAN BRD4 IN COMPLEX WITH BMS-986158, 2-{3-(1,4-dimethyl-1H-1,2,3-triazol-5-yl)-5-[(S)-(oxan-4-yl)(phenyl) methyl]-5H-pyrido[3,2-b]indol-7-yl} propan-2-ol. Protein Data Bank: 5s9r.

Sheriff, S. (2021). CRYSTAL STRUCTURE OF THE FIRST BROMODOMAIN OF HUMAN BRD4 IN COMPLEX WITH 2-{(7P)-7-(1,4-dimethyl-1H-1,2,3-triazol-5-yl)-8-fluoro-5-[(S)-(oxan-4-yl)(phenyl) methyl]-5H-pyrido[3,2-b]indol-3-yl} propan-2-ol. Protein Data Bank: 7mce.

Shi, R.; Manenda, M.S.; Picard, M.-E. (2021). Crystal structure of bH1 Fab variant (CDR H3 loop design 16_0325) in complex with VEGF. Protein Data Bank: 7kez.

Shi, R.; Picard, M.-E. (2021). Crystal structure of bH1 Fab variant (CDR H3 loop design 13_0346) in complex with VEGF. Protein Data Bank: 7kf0.

Shi, R.; Picard, M.-E.; Manenda, M.S. (2021). Crystal structure of bH1 Fab variant (CDR H3 loop design 14_0130) in complex with VEGF. Protein Data Bank: 7kf1.

Sintchak, M.; Lane, W.; Bump, N. (2021). Structure of SUMO1-ML00789344 adduct bound to SAE. Protein Data Bank: 6xoh.

Sintchak, M.; Lane, W.; Bump, N. (2021). Structure of SUMO1-ML786519 adduct bound to SAE. Protein Data Bank: 6xog.

Suits, M.D.L. (2021). SusE-like protein BT2857. Protein Data Bank: 7m1b.

Suits, M.D.L. (2021). SusE-like protein BT2857. Protein Data Bank: 7m1a.

Swinger, K.K.; Schenkel, L.B.; Kuntz, K.W. (2021). Human PARP14 (ARTD8), catalytic fragment in complex with RBN012759. Protein Data Bank: 6we2.

Van Herk, P.H.; Cleland, C.P.; Mosimann, S.C. (2021). Structure of the PTP-like myo-inositol phosphatase from Desulfovibrio magneticus (high salt). Protein Data Bank: 7k6y.

Vergunst, K.L.; Langelaan, D.N. (2021). Crystal structure of hydrophobin SC16, C2221. Protein Data Bank: 7s86.

Wang, F.; Cheng, W.; Shang, H.; Wang, R.; Zhang, B. et al. (2021). The Crystal Structure of human MTH1 from Biortus. Protein Data Bank: 7esf.

Wang, F.; Cheng, W.; Xu, C.; Qi, J.; Bao, X. et al. (2021). The Crystal Structure of human DHFR from Biortus. Protein Data Bank: 7ese.

Wang, F.; Lin, D.; Wang, R.; Wei, X.; Shen, Z. et al. (2021). The Crystal Structure of human UMP-CMP kinase from Biortus.. Protein Data Bank: 7e9v.

Wang, F.; Xu, C.; Qi, J.; Zhang, M.; Tian, F. et al. (2021). The Crystal Structure of D-psicose-3-epimerase from Biortus.. Protein Data Bank: 7e9w.

Wen, Y.; Campbell, R.E.; Lemieux, M.J.; Nasu, Y. (2021). Crystal structure of eLACCO1. Protein Data Bank: 7e9y.

Wen; Y.; Lemieux; J.M. (2021). Crystal structure of PhoCl barrel. Protein Data Bank: 7dnb.

Wen; Y.; Lemieux; J.M. (2021). Photocleavable Fluorescent Protein in green and red form. Protein Data Bank: 7dna.

Wen; Y.; Lemieux; M.J. (2021). Photocleavable Fluorescent Protein in green form. Protein Data Bank: 7dmx.

Workman, S.D.; Strynadka, N.C.J. (2021). Crystal structure of Bacillus subtilis UppS in complex with MAC-0547630. Protein Data Bank: 7jlm.

Workman, S.D.; Strynadka, N.C.J. (2021). Crystal structure of Bacillus subtilis UppS in complex with clomiphene. Protein Data Bank: 7jlj.

Workman, S.D.; Strynadka, N.C.J. (2021). Crystal structure of Bacillus subtilis UppS. Protein Data Bank: 7jli.

Workman, S.D.; Strynadka, N.C.J. (2021). Crystal structure of Bacillus subtilis UppS in complex with JPD447. Protein Data Bank: 7jlr.

Worrall, L.J.; Sun, T.; Mulligan, V.K.; Strynadka, N.C.J. (2021). Structure of NDM-1 in complex with macrocycle inhibitor NDM1i-1G. Protein Data Bank: 6xbf.

Worrall, L.J.; Sun, T.; Mulligan, V.K.; Strynadka, N.C.J. (2021). Structure of NDM-1 in complex with macrocycle inhibitor NDM1i-1F. Protein Data Bank: 6xbe.

Xu, S.; Grochulski, P.; Tanaka, T. (2021). X-ray crystallographic structure model of Lactococcus lactis prolidase mutant D36S. Protein Data Bank: 7n02.

Zielinski; M.; Berghuis; A.M. (2021). Erythromycin esterase mutant EreC H289N in its open conformation. Protein Data Bank: 6xcs. Columbia. http://hdl.handle.net/2429/74692

DOCTORAL THESIS

Bhagavathula, Kapil Bharadwaj (2021). Density, Microstructure, and Strain Rate-Dependent Behaviour of Polymeric Foams. Supervisor: Hogan, James. Alberta, Canada: University of Alberta. https://era.library.ualberta.ca/items/c86d71cd-8ce3-48d1-b9bf-b59a1d77d83d.

Christopher Dydula (2021). Development of x-ray coherent scatter projection imaging systems. Supervisor: Johns, Paul C.. Ontario, Canada: Carleton University. https://doi.org/10.22215/etd/2021-14418.

Rathinaswamy, Manoj Kumar (2021). Molecular basis for the regulation of phosphoinositide 3-kinase γ (PI3Kγ). Supervisor: Burke, John. British Columbia, Canada: University of Victoria. http://hdl.handle.net/1828/13168.

Roby Gauthier (2021). Understanding and Preventing Lifetime Failure in Lithium-Ion Batteries. Supervisor: Dahn, Jeff. Nova Scotia, Canada: Dalhousie University. https://dalspace.library.dal.ca/handle/10222/80722.

Sudheesh Kumar Veeranmaril (2021). Designing Sinter-Resistant Monometallic and Bimetallic Nanomaterials for Catalysis. Supervisor: Scott, Robert W. J.. Saskatoon: University of Saskatchewan..

Sun, Tianxiao (2021). Experimental Study on the Soft X-ray Spectro-Microscopy. Supervisor: Tai, Renzhong. Shanghai, China: The University of Chinese Academy of Sciences / Shanghai Institute of Applied Physics, CAS..

Tyler A. Morhart (2021). Surface-Enhanced Spectroelectrochemistry using Synchrotron Infrared Radiation. Supervisor: Burgess, Ian J.. Saskatchewan, Canada: University of Saskatchewan. https://harvest.usask.ca/handle/10388/13617.

Vanessa Orr (2021). Rotational and Vibrational Spectroscopy and Structure Determination of Organic Molecules of Astrochemical Relevance. Supervisor: McMahon, Robert; Claude, Woods. Wisconsin, USA: University of Wisconsin-Madision..

Wenshuai Li (2021). Tracing chemical weathering using lithium and potassium isotopes. Supervisor: Liu, Xiao-Ming; Teng, F.-Z.; Wasylenki, L.; Benninger, L.; Barzyk, J.. North Carolina, USA: University of North Carolina at Chapel Hill. https://doi.org/10.17615/jmxm-4116.

Wiewiora, Rafal Piotr (2021). Rigorous Construction of Markov State Models for Conformationally Selective Drug Design. Supervisor: Chodera, John D.. New York, United States: Weill Medical College of Cornell University.. Abdelrasoul, Amira (2021). Investigation on Hemodialysis Membranes Morphology and Human Serum Proteins Depositions Using Synchrotron-based Imaging.. 10.11159/icbes21.117.

Berkenbrock, Jose Alvim; Suzuki, Daniela Ota Hisayasu; Wells, Garth; Mail, Matthias; Scherer, Torsten et al. (2021). Analysis of High Aspect Ratio Nanopores for Resistive Pulse Sensing Applications Through Numerical Simulations.. 10.1109/nmdc50713.2021.9677508.

Cron, Brandi; Macalady, Jennifer L.; Cosmidis, Julie (2021). Organic stabilization of extracellular elemental sulfur in a Sulfurovum-rich biofilm: a new role for EPS?. Patent Number: 10.1101/2021.06.03.446708.

Simonson, N. A.; Sigari, Y.Y; M. J. Boland (2021). X-Ray Double Slit Interferometer Progress at CLS.

MASTERS THESIS

Casali; Juliana (2021). Hydrothermal Alteration Footprint of the Monument Bay Project, Manitoba, Canada. Supervisor: Banerjee, Neil R.; Van Loon, Lisa. Ontario, Canada: The University of Western Ontario. https://ir.lib.uwo.ca/cgi/viewcontent.gi?article=10085&context=etd.

Denys Vidish (2021). Functional nanoparticles: tin monoxide and molybdenum disulfide quantum dots on graphene nanosheets. Supervisor: Fanchini, Giovanni; Sham, Tsun-Kong. Ontario, Canada: The University of Western Ontario. https://ir.lib.uwo.ca/etd/8171.

Dong, Zhi Liang (2021). X-ray Absorption Spectroscopy, and Optical Luminescence Studies of Undoped and P-doped ZnO Nano/Microparticles. Supervisor: Sham, Tsun-Kong. Ontario, Canada: The University of Western Ontario. https://ir.lib.uwo.ca/etd/8052.

Dylan Sidney Blair Scheibelhoffer (2021). Enzymatic Hydrolysis of Flaxseed Oil to Produce Free Fatty Acids. Supervisor: Dalai, Ajay K. Saskatchewan, Canada: University of Saskatchewan. https://harvest.usask.ca/handle/10388/13187.

Forand, Ariana Dylis (2021). The Cell Wall as a Barrier Against Water Loss and Plant Pathogens. Supervisor: Tanino, Karen. SK, Canada: University of Saskatchewan. https://harvest.usask.ca/handle/10388/13497.

Hao; Chunyi (2021). Geometallurgy and Gold Mineralization of the Monument Bay Project, Stull Lake Greenstone Belt, Manitoba, Canada. Supervisor: Banerjee, Neil R.; Van Loon, Lisa L.. Ontario, Canada: The University of Western Ontario. https://ir.lib.uwo.ca/cgi/viewcontent.cgi?article=10079&context=etd.

Hisan Waleed Shafaque (2021). Improving the Performance of Membrane Electrode Assembly CO2 Electrolyzers. Supervisor: Bazylak, Aimy. Ontario, Canada: University of Toronto. https://tspace.library.utoronto.ca/handle/1807/106383.

Junseob Kim (2021). Novel Porous Transport Layers with Through Pores for Polymer Electrolyte Membrane Electrolyzers. Supervisor: Bazylak, Aimy. Ontario, Canada: University of Toronto. https://tspace.library.utoronto.ca/handle/1807/104998.

Kevin Krause (2021). Characterizing Unstable Operation in Flow Cells for CO2 Electroreduction. Supervisor: Bazylak, Aimy. Ontario, Canada: University of Toronto. https://tspace.library.utoronto.ca/handle/1807/104877.

Mackenzie J. Wieler (2021). Molecular Level Speciation of Phosphorus in Suspended and Streambed Fluvial Sediments. Supervisor: Hu, Yongfeng; Wang, Hui. Saskatchewan, Canada: University of Saskatchewan. https://harvest.usask.ca/handle/10388/13640.

Ngoc Ton (2021). Developing a Microbubble-based Contrast Agent for X-ray Phase Contrast Imaging to Detect Neovasculature in Breast Cancer. Supervisor: Machtaler, Steven; Wiebe, Sheldon. Saskatchewan, Canada: University of Saskatchewan. https://harvest.usask.ca/handle/10388/13397.

Olumorin, Theo (2021). Investigation of Size Specific Fe2O3 nanoparticles: Towards Single Nanoparticle Resolved Spectro-ptychography. Supervisor: Urquhart, Stephen G.. Saskatchewan, Canada: University of Saskatchewan..

Scire, Michelle Denise (2021). Structure and Function of MUC1 Specific Monoclonal Antibodies. Supervisor: Brooks, Cory L.. California, United States: California State University, Fresno. https://www.proquest.com/openview/5490f79cdbfb3740264d2fb8533321b1/.

Spencer Sterling (2021). Structural Studies of Boron Nitride Compounds Under Extreme Conditions. Supervisor: Desgreniers, Serge. Ontario, Canada: University of Ottawa. https://ruor.uottawa.ca/handle/10393/42856.

Yuzhou Zhang (2021). Visualization of Thawing and Desaturation in Frozen Gas Diffusion Layers of Proton Exchange Membrane Fuel Cells via Synchrotron X-ray Computed Tomography. Supervisor: Zhang, Lifeng. Saskatchewan, Canada: University of Saskatchewan. https://harvest.usask.ca/handle/10388/13388.

Zhi Liang Dong (2021). X-ray Absorption Spectroscopy, and Optical Luminescence Studies of Undoped and P-doped ZnO Nano/MicroparticlesStudies of Undoped and P-doped ZnO Nano/Microparticles. Supervisor: Tsun-Kong Shan. Ontario, Canada: The University of Western Ontario..

Zhi Liang Dong (2021). X-ray Absorption Spectroscopy, and Optical Luminescence Studies of Undoped and P-doped ZnO Nano/Microparticles. Supervisor: Tsun-Kong Sham. Ontario, Canada: Western University.

Canadian Light Source | Centre canadien de rayonnement synchrotron

The Canadian Light Source is a national research facility of the University of Saskatchewan.

University of Saskatchewan

Canadian Light Source Inc

44 Innovation Boulevard, Saskatoon, SK, Canada S7N 2V3 | Phone: (306) 657-3500 | cls@lightsource.ca

www.lightsource.ca **canlightsource**